Inaugural dissertation

for

obtaining the doctoral degree

of the

Combined Faculty of Mathematics, Engineering and Natural Sciences

of the

Ruprecht – Karls – University

Heidelberg

Presented by

Christina Blume, M.Sc.

Born in: Zwickau, Germany

Oral examination: September 29, 2023

Characterization of inter- and intratumoral heterogeneity and the differential immune microenvironment during malignant progression in meningiomas

Referees: Prof. Dr. Benedikt Brors

Prof. Dr. Dr. med. Felix Sahm

ABSTRACT

Meningiomas are thought to arise from the arachnoid cells of the leptomeninx and make up the most common primary intracranial tumor in adults. They are usually benign, however in about 20 % of cases, tumors present with an aggressive phenotype and higher risk of recurrence. Risk stratification thereby remains challenging especially for *NF2*-mutated meningiomas, which make up about two thirds of all cases, as they can occur at the full spectrum of WHO grades in meningioma from 1 to 3. Recently, molecular profiling has gained importance for prognosis in meningioma with several classification systems that have been established mostly based on the DNA methylation of the tumors. However, the DNA methylation-based classification has not been extensively linked to phenotypic traits of the tumor. Nor have meningiomas been investigated regarding intratumoral subpopulations that may exist in parallel and may have different characteristics, especially regarding the stage of progression and ability to recur. In addition, the role of the immune microenvironment in meningiomas is poorly understood, despite the identification of an immune-enriched meningioma subgroup with beneficial outcome in two independent DNA methylation classification systems.

In this dissertation, I investigated the consistency of subgroups initially defined on epigenomic level across molecular levels by comparison to transcriptomic and proteomic data. Further, I leveraged single nuclei transcriptomic profiling to dissect intertumoral differences in the expression profile specific to the tumor cell population depending on the tumor subgroup, and to investigate the abundance and phenotype of intratumoral tumor cell subpopulations across samples. Similarly, I analyzed the single nuclei transcriptomic data to characterize tumor-infiltrating immune cells with respect to their abundance and activation status. I furthermore correlated the differences in immune infiltration with the progression-free survival of patients by deconvoluting DNA methylation array data according to their cellular composition.

These analyses underlined the coherence of epigenomic meningioma subgroups across transcriptome and proteome. Moreover, I identified six tumor cell subpopulations that were defined by distinct expression profiles und could be identified across samples at varying abundancies depending on the stage of progression. Similarly, I observed profound differences in infiltrating immune cells between tumor subgroups, with a significant enrichment of tumor-associated macrophages in a benign subgroup of *NF2*-mutated meningiomas as compared to more progressed tumors. In parallel to their abundancy, macrophages changed in activation between benign and malignant cases from an anti- to a pro-tumorigenic phenotype. The evaluation of progression-free survival data revealed a positive correlation to the proportion of infiltrating immune cells as estimated from epigenomic profiles.

Altogether, these results highlight the role of multi-level molecular profiling for tumor grading in a paradigmatic, epidemiologically relevant tumor type. They further indicate an important role

of tumor-infiltrating macrophages during meningioma progression with possible consequences for risk prediction as well as therapeutic targets in meningioma.

ZUSAMMENFASSUNG

Meningeome entstehen nach aktuellem Kenntnisstand vermutlich aus den arachnoidalen Deckzellen der Leptomeninx und machen den größten Anteil primärer intrakranialer Tumore bei Erwachsenen aus. Sie sind für gewöhnlich benigne, können jedoch in rund 20 % der Fälle mit aggressivem Phänotyp und einem hohen Risiko für ein Rezidiv auftreten. Risikostratifizierung ist dabei oft problematisch, im Besonderen für *NF2*-mutierte Meningeome, welche etwa zwei Drittel aller Fälle ausmachen, da diese entlang des gesamten Spektrums an WHO-Graden für Meningeome, von 1 bis 3, vorkommen können. Kürzlich hat die molekulare Charakterisierung an Wichtigkeit für die Prognose bei Meningeomen aufgrund mehrerer Klassifikationssysteme, welche auf Grundlage des Tumorepigenoms etabliert wurden, gewonnen. Jedoch wurden die auf DNA-Methylierung basierenden Klassifikationen bisher kaum mit phänotypischen Eigenschaften des Tumors in Verbindung gebracht. Gleichsam wurden Meningeome bisher nicht bezüglich intratumoraler Subpopulationen untersucht, welche gleichzeitig innerhalb eines Tumors existieren, doch dabei unterschiedliche Merkmale insbesondere hinsichtlich der Progressionsstufe und Fähigkeit zu rezidivieren aufweisen könnten. Des Weiteren ist die Rolle des Immunmikromilieus in Meningeomen kaum untersucht, obwohl eine immun-angereicherte Subgruppe von Meningeomen mit günstiger Prognose in zwei unabhängigen epigenomischen Klassifikationssystemen identifiziert wurde.

In dieser Dissertation untersuche ich die Vereinbarkeit von epigenomischen Subgruppen über molekulare Ebenen hinweg mit dem Transkriptom sowie Proteom. Zudem nutze ich die Profilierung des Transkriptoms auf Einzelzellebene, um Tumorzell-spezifische Unterschiede im Expressionsprofil zwischen Tumoren in Abhängigkeit zur Tumorsubgruppe aufzudecken sowie das Vorkommen und den Phänotyp von intratumoralen Tumorzellsubpopulationen zu untersuchen. Ebenso analysiere ich die Einzelzell-Transkriptomdaten, um die den Tumor infiltrierenden Immunzellen hinsichtlich ihres Vorkommens und ihres Aktivierungsstatus zu charakterisieren. Darüber hinaus korreliere ich die Unterschiede in der Immuninfiltration mit dem progressionsfreien Überleben der Patienten, indem ich epigenomische Daten hinsichtlich ihrer zellulären Komposition aufschlüssele.

Diese Analysen bekräftigen die Kohärenz von Meningeom-Subgruppen, welche ursprünglich auf epigenomischer Ebene definiert wurden, in Transkriptom und Proteom. Darüber hinaus identifiziere ich sechs Tumorzellsubpopulationen, welche sich durch individuelle Expressionsprofile auszeichnen und in verschiedenen Tumoren in variierender Menge je nach Progressionsstufe nachgewiesen werden konnten. Gleichermaßen konnte ich ausgeprägte Unterschiede in den infiltrierenden Immunzellen abhängig von der Tumorsubgruppe beobachten, wobei Tumor-assoziierte Makrophagen in einer Subgruppe von benignen Meningeomen mit *NF2*-Mutation im Vergleich zu malignen Meningeomen signifikant angereichert waren. Neben ihrer

Abundanz wechselten die Makrophagen auch in ihrer Aktivierung zwischen benignen und malignen Fällen von einem anti- zu einem protumorigenen Phänotyp. Die Auswertung des progressionsfreien Überlebens zeigte zudem eine positive Korrelation mit dem Anteil der infiltrierenden Immunzellen, welche auf Grundlage von epigenomischen Daten bestimmt wurde, auf.

Zusammen genommen verdeutlichen diese Ergebnisse die Bedeutung einer mehrstufigen molekularen Auswertung in der Bewertung eines paradigmatischen, epidemiologisch relevanten Tumortyps. Zudem weisen sie auf eine wichtige Rolle von infiltrierenden Makrophagen während der Tumorprogression hin, welche möglicherweise Auswirkungen auf die Risikobewertung sowie therapeutische Ansätze bei Meningeomen hat.

ACKNOWLEDGEMENTS

I am more than grateful for all the people who have accompanied me on my path to this dissertation and without whose support I would not have gotten this far.

First and foremost, I would like to thank **Prof. Dr. Dr. med. Felix Sahm** for providing me with the opportunity of a PhD position in his group. Thank you for your supervision and guidance. I highly appreciate the support I have received, enabling me to learn and grow scientifically as well as personally.

Moreover, I would like to thank **Prof. Dr. Matthias Schlesner**, who has been an excellent second supervisor and has provided me with support especially on, but not limited to, the bioinformatics side of my projects. Your ideas and feedback are always inspiring and have been more than valuable during this time. Thank you also for your continuous support after leaving Heidelberg.

I would further like to thank **Prof. Dr. Benedikt Brors** for offering his help and guidance, his valuable feedback during my TAC meetings, and for being a referee in my PhD defense. Thank you also to **Dr. Carl Herrmann** for his helpful input during my TAC meetings. Furthermore, I would like to thank **Dr. Simon Anders** and **Dr. Angela Goncalves** for participating in my thesis defense.

I am very grateful to have been part of such a fun and amazing lab. I could not have wished for a better environment during my PhD. I was especially fortunate to have started out together with **Areeba Patel**, who has been so much more than a colleague and office mate to me. I could not have wished for a better person to exchange and share all PhD (and non-PhD related) experiences with. Thank you for enlightening me in so many ways – scientifically, linguistically, as well as personally. You always provided a consistent flow of information. I would also like to express my deep gratitude to **Michael Ritter**, who has not only taken care of the wet lab side of things many times for me, but who has also been the best bouldering partner and supporter on and off the wall I could imagine (his taste in bouldering routes aside). I will absolutely miss your sense of humor; it truly is one of a kind! A huge thank you furthermore to **Helin Dogan**, who has most importantly done such a tremendous work in the wet lab, by which she has laid the foundations for my dissertation. I will always admire your motivation and dedication.

I would also like to extend my gratitude to the **BODAs**, who have welcomed me in their group as one of their own and provided such a great environment. I greatly enjoyed all the social activities together, in person and online!

I am truly thankful to the **LUGAs**: **Areeba Patel**, **Enrique Blanco Carmona**, and **Dina ElHarouni** (and Carl, of course), for making it always so worthwhile to come to the office. Thank you for being able to share all our delight and successes as well as frustration and failures. I do not think a day has passed in which you did not conjure a smile in my face. I will never find office mates (not only) like you again – this will be a tough adjustment in the future. An especially big

thank you goes to **Enrique Blanco Carmona**. You have been such a great source of support in the most difficult times, but also a person to easily make me laugh (and not just because of our misunderstandings now and then). You are the reason I have kept my sanity during the pandemic and in my efforts towards this thesis. I am deeply grateful that this PhD has made us cross paths. Be mindful to safely circumvent any rocks in your path in the future though!

I would also like to thank **Beatrice Casati**, who I met under the most difficult conditions (during an online workshop in the middle of the pandemic!), but still became such a great friend. Thank you for always offering valuable advice and support, and thank you for all these wonderful moments we shared.

I am eternally grateful for **"Die Hinterbliebenen"**: **Laura Gloßner**, **Raul Magyar**, and **Tom Zimmermann**. You have been accompanying me ever since our Bachelor's, and even though we have been separated by physical distance, I know that I can always count on you. We have shared so many laughs and memories, and I hope for many more to come. Thank you for always being there, despite my disabilities when it comes to text messaging.

A very special thanks goes to my **Mom** and **Dad**. Without both of you, I would not be who I am and where I am today. Thank you for your constant encouragement in everything I am doing and always believing in me. I am deeply grateful to know that I can always turn to you, and I will always rely on your advice.

Finally, the most important thank you goes to **Frank**. Thank you for all the love and support I have received from you. I do not even know how to begin to express my deep gratitude to you for moving to a new city in the middle of a pandemic entirely on my behalf. Thank you for always being there, for keeping me in a healthy work attitude, and for helping me focus on what is important in life.

List of Abbreviations

ATAC-Seq … assay for transposase-accessible chromatin using sequencing

CNS … central nervous system

CNV … copy number variation

DE … differential expression

ECM … extra-cellular matrix

EMT … epithelial-mesenchymal transition

FFPE … formalin-fixed, paraffin-embedded

H&E … Hematoxylin & Eosin

IBS … Integrated Brier score

IL … interleukin

ISH … *in-situ* hybridization

ISS … *in-situ* sequencing

LSI … latent semantic indexing

MC … methylation class

NGS … next generation sequencing

NMF … non-negative matrix factorization

PC … principal component

RNA-Seq … RNA-Sequencing

scATAC-Seq … single-cell ATAC-Sequencing

scRNA-Seq … single-cell RNA-Sequencing

SNF … similarity network fusion

TAM … tumor-associated macrophage

TME … tumor microenvironment

UCSF … University of California San Francisco

UMAP … Uniform Manifold Approximation and Projection

WHO … World Health Organization

TABLE OF CONTENTS

I. Introduction

1.1. Meninges and Meningioma

Healthy meninges

The connective tissue surrounding the central nervous system (CNS) is called the meninges. The meninges can be separated into three layers: the dura mater, the arachnoid mater, and the pia mater. The dura is the thickest and outermost membrane of the three, directly adjacent to the skull (**Figure 1**). It consists of dense fibrous tissue as well as blood and lymphatic vasculature, and surrounds the dural sinuses (Derk et al. 2021). Underneath the dura lies the thinner and transparent arachnoidea. Within the arachnoidea, the arachnoid cells facing the dura form a tightly connected layer of cells called the arachnoid barrier (Weller et al. 2018). The arachnoid barrier constitutes the barrier between the blood circulation in the dura and the cerebrospinal fluid in the so-called subarachnoid space between the arachnoidea and the pia below (Davson and Segal 1996). Fibrous trabeculae extend from the arachnoidea into the subarachnoid space (**Figure 1**). The pia as the innermost membrane is the most delicate layer, mostly consisting of just a single cell layer and directly adherent to the brain and spinal cord (Weller et al. 2018).

Together, arachnoid and pia mater, including the subarachnoid space in between, form the leptomeninx. Cells forming these membranes originate in the neural crest, while the cells forming the dura stem from the embryonal mesoderm (O'Rahilly and Müller 1986). Meningiomas are thought to arise from arachnoid cells of the leptomeninx (Kalamarides et al. 2011).

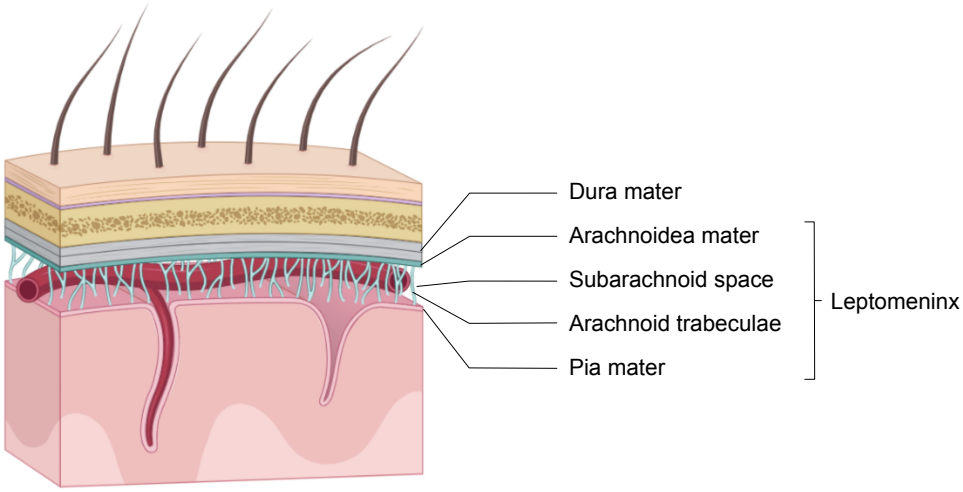

Figure 1. *Anatomy of the human meninges. [Created with BioRender.com.]*

Epidemiology and phenotypes of meningiomas

Meningiomas are the most frequent primary CNS tumor, making up 39 % of all CNS tumors (Ostrom et al. 2021). These tumors are typically slow growing (Buerki et al. 2018) and can occur both intracranially and in the spine, with spinal lesions making up 4.2 % of meningiomas (Ostrom et al. 2021). They are only rarely observed in children, their incidence increasing with age, and more frequently diagnosed in females with a male:female ratio of 0.43 for non-malignant meningiomas and 0.92 for malignant tumors (Ostrom et al. 2021).

Meningiomas can be divided into 15 subtypes based on their histology (Louis et al. 2021). Nine of these subtypes are usually associated with a more favorable prognosis: fibrous, meningothelial, mixed, angiomatous, psammomatous, secretory, microcystic, metaplastic, and lymphoplasmacyte-rich meningiomas. Meningiomas of a clear cell or chordoid histology have a higher risk to recur (Louis et al. 2021). For rhabodoid and papillary meningiomas on the other hand it has not sufficiently been demonstrated whether they are indeed associated with a more aggressive behavior. The two remaining subtypes however are determinative of aggressiveness and irrespective of the underlying subtype: atypical, and the most aggressive subtype of anaplastic meningioma (Louis et al. 2021).

Risk factors for developing a meningioma include ionizing radiation and obesity, as well as the occupational exposure to herbicides (Wiemels, Wrensch, and Claus 2010; Takahashi et al. 2019; Samanic et al. 2008). In addition, some familial syndromes such as neurofibromatosis type 2 and familial schwannomatosis are associated with an increased risk for meningioma (Kresak and Walsh 2016).

Molecular landscape of meningiomas

Genetically, meningiomas can be broadly separated into two major groups. Namely, meningiomas that harbor a mutation in the *NF2* gene, making up about two thirds of all cases, and meningiomas without a loss of *NF2* (Zhang et al. 2014). The latter is usually associated with a favorable course of disease and displays mutations in other genes such as *TRAF7*, *AKT1*, *KLF4*, *SMO*, *POLR2A*, and *PIK3CA* (Clark et al. 2013; Brastianos et al. 2013; Reuss et al. 2013; Yuzawa, Nishihara, and Tanaka 2016). For tumors with *NF2* loss, the range of outcomes is broad, covering slow-growing cases that almost never recur as well as cases with aggressive growth and high risk of recurrence (Yuzawa, Nishihara, and Tanaka 2016; Sahm et al. 2017). The gene product of *NF2*, Merlin, influences several downstream signaling pathways, such as the Hippo, PI3K, MAPK, and Wnt signaling pathways (Stamenkovic and Yu 2010; Cui et al. 2019). It regulates the cytoskeleton by linking actin filaments and transmembrane receptors and can attenuate proliferation through contact inhibition (Stamenkovic and Yu 2010). Mutations in this gene are usually nonsense,

frameshift, or splice site mutations, resulting in a loss of *NF2* (Ahronowitz et al. 2007). *NF2* loss in meningioma is associated with certain histopathological subtypes, mostly the fibroblastic and the transitional subtype. On the other hand, *KLF4* and *TRAF7* mutations are linked to a secretory histology, and mutations in *AKT1* are frequently observed in meningothelial meningiomas (Brastianos et al. 2013). Mutations in *TRAF7* often occur in combination with *KLF4*, *AKT1*, and *PIK3CA* mutations (Zotti et al. 2017; Abedalthagafi et al. 2016), although they can also present in isolation (**Figure 2**). By contrast, mutations in *SMO* and *POLR2A* are typically mutually exclusive (Yuzawa, Nishihara, and Tanaka 2016).

Besides gene mutations, meningiomas frequently display copy number variations (CNVs). By far the most common alteration is the deletion of chromosome 22q, being deleted in 68% of all cases, which is also the gene locus of the *NF2* gene (Maas et al. 2021). Other common CNVs include the deletion of chromosomes 1p, 6q, 7p, 10q, 14q, and 18q (Maillo et al. 2003; Riemenschneider, Perry, and Reifenberger 2006; Ketter et al. 2007; Maas et al. 2021). The number of alterations typically increases with malignancy.

Other common alterations in meningioma are the deletion of the *CDKN2A/B* gene locus as well as *TERT* promoter mutations, which are both associated with an aggressive behavior of the tumor (Goutagny et al. 2014; Sahm et al. 2015; Sievers et al. 2020). Further connected with increased malignancy is the elevated activity of the transcription factor *FOXM1* (Paramasivam et al. 2019). *FOXM1* may play a role in the promotion of tumor cell proliferation and their epithelial-mesenchymal transition as well as angiogenesis within the tumor (H. Kim et al. 2020).

The evaluation of molecular alterations has recently gained significance in risk stratification for meningioma patients (Louis et al. 2021).

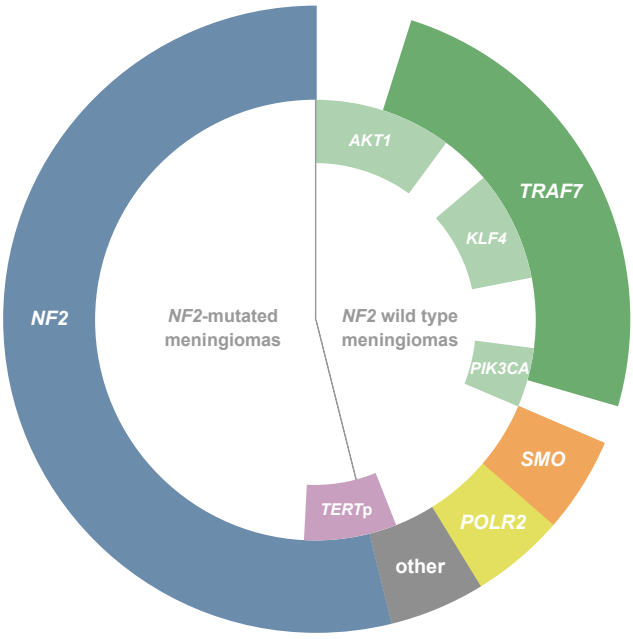

***Figure 2**. Genetic alterations in meningiomas. [Adapted from* Lee and Lee 2020.*]*

THE MENINGIOMA-SPECIFIC TUMOR MICROENVIRONMENT

The behavior and aggressiveness of tumor cells is heavily influenced by the surrounding tissue and infiltrating non-malignant cells, such as immune cells or fibroblasts, as well as the proteins that they produce, including extra-cellular matrix (ECM) components, cytokines, chemokines, and growth factors. Together, these cells and their secreted proteins are referred to as the tumor microenvironment (TME). In meningiomas specifically, the TME consists of non-cancerous fibroblasts, endothelial cells, and immune cells, as well as the ECM (Sahab-Negah and Gorji 2020). Importantly, the TME in meningioma is not limited by the blood brain barrier, as is the case for parenchymal CNS tumors. The most frequent infiltrating cell type are myeloid cells, of which macrophages make up the largest component (Fang et al. 2013). Macrophages that are observed in the healthy meninges compose a strongly specialized subtype of macrophages and are therefore often referred to as border-associated macrophages (Utz and Greter 2019). Besides macrophages, the immune cell compartment within meningiomas includes microglia, T cells, most of which are CD8 positive, NK cells, and to a lesser extent B cells and regulatory T cells (Fang et al. 2013). Macrophages and microglia have largely overlapping expression profiles and share the same embryonic origin, so that discrimination of both cell types can be challenging; however, some cell type specific markers have been established for both (Gomez Perdiguero et al. 2015; Ginhoux et al. 2010; Haage et al. 2019). Furthermore, myeloid derived suppressor cells have been reported in meningiomas, at higher proportions in high grade tumors as compared to WHO grade 1 tumors (Pinton et al. 2018). These cells are known to have an immunosuppressive activity and promote tumor vascularization (Veglia, Sanseviero, and Gabrilovich 2021). In addition, they might facilitate immune escape of the tumor by enhancing PD-L1 expression. PD-L1 expression has been demonstrated to be increased in anaplastic meningioma (Du et al. 2015).

Overall, the presence or absence of certain immune cell types heavily influences the malignancy of the tumor. However, the composition and behavior of the meningioma TME is not extensively studied thus far.

WHO GRADING OF MENINGIOMAS

Meningiomas occur at WHO grades 1 to 3. Their grading has previously been purely based on histopathological evaluation, but in the most recent 2021 WHO classification also molecular markers have been introduced (Louis et al. 2021). Still, meningiomas are assigned an atypical subtype and thereby classified as WHO grade 2 if they either have a mitotic rate of four to 19 mitoses per mm^2, present with brain invasion, or display three of the five histological features defined as atypical by the WHO. These are: spontaneous intratumoral necrosis, high cellularity, prominent nucleoli, a low cytoplasm to nucleus ratio, and a pattern-less or sheeted architecture

(Louis et al. 2021). Meningiomas of a chordoid and clear cell subtypes are also assigned as WHO grade 2. Anaplastic meningiomas, which are classified as WHO grade 3, are defined by their high mitotic rate of more than 20 mitoses per mm^2, or alternatively frank anaplasia that is linked to a loss of the meningothelial differentiation. In addition, two genetic alterations have been included in the 2021 WHO classification as indicative of WHO grade 3 tumors: A homozygous deletion of *CDKN2A/B*, and *TERT* promoter mutations (Louis et al. 2021).

Besides that, some genetic characteristics are frequently associated with malignancy, although they are not decisive for tumor grading. *NF2*-mutated meningiomas for example are more often classified as WHO grade 2 or 3. Furthermore, a loss of H3K27 trimethylation also points towards an increased risk of recurrence and more aggressive behavior (Katz et al. 2018; Behling et al. 2021; Nassiri, Wang, et al. 2021; Torp, Solheim, and Skjulsvik 2022).

The majority of all meningiomas, namely 80 %, are assigned as WHO grade 1 (Ostrom et al. 2021). The ten-year overall survival rate for these tumors after resection is with around 83.7 % quite high (Ogasawara, Philbrick, and Adamson 2021). This rate is decreased to 53 % for WHO grade 2 meningiomas, which make up 18.3 % of all cases. The by far smallest proportion are WHO grade 3 meningiomas with 1.6 % (Ostrom et al. 2021). These tumors usually have a poor prognosis and five-year overall survival rate of 0 % (Ogasawara, Philbrick, and Adamson 2021).

As histopathological evaluation for grading is nonetheless prone to sampling error as well as to some degree subjectiveness of the pathologist, the WHO grading has recently been further refined through epigenetic profiling. The existing classification systems based on the meningioma methylome are described in detail in the following section.

1.2. Molecular grading systems for meningioma

Heidelberg Methylation Classifier

At the University Hospital Heidelberg, a classification system for meningiomas was derived based on unsupervised clustering of meningioma epigenomic profiles. It distinguishes six so-called methylation classes (MCs). These comprise three benign classes, MCs ben-1, ben-2, and ben-3, with usually good prognosis, one malignant class, MC mal, characterized by aggressive growth and high risk of recurrence, and two intermediate classes, MC int-A and int-B, with an intermediate outcome (Sahm et al. 2017). Apart from their epigenetic profile tumors of the same MC tend to share other characteristics regarding mutations, CNVs, as well as the anatomic location at which they typically present. *NF2* mutations and a deletion of chromosome 22q for example are frequently observed in ben-1, int-A/B, and mal tumor, but mostly absent in MCs ben-2. MC ben-3 tumors in turn more often harbor chromosomal gains than other tumors, such as a gain in

chromosome 5 (Sahm et al. 2017; Maas et al. 2021). Overall, chromosomal changes accumulate with increasing malignancy.

This classification system has been demonstrated to be superior in risk stratification to the conventional 2016 WHO grading and is thus now considered in the most recent 2021 WHO grading (Sahm et al. 2017; Louis et al. 2021).

UCSF Methylation Classifier

With a similar background, the University of California San Francisco (UCSF) has derived another classification system based on the clustering of meningioma methylation profiles (Choudhury, Magill, et al. 2022). This classification only discriminates three meningioma subgroups, however: Merlin-intact, immune-enriched, and hypermitotic meningiomas. Merlin-intact tumors are here characterized by a copy number neutral state of chromosome 22q as well as an intact *NF2* gene locus and the expression of *NF2*. Moreover, they often harbor gains of chromosome 5 and a loss of chromosome 6p (Choudhury, Magill, et al. 2022). Most cases in the Merlin-intact subgroup (81 %) are classified as grade 1 through WHO grading. Immune-enriched meningiomas usually follow a benign course as well, with 75 % being classified as WHO grade 1. While those tumors usually present with a chromosome 22q deletion, they are characterized by an elevated HLA gene expression, often with chromosomal gains on chromosome 6p, which harbors the HLA gene locus, and a hypomethylation of the HLA as well as lymphatic gene loci (Choudhury, Magill, et al. 2022). The hypermitotic subgroup was the most aggressive type, with only 43 % of tumors being assigned to WHO grade 1. Meningiomas of this subgroup harbored the most CNVs, most frequently chromosomal losses on 22q, 1p, 6p, and 9p, as well as chromosomal gains on 1q. They also displayed an elevated *FOXM1* expression and a hypermethylation of the *CDKN2A/B* gene locus (Choudhury, Magill, et al. 2022).

Toronto Methylation Classifier

A third classification system was developed by the University of Toronto (Nassiri, Liu, et al. 2021). This system however does not only consider the epigenomic profile, but also CNVs as well as the transcriptome for identification of subgroups. It separates four subgroups: immunogenic, *NF2* wild type, hypermetabolic, and proliferative meningiomas. While the immunogenic subgroup mostly contained benign meningiomas, high grade meningiomas were enriched in the hypermetabolic and proliferative subgroup, of which the proliferative displayed the most unfavorable clinical course, and both of which accumulated CNVs and mutations in oncogenic driver genes (Nassiri, Liu, et al. 2021). *NF2* wild type meningiomas on the other hand displayed virtually no chromosomal deletions and, as the name suggests, rarely harbored mutations in the

NF2 gene. Instead, frequently mutated genes in this subtype were *TRAF7*, *AKT1*, *KLF4*, and *POL2RA*. If none of these mutations were present, usually chromosomal gains, for example on chromosome 4, 12, 13, 17, or 20 could be observed (Nassiri, Liu, et al. 2021). Immunogenic meningiomas mostly exhibited flat CNV profiles, apart from chromosome 22q deletions. The subgroups also differed in their gene expression profiles, with genes connected to immune-related pathways being enriched in the immunogenic subgroup, and angiogenesis-related genes enriched in the *NF2* wild type subgroup. The hypermetabolic and proliferative subgroup displayed elevated expression levels of genes related to the cell metabolism and the cell cycle, respectively (Nassiri, Liu, et al. 2021).

Comparison of existing methylation classification systems

Interestingly, all the three methylation classifiers described above identify a different set of subgroups, even though they are all based on unsupervised clustering of meningioma epigenomic profiles. The Heidelberg classifier defines six groups, while UCSF and Toronto distinguish three and four groups, respectively. Nonetheless, some similarities between the three systems can be observed. All the classifiers for example identify a subgroup of tumors that harbors no loss of the *NF2* gene, namely the Merlin-intact tumors in the UCSF classifier, the *NF2*-wild type for Toronto, and MC ben-2 meningiomas in the Heidelberg classifier (Sahm et al. 2017; Choudhury, Magill, et al. 2022; Nassiri, Liu, et al. 2021). MCs ben-2 and ben-3, which also have comparatively few *NF2* alterations, hereby differ in the Heidelberg classification system by the CNV profile, which is virtually flat in ben-2 and enriched for chromosomal gains in ben-3; an observation that was also made within the Toronto *NF2*-wild type group. In addition, the UCSF immune-enriched and the Toronto immunogenic subgroup share their enrichment in immune-related processes and the beneficial prognosis. The UCSF hypermitotic subgroup, the Toronto hypermetabolic and proliferative subgroups, and the Heidelberg MC mal all share the accumulation of CNVs and mutations as well as the aggressive behavior. A recent publication has even demonstrated that the hypermetabolic and proliferative subgroup in the Toronto system can indeed be regarded as a further subgrouping of the UCSF hypermitotic subgroup (Choudhury, Chen, et al. 2022). This leaves the two intermediate subgroups, MCs int-A and int-B, of the Heidelberg classifier without immediate counterpart, which raises the question whether these add prognostic value in comparison to the other two systems. So far however, little is known regarding the molecular subgroups in terms of cellular composition, tumor microenvironmental changes, and the regulatory mechanisms leading up to tumor progression.

1.3. Single cell and spatial transcriptomics

Benefits of single cell transcriptomics

The classification and characterization of the above-named subgroups of meningioma relies mostly on epigenomic and transcriptomic data obtained from bulk. While this can identify global differences between tumors, it is often difficult to impossible to distinguish whether observed changes originate from the tumor cells themselves or from the infiltrating cell populations, or whether they may be due to changes in the composition of cell types. Investigating tissue on a cellular level overcomes these difficulties. Due to that, single cell sequencing methods have gained importance in the last years, and the range of available technologies is growing. They enable the identification of the cell types present in a tissue as well as their proportions and allow a comparison of certain cell populations between conditions. Increasing throughput and decreasing costs for single cell sequencing experiments allow for broader application of these methods.

Single cell RNA-Sequencing methods

Methodologies for single-cell RNA-Sequencing (scRNA-Seq) can in general be well-based, e.g. Smart-Seq2, or droplet-based, e.g. 10X Chromium. For well-based approaches, cells are first sorted into individual wells. Here, cells are lysed, mRNA is reverse transcribed to cDNA and amplified, and sequencing adapters are added before pooling the wells for sequencing (Picelli et al. 2014). The usage of well plates limits however the throughput to a few hundred cells. While this may already be a good number of cells, it is often not enough to recapitulate the full diversity of cell types and subtypes. The droplet-based Chromium device from 10X Genomics overcomes this limitation by enabling the simultaneous profiling of thousands of cells, making it one of the most widely applied technologies. This methodology is based on microfluidics, through which the cells are placed into individual gel beads, each of them containing barcoded primers and enzymes which allows capturing and barcoding of the RNA molecules of each single cell (**Figure 3**). Afterwards, they can be pooled for generation of sequencing libraries. While the throughput in terms of cell numbers for this method is much higher compared to the well-based Smart-Seq2 protocol, it identifies less transcript per cell and has a higher dropout rate, meaning genes for which no expression could be detected due to technical issues (X. Wang et al. 2021). In addition, the 10X protocol requires the Chromium device, whereas Smart-Seq2 runs without any specific devices. Still, the better coverage of cells with the 10X Chromium allows for the detection of rare cell populations, aside from providing a larger sample size. Thus, the choice of method always must be made based on the aim of the study.

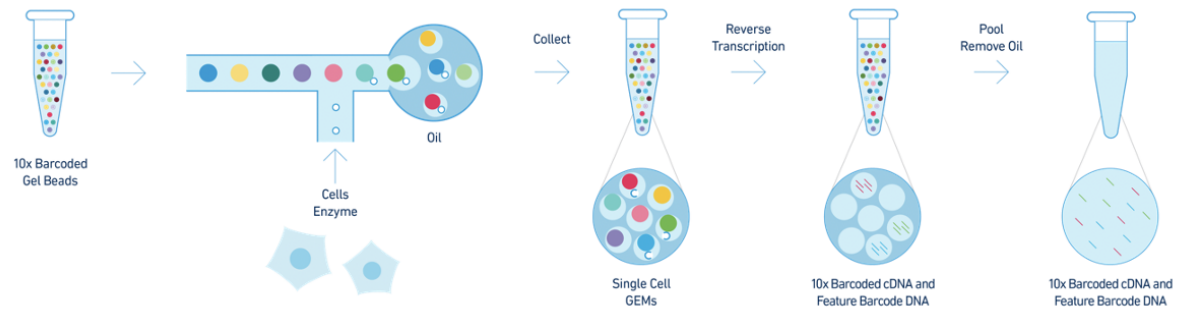

Figure 3. *Droplet-based scRNA-Seq approach using the 10X Chromium platform. [Taken from 10X Genomics.]*

Benefits of spatial transcriptomics

Single cell sequencing methods allow for a characterization of cellular types and subtypes present within a sample. They do not, however, permit any predictions where in the tissue these cell populations are located, as samples need to be dissociated into single cell suspensions. Nonetheless, this information can be important, as the tissue architecture is known to strongly influence biological function, and one can infer interacting cell populations based on their neighborhood as well as cellular niches. Spatial transcriptomics enable these kinds of investigations by placing the detected RNA expression at its respective location within the tissue.

Spatial transcriptomics methods

Broadly, methods for investigating transcriptomics on spatial level can be separated into next-generation sequencing (NGS) based methods, and imaging-based methods (Rao et al. 2021). However, also methods that leverage aspects of both exist. Imaging-based methods either rely on *in-situ* hybridization (ISH), where a complementary probe with a fluorescent marker aligns to RNA molecules in the tissue which can subsequently be imaged (**Figure 4**c), or they rely on *in-situ* sequencing (ISS). For the latter, the RNA is captured with targeted so-called padlock probes, which are amplified through a rolling circle amplification. This attaches a specific barcode sequence to the RNA molecule which can then be decoded sequentially using fluorescently labeled oligonucleotides (**Figure 4**b). Both ISH and ISS thereby require a pre-selection of the probes and thus the RNA molecules to be queried, making them targeted approaches. NGS-based methods, on the other hand, are unbiased as they capture all polyadenylated RNA. They are based on oligo-coated slides, where each oligo sequence encodes a specific spot of a certain diameter on the slide. Tissue is placed on the slide and lysed, whereby the mRNA anneals to the primers on the slide and the barcode is ligated in the subsequent reverse transcription and cDNA generation. The barcoded cDNA is then basis for sequencing library generation (**Figure 4**a). A commercial application of this technique is the Visium platform (10X Genomics). While this approach can be applied without

prior feature selection, its resolution is limited by the size of the spots. In the case of Visium, spots have a diameter of 55 µm, which is of course well beyond the size of most cells, rendering spatial profiling at single cell resolution impossible. The resolution of imaging-based methods is much better, allowing even for subcellular localization. However, NGS-based methods are still rapidly improving in resolution. Another disadvantage of NGS-based methods is their low sensitivity. Image-based methods have a much higher detection efficiency, especially ISH can detect lowly expressed RNA molecules with high sensitivity. Nonetheless, NGS-based methods are the method of choice for an unbiased approach without feature selection and are often easier to apply due to the availability of commercial solutions.

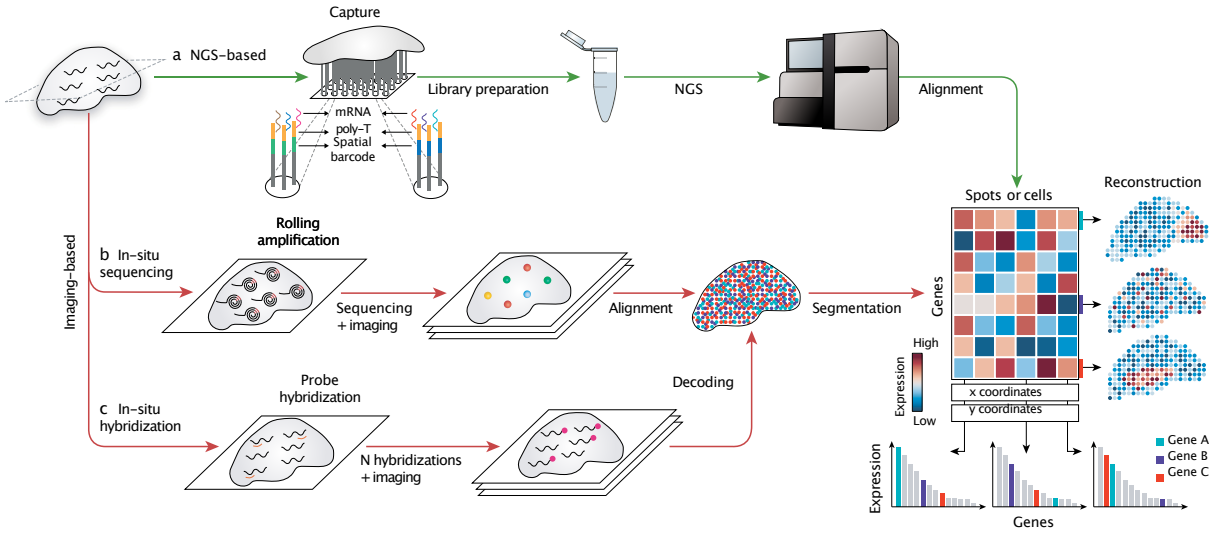

Figure 4. *Available spatial transcriptomics approaches. [Taken with permissions from* Rao et al. 2021.*]*

1.4. Aim

As molecular classification is gaining increasing importance for meningioma and has recently been included in the 2021 CNS WHO classification, this thesis aims to further characterize the methylation classes that were previously established by the Heidelberg University Hospital and thus improve risk stratification for meningioma patients. While commonalities regarding the epigenome, CNV status, and mutational profile have been investigated between the individual MCs, nothing is known about the differences in cellular processes and regulatory mechanisms that might cause the differences in patient outcome. Here, I leveraged bulk transcriptomic and proteomic data to investigate whether the MCs that have been defined based on the level of the epigenome can be recapitulated on RNA and protein level. In addition, these data are basis for enrichment and pathway analyses to highlight the underlying features of each MC.

However, differences in tumor class might not be caused by global changes in the tumor cell population. It is more likely that changes are gradual, and a single tumor might comprise tumor cell subpopulations at different stages of progression, or with different tendencies towards progression. Thus, I investigated subpopulations of cells that are shared or distinct between tumor classes using meningioma scRNA-Seq data. Finding tumor cell subpopulations that are present across all stages of malignancy or ones exclusive to benign or malignant tumors, respectively, can give indications what cellular states might be responsible for tumor progression. The primary and recurrent tumor pairs from the same patient, that are also included in the data set, can facilitate this by allowing a direct comparison between the initial tumor and its recurrence. Subsequently, spatial transcriptomics data for a set of meningiomas allowed me to examine the location of cell subpopulations within the tumor tissue and their association with histological structures.

The scRNA-Seq data also enabled me to put known molecular risk factors into perspective on single cell level. The *CDNK2A/B* gene locus for example is often deleted in high grade meningioma (Sievers et al. 2020). However, it has not been investigated thus far whether this deletion occurs homogeneously across cells and whether regulatory mechanisms that facilitate the loss of this gene locus may be activated during meningioma progression. I not only probed the single cell transcriptomic data to investigate *CDKN2A* expression and its potential heterogeneity on single cell level, but also leveraged single-cell ATAC-Sequencing (scATAC-Seq) data that was additionally obtained for *CDKN2A/B* homozygous deleted and non-deleted cases to examine the differences in chromatin status. Similarly, *FOXM1* expression, which is a known risk factor for high-grade meningiomas (Louis et al. 2021), has not been explored on single cell level. Here, I assessed in the scRNA-Seq data whether the expression of this genes is indeed upregulated in tumor cells and whether this is a global change or only caused by a specific cell subpopulation.

In addition, I leveraged the single cell transcriptomic data to closer investigate the endothelial structures of meningiomas with an angiomatous subtype. A high amount of vascularization is characteristic for this histological subgroup. However, it has not been conclusively determined whether these blood vessels are formed by endothelial cells infiltrating the tumor based on angiogenic signals, or whether the vessels are in fact formed by tumor cells. The question is addressed in this thesis by examining vascular markers as well as copy number changes in the individual cell populations of these tumors.

Since not only tumor cells are captured by the scRNA-Seq data but also the range of infiltrating cell populations, I subsequently aimed to define the cell types typically present in meningiomas and the changes in immune cell populations that can be observed between low- and high-grade tumors, including tumor associated macrophages and lymphocytes. The query of spatial transcriptomic data allowed inferences on the colocation of immune and tumor cells as well as the association of immune cells and immune cell subtypes with histological features. Thereby,

information on the tumor microenvironment can be appended to the epigenetic classification system. This is of especial interest as two of the alternative methylation classification systems, the UCSF and the Toronto classifier, both identify a benign subgroup that is enriched for immune signatures (Choudhury, Magill, et al. 2022; Nassiri, Liu, et al. 2021).

Altogether, in this thesis I aimed to consolidate the added value of molecular classification for meningiomas to the conventional WHO grading and the consistency of epigenomic classes on transcriptomic and proteomic level. A special focus was thereby on the infiltrating non-tumor cell populations that will not only affect any results on bulk level, but also strongly interact with the tumor cell populations. The gathered information will be valuable for understanding the meningioma TME, the molecular mechanisms of progression in meningiomas, and thereby the identification of molecular markers for risk prediction.

II. Material & Methods

2.1. Materials

This section gives on overview on the datasets used for my analyses and how they were derived. This part has not been performed by me but by colleagues in the wet lab, especially thanks to Helin Dogan and Michael Ritter.

Bulk RNA-Seq data

Bulk RNA-Seq data was obtained by Helin Dogan and lab technicians as described in Stichel et al. 2019. In short, the TruSeq RNA Library Prep for Enrichment kit (Illumina) was used to generate libraries from formalin-fixed, paraffin-embedded (FFPE) tissue. Paired-end reads with a length of 75 bp were sequenced using a NextSeq 500 device (Illumina). By applying the in-house pipeline for the processing of RNA-Seq data, adapters were trimmed, reads were aligned to the human genome (GRCh37) with the STAR aligner (Dobin et al. 2013), and subsequently quantified using RSEM (Li and Dewey 2011). The thus generated count matrices were basis for all further analysis performed by me as described in the methods section.

Proteomics & phosphoproteomics data

Generation of proteomics and phosphoproteomics data was generated from FFPE tissue samples by Lisa Schweizer and Sophia Doll at the Max Planck Institute of Biochemistry, Martinsried, according to the previously described workflow (Coscia et al. 2020). After enrichment for phosphorylated peptides, liquid chromatography – mass spectrometry measurements were performed, and mass spectrometry data was acquired in either data-independent mode or data-dependent mode. The data were further processed by combining the SpectronoutTM and the SprectromineTM software. MaxQuant was used for analysis of phosphoproteomic data. Counts matrices were further processed by me as described in the methods section.

Single nuclei RNA-Seq data

Single nuclei RNA-Seq data was obtained in two batches, between which the nuclei isolation protocol underwent some optimization. They are described separately in the following.

Batch 1 – original nuclei isolation protocol

Single nuclei isolation and library preparation for this batch were conducted by Laura Dörner and Lea Hofmann. To this end, 20 to 30 mg of tissue were mechanically broken up using a scalpel under addition of lysis buffer. The suspension was transferred to a Douncer and further lysed by eight strokes each with two types of pestles. The lysate was subsequently filtered and washed. After resuspension of the nuclear pellet, a nuclei suspension was obtained that was basis for single nuclei library preparation.

Batch 2 – optimized nuclei isolation protocol

Single nuclei suspensions were obtained from frozen tumor and library preparation for this batch was performed by Helin Dogan. Therefore, 150 µm tissue sections of 10 mg are lysed in lysis buffer and suspended by repeated pipetting. The suspension was transferred to a Douncer and further lysed by 15 strokes each with two types of pestles. The lysate was subsequently filtered and washed. Nuclei concentration was adjusted to 450 nuclei per µl for library preparation.

Library preparation

Single nuclei RNA-seq libraries were obtained from nuclei suspensions using the Chromium Next GEM Single Cell 3' Reagent Kits v2 (10X Genomics). Sequencing was performed on a NovaSeq 6000 (Illumina).

Single nuclei combined RNA- & ATAC-Seq data

Single nuclei isolation and library preparation for combined RNA- and ATAC-Seq was performed by Helin Dogan. Nuclei isolation was performed as for single nuclei RNA-Seq in Batch 2; however, nuclei concentration was adjusted to only 225 nuclei per µl. Library preparation for RNA- and ATAC-Seq was conducted according to the Chromium Next GEM Single Cell Multiome ATAC + Gene Expression Reagent Kits User Guide (10X Genomics). Sequencing was performed on a NovaSeq 6000 (Illumina).

Spatial transcriptomics data

Spatial transcriptomics data acquisition was performed by Michael Ritter. Sample preparation was carried out as described in the Visium Spatial Gene Expression Reagent Kits User Guide (10X Genomics). In short, 10 µm thick fresh frozen tissue slices were placed on the capture frame of a Visium spatial expression slide and stained with hematoxylin and eosin (H&E) after fixation with Methanol. The slides were imaged on an Aperio AT2 Slide Scanner (Biosystems Switzerland AG). After imaging, the RNA was released, and the cDNA synthesized. The released

cDNA was then used for library generation. Sequencing was performed on a NextSeq 500 (Illumina) with 28 bp for Read 1 and 90 bp for Read 2.

Methylation array data

Methylation data were generated from frozen tissue by lab technicians using the Illumina HumanMethylation450 (450k) array platform (Illumina) as previously described (Capper et al. 2018). DNA methylation status of 10,000 CpG sites was analyzed on the current version v12b4 of the MNP Classifier (www.molecularneuropathology.org) to determine the MC of each sample.

Immunohistochemistry

Immunohistochemistry was performed by Helin Dogan on a BenchMark XT immunostainer and on a BenchMark Ultra immunostainer (Ventana Medical Systems). Dilutions and antibody details are provided in **Supplementary Table 1**. Slides were scanned on an Aperio AT2 Slide Scanner (Biosystems Switzerland AG).

2.2. Methods

All further analyses described here were performed by me.

Analysis of bulk RNA-Seq data

Expected counts obtained from bulk RNA-Seq as described above were further analyzed in R v.4.2.0 using DESeq2 v.1.36.0 (Love, Huber, and Anders 2014). Genes with a total count of less than ten across all samples were excluded from analysis. Size factors and dispersion were estimated for each sample, a negative binominal generalized linear model was fitted, and Wald statistics calculated (*DESeq()*) with the tumor MC included as variable in the design for later differential expression (DE) analysis. P-values and fold changes were calculated always comparing one MC against all other MCs (*results()*). P-values were adjusted for multiple testing through Benjamini-Hochberg (*pAdjustMethod = "BH"*).

Cell type deconvolution from bulk RNA-Seq

The enrichment of infiltrating cells, including immune and stromal cells, was predicted from bulk RNA-Seq data using the xCell R package (Aran 2020). xCell's intrinsic dataset containing 64

human stroma and immune cells was used as reference. Bulk gene expression levels were ranked per sample. Gene set enrichment analysis was performed on the ranked expression for cell type-specific signatures, with each cell type being represented by several signatures, and scores for signatures of each cell type were averaged (*rawEnrichmentAnalysis()*). The thus obtained enrichment scores were transformed to a linear scale to resemble percentages (*transformScores()*). Finally, a compensation by spill-over was performed on the scores to account for dependencies between the scores of cell types that are closely related (*spillOver()*).

Pathway analyses for bulk RNA-Seq and proteomics

Pathway enrichment analyses were performed via Ingenuity Pathway Analysis (IPA), a web-based software application (QIAGEN Inc., https://www.qiagenbioinformatics.com/products/ingenuity-pathway-analysis), based on all differentially expressed genes with an adjusted p-value smaller than 0.05 and for RNA-Seq data additionally with a log fold change of at least one.

Similarity network fusion analysis

For similarity network fusion (SNF) analysis, Euclidean distances were calculated individually in the proteomics count data and the variance stabilizing transformed RNA-Seq count data between each sample pair. In a secondary SNF analysis, this was analogously performed for the phosphoproteomics count data. For each of the thus obtained distance matrices an affinity matrix was generated (*affinityMatrix()*) using the R package SNFtool v.2.3.1 (B. Wang et al. 2018), with the number of nearest neighbors set to ten (*K = 10*) and the variance of the local model to 0.5 (*sigma = 0.5*). The affinity matrices were then used as input for construction of a consensus network (*SNF()*), with the number of nearest neighbors set to ten (*K = 10*) and ten iterations for the diffusion process (*t = 10*). For the secondary SNF analysis that included the phosphoproteome data, the number of nearest neighbors for affinity matrix generation and consensus network construction was set to three (*K = 3*) due to the limited number of phosphoproteomics samples.

Kinase perturbation analysis from phosphoproteome

Kinase activities were inferred from the phosphorylation status of their respective target proteins using the KSEApp R package (Wiredja 2017) using KSEA's integrated kinase-substrate database (2016). First, fold changes in the phosphorylation status and matching p-values for each phosphorylation site were calculated comparing each MC against the remaining MCs. These served then as input for calculating KSEA kinase scores in each comparison individually as Z scores, and p-values as statistical assessment of the Z scores for all kinases with at least one

identified substrate (*KSEA.Scores()*). P-values were adjusted for multiple testing by applying the Benjamini-Hochberg method.

SINGLE NUCLEI RNA-SEQ DATA ANALYSIS

Sequencing data from the Illumina runs was converted into FASTQ format using Cell Ranger v.6.1 (10X Genomics) in *cellranger mkfastq* mode with default parameters. Alignment to the human genome (GRCh38) and read counting were performed in *cellranger count* mode (Cell Ranger v.6.1, 10X Genomics) with default parameters. All further analysis was conducted in R v.4.2.0 with the Seurat package v.4.0.0 (Hao et al. 2021) unless otherwise specified. At this, I removed cells with less than 200 detected features or a median absolute deviation of more than three times in their detected features for analysis. Similarly, I filtered out cells with a percentage of mitochondrial genes three times higher than the median value across all cells. Doublets were subsequently removed using the DoubletFinder R package v.2.0.3 (McGinnis, Murrow, and Gartner 2019). To this end, the number of principal components (PCs) was set to 15 (*PCs = 15*), the number of artificial doublets to 0.25 (*pN = 0.25*), and the number of expected doublets (*nExp*) was calculated as the number of cells in the sample times 0.8 divided by 100,000, as suggested as expected doublet rate by 10X Genomics. The PC neighborhood size (*pK*) was determined using the *paramSweep_v3()*-function. In Seurat, PCA dimensionality reduction was performed (*RunPCA()*) on the 2,000 most variable features and nearest neighbors were computed (*FindNeighbors()*) on the first 20 PCs. Clusters of cells were identified based on the shared nearest neighbors (*FindClusters()*) with a resolution of 0.6. Uniform Manifold Approximation and Projection (UMAP) reduction was performed on the first 20 PCs (*RunUMAP()*).

Cell type annotation

For the annotation of cell types, I leveraged several sources of information. This included the Human Primary Cell Atlas (Mabbott et al. 2013), which served as reference for automized cell type annotation with the R package SingleR v.1.10.0 (Aran et al. 2019). Thereby obtained annotations were validated by examination of cell type specific marker genes as listed in PanglaoDB (Franzén, Gan, and Björkegren 2019). The annotation of presumed neoplastic cells was in the following validated by presence of copy number alterations.

CNV calling from single cell expression profiles

CNV profiles were estimated using the InferCNV R package v.1.12.0 (Tickle et al. 2019). Non-malignant cells were hereby used as a reference. The size of the sliding window across which gene

expression was averaged was set to 201 neighboring genes (*window_size = 201*). The obtained expression matrix was then median filtered across 15 neighboring genes (*window_size = 15*).

Batch effect correction

As the scRNA-Seq data was obtained in two rounds by different people and with considerable lag of time and modifications to the nuclei isolation protocol, I performed batch correction between these two batches as well as between samples using the Harmony R package (Korsunsky et al. 2019). Parameters were empirically chosen based on their ability to cluster cell types across samples. For correction between the first and second round of data acquisition, parameters were set to $\lambda = 10$ and $\theta = 0.1$, and for correction between samples to $\lambda = 1$ and $\theta = 2$.

Differential expression analysis

A differential expression (DE) analysis was applied using the Libra R package v.1.7 (Squair et al. 2021) to compare cell populations of interest (tumor cells and macrophages, respectively) across tumor classes. In this approach I chose Libra's edgeR-LRT pseudobulk method. To this end, counts from cells of the same type and sample are summarized into a "pseudobulk", for which differentially expressed genes are calculated as for bulk transcriptomic data, applying a likelihood ratio test with edgeR (Robinson, McCarthy, and Smyth 2010). Comparisons were always made between one MC and all other MCs. Thereby obtained differentially expressed genes were basis for further pathway enrichment analyses.

Specifically, enrichR (Kuleshov et al. 2016) was applied for comparison of enriched Molecular Signature Database hallmark gene sets (Liberzon et al. 2015) in the neoplastic cell populations between tumor classes. Thereby, genes with a fold change with a log base 2 of at least one ($log2FC > 1$) and with an adjusted p-value smaller than 0.05 were considered differentially expressed and supplied as input to enrichR.

Macrophage populations were only queried for Reactome pathways (Gillespie et al. 2022) pertaining interleukin signaling pathways. Their enrichment was determined through hypergeometric testing based on the genes participating in the respective pathways on one side, and the genes differentially expressed for the respective tumor class ($log2FC > 1$, adjusted p-value < 0.05) on the other side.

Inference of transcription factor activities

Activities of transcription factors were inferred from the expression levels of their respective target genes using the DoRothEA R package v.1.8.0 (Garcia-Alonso et al. 2019). I used DoRothEA's internal database to determine transcription factor-target regulons, restricting the regulons to those annotated with confidence levels A, B, or C. These were basis for the virtual inference of

protein-activity by enriched regulon analysis using viper v.1.30.0 (Alvarez et al. 2016). Single cell signatures were thereby computed using the rank method (*method = "rank"*). Regulons were further restricted to those with a minimum of four targets (*minsize = 4*). The dataset was not limited to the genes represented in the interactome (*eset.filter = FALSE*).

Prediction of ligand-receptor interactions between cell types

Cell-cell interactions were predicted on an individual sample level based on the matched expression of a ligand in one cell population and the expression of its respective receptor in the other cell population using the LIANA R package v.0.1.5 (Dimitrov et al. 2022). This framework combines five methods for ligand-receptor interaction inference and the information from 16 databases of ligand-receptor interactions (*liana_wrap()*). Aggregate consensus ranks were calculated across methods (*liana_aggregate()*), denoting the significance of each interaction. SingleCellSignalR's LRscore was chosen to depict the magnitude of expression, i.e., the expression levels of ligand and receptor in the respective cell populations. Scores for each interaction were then averaged across samples, which served as final interaction scores.

Identification of tumor subpopulations with shared transcriptional programs

To identify shared signatures in the expression profiles of tumor cells across samples, I applied a non-negative matrix factorization (NMF) approach. First, NMF was performed on the tumor cell populations individually for each sample, which segregated the expression matrix into a coefficient and a factor matrix with a fixed number of factors as determined by the factorization rank. To this end, the expression data was centered and scaled across all cells of the respective sample. Then, NMF was performed using the NMF R package (Gaujoux and Seoighe 2010) with several factorization ranks in the range between two and four (*rank = 2:4*), with ten runs (*nrun = 10*), and using the Alternating Least Square approach (Hyunsoo Kim and Park 2007) (*method = "snmf/r"*). In the final analysis, a factorization rank of three was empirically chosen based on its ability to create unique clusters in a correlation of all thereby across samples obtained factors without too large of an overlap between clusters. For each of the three factors in every sample the top 30 genes contributing to the respective factor were selected as those genes with highest NMF scores. These genes were selected as gene signature specific for the respective factor. Each gene signature was then assigned a cell-wise score. Scoring was performed by first determining those 100 genes with smallest difference in mean expression to the respective signature genes across all cells. Then, the difference in expression of each signature gene to the mean expression of the 100 selected genes was calculated on a cellular level. Scores for all genes in the same signature were averaged. This average resembled the signature-specific score for each individual cell. The gene signatures of all samples were subsequently hierarchically clustered based on their cell-wise

signature scores. On this basis, six clusters of gene signatures with similar patterns of cell-wise signature scores were identified. The cell-wise scores of all signatures in the same cluster were averaged and cells assigned to one of the clusters based on their highest average score. To identify the gene signatures specific for each of the clusters, all genes contributing to any of the gene signatures summarized in the respective clusters were scored within all cells assigned to that cluster. Therefore, again those 100 genes with smallest difference in mean expression to the respective genes across all cells were determined and the difference in expression between the gene and the mean expression of the 100 selected genes calculated for each cell. Those 50 genes with the highest average scores across all cells from one cluster were selected as transcriptional signature specific to the respective cluster.

Analysis of combined RNA- and ATAC-Seq data for single nuclei

Sequencing data from the Illumina runs was converted into FASTQ format using Cell Ranger ARC v.2.0.0 (10X Genomics) in *cellranger-arc mkfastq* mode with default parameters. Alignment to the human genome (GRCh38), peak calling from ATAC, and read counting from RNA were performed in *cellranger-arc count* mode (Cell Ranger ARC v.2.0.0, 10X Genomics) with default parameters. All further analysis was conducted in R v.4.2.0 with Seurat v.4.0.0 (Hao et al. 2021) for the RNA assay and Signac v.1.9.0 (Stuart et al. 2021) for the ATAC assay unless otherwise specified. Cells with less than 1,000 or more than 100,000 ATAC peaks and with less than 1,000 or more than 25,000 UMIs in the RNA assay were filtered out. Cells with a transcription start site enrichment score of less than one were removed from the analysis as well. For the RNA assay, reads were normalized and scaled using regularized negative binominal regression (*SCTransform()*), PCA dimensionality reduction was performed (*RunPCA()*), and UMAP reduction calculated based on the first 50 PCs (*RunUMAP()*). The ATAC assay was normalized through frequency inverse document frequency normalization (*RunTFIDF()*). Subsequently, singular value decomposition was performed (*RunSVD()*) and UMAP reduction was calculated (*RunUMAP()*) based on latent semantic indexing (LSI) components two to 50 (*reduction = 'lsi'*). Both assays were combined in a weighted nearest neighbor graph that was calculated on the PCA reduction of the RNA assay and the LSI reduction of the ATAC assay (*FindMultiModalNeighbors()*). Another UMAP reduction was performed on the weighted nearest neighbor graph (*RunUMAP()*) and clusters were calculated based on shared nearest neighbors (*FindClusters()*) with a resolution of 0.5 from this combined graph. Cell type annotation as well as CNV calling was performed solely based on the RNA assay analogous to the description of the procedures for the scRNA-Seq data above. The ATAC assay was used to predict transcription factor activities based on the accessibility of their matching motifs using chromVAR v.1.18.0 (Schep et al. 2017) with default parameters (*RunChromVAR()*).

SPATIAL TRANSCRIPTOMICS DATA ANALYSIS

The Visium platform (10X Genomics) was utilized by Michael Ritter as described above to generate spatial sequencing data. For downstream analysis, I deployed the Space Ranger software v1.3.0 (10X Genomics) in *spaceranger mkfastq* mode to generate FASTQ files from the Illumina runs and subsequently in *spaceranger count* mode for alignment to the human genome (GRCh38) and counting. Any further analysis was performed in R using the Seurat package v.4.0.0 (Hao et al. 2021) unless otherwise specified. Spots with less than 500 UMIs were excluded from analysis. Normalization and variance stabilization were performed using regularized binominal regression (*SCTransform()*), correcting for the number of UMIs per spot (*vars.to.regress = "nCount_Spatial"*). PCA dimensionality reduction was applied using default parameters (*RunPCA()*), nearest neighbors were computed on the first 30 PCs (*FindNeighbors()*), and clusters of spots identified with a resolution of 0.5 (*FindClusters()*). UMAP reduction was performed on the first 30 PCs (*RunUMAP()*).

CNV calling from transcriptomic profiles of single spots

CNV profiles were inferred for each spot based on the expression data using the SPATA2 R package v0.1.0 (Ravi et al. 2022), which employs InferCNV (Tickle et al. 2019) for CNV calling. Specifically, I applied the *runCnvAnalysis()*-function with default parameters and using SPATA2's built-in reference of healthy human brain tissue.

Integration of Visium with scRNA-Seq data

To determine the cellular composition of each individual spot, transcriptomic signatures were decomposed using the scRNA-Seq dataset for reference. First, anchors between both data modalities were determined (*FindTransferAnchors()*). Then, enrichment of cell types was inferred for each spot in the spatial transcriptomic data (*TransferAnchors()*) based on the PCA dimensionality reduction and using the first 30 PCs for anchor weighting (*dims = 1:30*) through probabilistic transfer of the annotations (Stuart et al. 2019).

CELL TYPE DECONVOLUTION FROM EPIGENOME

Methylation data obtained from Illumina HumanMethylation450 (450k) array platform as described above was deconvoluted to predict the proportion of the infiltrating immune cell compartment using the Edec R package v.0.9 (Onuchic 2022). To this end, a set of methylation array data from macrophages, CD3+ T cells, endothelial cells, and fibroblasts (Dekkers 2019; Hassler et al. 2016; Lucero et al. 2020; Vizoso et al. 2015) served as cell type references. Loci were restricted to those that were most informative by selecting the 500 most hyper- or

hypomethylated loci (*run_edec_stage_0()*) with a p-value of less than 0.00001 (*max_p_val = 1e-5*) when comparing each reference cell type with the remaining reference cell types (*version = "one.vs.rest"*) in a t-test. Subsequently, the number of constituent cell types in the bulk methylation array samples was estimated (*estimate_stability()*) based on the informative loci by creating five random subsets of the samples (*num_subsets = 5*) and including 80 % of the data in each of these subsets (*subset_prop = 0.8*) with a maximum of 800 iterations (*max_its = 800*). Thereby an optimal number of three constituent cell types was obtained, which correlated to a population of immune cells including macrophages and T cells that could not be further discriminated, as well as two distinct populations of fibroblasts. The informative loci were further used to estimate the average methylation profile for each of the three constituent cell type and the respective proportion of the constituent cell types in the bulk methylation array samples (*run_edec_stage_1()*). The thus estimated proportion of the immune cell type was basis for further analysis.

Modelling of progression free survival

A Cox proportional hazard model with risk factors as covariates was generated to estimate the hazard ratio of the respective risk factors, in this case MC, WHO grade, and/or proportion of infiltrating immune cells for each sample using the survival R package v.3.3-1 (Therneau et al. 2022). The factor level with the lowest risk for each risk factor was chosen as the reference level. Cumulative prediction error (Brier score) curves were calculated and the integrated Brier score at ten years determined with the pec R package v.2022.05.04 (Mogensen, Ishwaran, and Gerds 2012).

Prediction of UCSF meningioma subtype from methylation array data

A linear support vector machine was trained according to the code and annotated training data with the UCSF meningioma subtypes "Merlin-intact", "immune-enriched", and "hypermitotic" as published by Choudhury *et al*. (Choudhury, Magill, et al. 2022). The Illumina MethylationEPIC (850k) array UCSF training data therefore had to be restricted to loci present in the Illumina HumanMethylation450 (450k) array that was obtained here. I then applied the linear support vector machine to the in-house methylation array data, generated as described above, and each sample was thus assigned to one of the three UCSF subtypes.

III. Results

3.1. Recapitulating epigenetic classes on transcriptomic and proteomic levels

The existing subgroups for meningioma that extend beyond the conventional WHO grading and have been demonstrated to be clinically relevant are derived solely from the epigenetic profile of the tumors (Sahm et al. 2017). Thus far, it has not been investigated in depth how the Heidelberg MCs correlate on levels downstream of the epigenome, specifically the transcriptome and the proteome. To characterize these previously established epigenetic meningioma subtypes at the transcriptional as well as proteomic level, RNA sequencing (RNA-Seq) and proteomics data were generated for a cohort of 44 meningioma samples covering WHO grades 1, 2, and 3, and MCs ben-1/2, and mal (**Figure 5**a). Proteomics data was available for all samples, RNA-Seq data for 40 of the 44 samples. For a subset of eight samples across WHO grades and MCs, phosphoproteomic data was additionally obtained.

Differential expression signatures on transcriptomic level

For comparison of the epigenetic subgroups on transcriptomic level, I applied a differential expression (DE) analysis. To this end, RNA-Seq data for samples of one MC were compared to all others and a pathway analysis was performed on all genes determined as differentially expressed in each of these comparisons. Thereby, MC-specific transcriptomic signatures could be observed. While genes related to the cell cycle were expressed at elevated levels in MC mal samples compared to MC ben-1/-2 samples, MC ben-1 tumors displayed a strong enrichment for pathways related to the immune system (**Figure 5**c). Interestingly, also a differential regulation pertaining neuronal related processes could be observed, albeit no neuronal cells are to be expected in meningioma tissue. Furthermore, differences in signaling pathway activities were detected. However, there seemed to be no association of a tumor class with the activity of any specific signaling pathway.

Differential expression signatures on proteomic level

As clear differences could be observed between meningioma MCs on transcriptomic level, I subsequently investigated whether these differences were preserved on proteomic level. On the level of single genes, the MCs did not share a large overlap in differentially regulated genes

between the RNA and protein datasets (**Figure 5**b). On pathway level however, MC ben-1 samples were indeed strongly enriched for immune-related pathways, similarly as observed on RNA level (**Figure 5**d). The elevated expression levels for cell cycle-related pathways on the other hand could not be observed in the proteome of MC mal to a similar extent as on transcriptomic level. Also signaling pathways were not consistently differentially regulated on RNA and protein level. Thus, even though parallels in the MC-specific pathway enrichment were detected between transcriptome and proteome, not all differences could be observed across both levels.

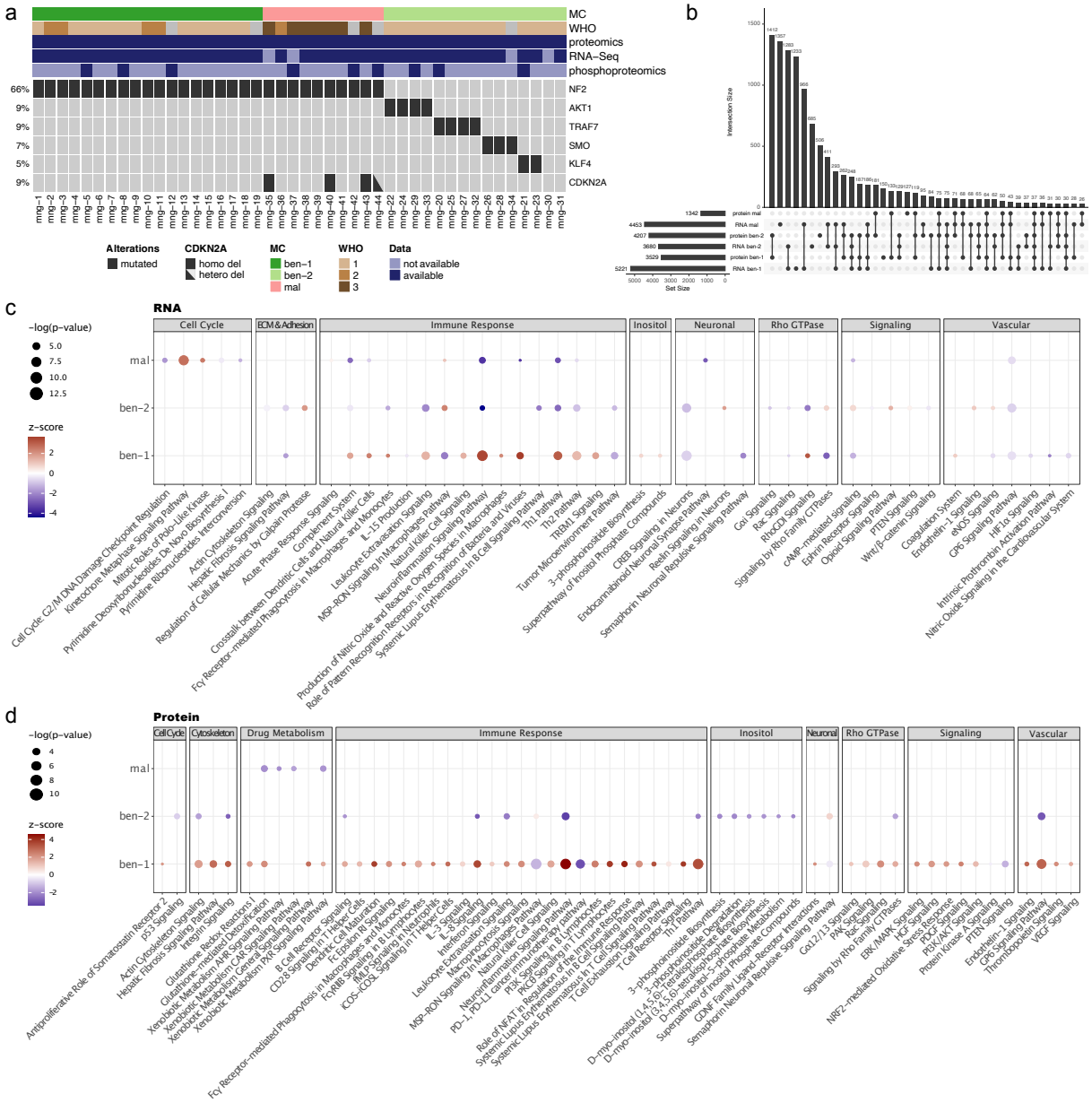

*Figure 5. **a** Meningioma samples included in the bulk transcriptome and proteome datasets and their mutational status. homo/hetero del … homozygous/heterozygous deletion. **b** Overlap in differentially expressed genes between transcriptomic and proteomic data and between MCs. **c** Differentially regulated pathways on transcriptomic level. **d** Differentially regulated pathways on proteomic level.*

Consistency of subgroups across transcriptomic and proteomic level

Given the differences in differentially regulated genes and pathways between RNA and protein level, I aimed to investigate whether a combination of both levels would be able to successfully separate MCs. To this end, I employed similarity network fusion (SNF) analysis which integrates data modalities by creating a weighted network for each data layer and encapsulating those in one joint network. In the combined SNF analysis for transcriptomic and proteomic data, the three MCs ben-1, ben-2, and mal clearly separated (**Figure 6**), even though according to the DE analysis only a fraction of genes was commonly differentially expressed between both layers (**Figure 5**b). An interconnection of samples across MCs was only observed for two pairs of samples, namely between the MC ben-1 tumor mng-14 and MC ben-2 tumor mng-25, and between MC ben-2 tumor mng-29 and MC mal tumor mng-36. Given the difference in the genetic background, these intersections with the MC ben-2 tumor class were unexpected. Nonetheless, all remaining connections were formed within the same MC, which highlights the consistency of epigenomic meningioma subgroups on transcriptomic and proteomic level.

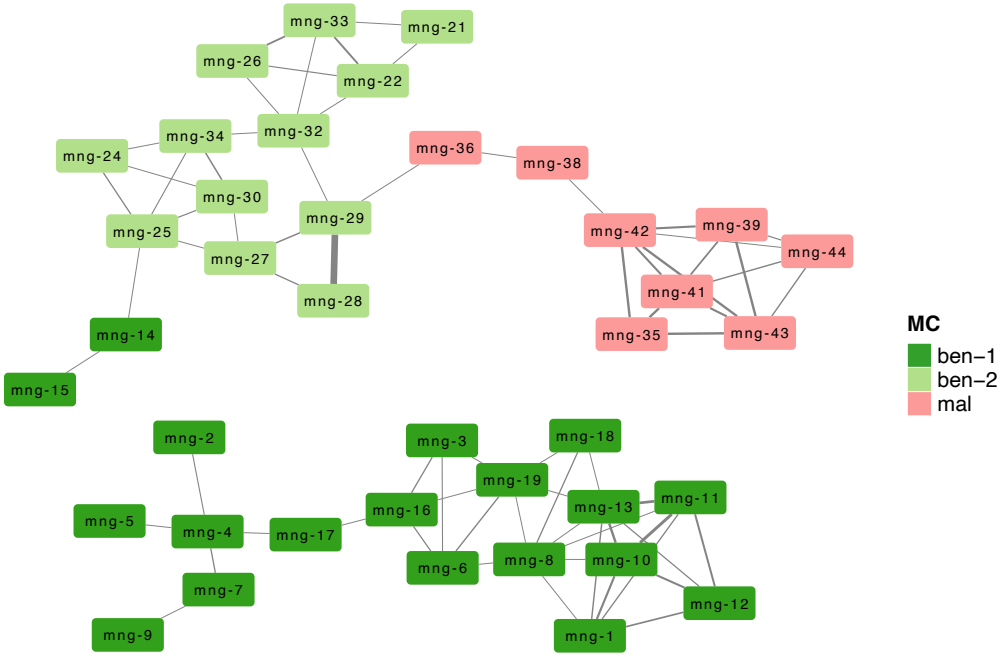

Figure 6. Similarity network fusion graph combining transcriptomic and proteomic data. Nodes represent samples, edges indicate similarity between samples. Edge widths are proportional to the extent of similarity.

Subclass-specific changes of the phosphoproteome

As activated pathways and processes are better understood by monitoring the phosphorylation status of proteins participating in these pathways than by examining their respective expression alone, I leveraged phosphoproteomic data for eight meningiomas to investigate the activities of regulatory signaling pathways, for which no clear patterns were found in the differential gene and protein expression analysis above. Kinase perturbation analysis infers

kinase activities based on the phosphorylation status of their respective targets. Employing it here, again comparing one MC against the remaining two, revealed an activation of MAPK kinases in MC ben-1 and ben-2 meningiomas, specifically of *MAPK1*/ERK2, *MAPK3*/ERK1, and *MAPK14*/p38α (**Figure 7**). *AKT1* kinase activity was in addition increased in MC ben-2 tumors. In MC mal meningiomas, on the other hand, kinases regulating the cell cycle, such as *CDK2* and *CDK7*, displayed elevated activities, in line with the elevated expression of cell cycle-related genes observed on RNA level.

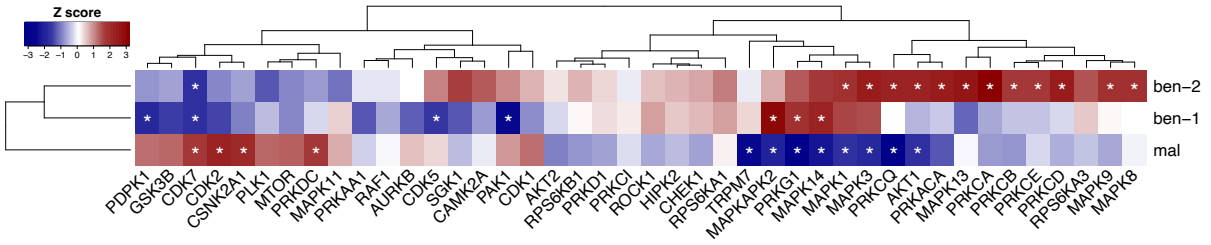

Figure 7. *Kinase activities as inferred from the phosphorylation status of their respective target proteins. Colors represent Z scores. Asterisks indicate significant differences in activation.*

Including the phosphoproteomic data in the SNF analysis revealed a consistent separation of the three MCs (**Supplementary Figure 1**). This further underlines the robustness of epigenetic subtypes not only on levels of gene and protein expression, but also protein regulation. Interestingly, the analysis suggests a closer interconnection between MC ben-2 and MC mal tumors and none between MC ben-1 and MC mal, despite the shared *NF2* loss and chromosome 22 deletion in both these MCs. However, the small sample size of the phosphoproteomic dataset certainly limits final conclusions.

3.2. Tumor cell populations on single cell level

While these data from bulk facilitate the understanding of general differences in the active processes between tumors, they do not allow for a further subdivision into processes related to certain cell populations. The observed enrichment for pathways related to the immune system that was observed in MC ben-1 tumors in the RNA-Seq and proteomics data above for example most likely originates not from the tumor cell population itself, but immune cells that may be infiltrating the tumor. To distinguish the exact source for such differential expression patterns is however impossible from bulk data. Hence, I leveraged single nuclei RNA-Seq data, for simplicity further referred to as single cell RNA-Seq (scRNA-Seq), to compare specifically the tumor cell population between meningioma subgroups. Not only does this permit the identification of expressional differences between stages of progression specific to the tumor cells, but it also allows for an identification of tumor cell subpopulations within the same tumor, and the comparison of their presence and phenotype across tumor stages.

Sample and cell type composition of the scRNA-Seq dataset

The scRNA-Seq dataset that was basis for the further analyses comprised 48 meningioma samples from 43 patients and 257,282 cells in total. The included tumors span all WHO grades 1 to 3 and all six MCs (**Figure 8**a, **Supplementary Table 2**). I integrated the data under removal of batch effects between the two batches in which the data was generated (see Methods) as well as between individual samples and subsequently annotated cells based on comparison to the human primary cell atlas (Mabbott et al. 2013) and the expression of cell type-specific marker genes. A joint clustering of all samples in a UMAP representation revealed five major clusters of different cell types: the largest cluster comprising neoplastic cells, and in addition four clusters of infiltrating cells, namely macrophages, endothelial cells, lymphocytes, and mast cells (**Figure 8**b). Annotation of neoplastic cells was confirmed based on alterations in the cellular CNV profile. CNV profiles inferred from single cell expression data greatly matched the respective CNV profiles obtained from bulk methylation array data. While tumor cells from MC mal meningiomas generally displayed the most copy number alterations, CNV profiles of MC ben-2 tumors were virtually flat (**Supplementary Figure 2**). This is in line with previous findings on MC-specific copy number changes (Sahm et al. 2017; Maas et al. 2021).

The neoplastic cells were isolated in the following for further analysis.

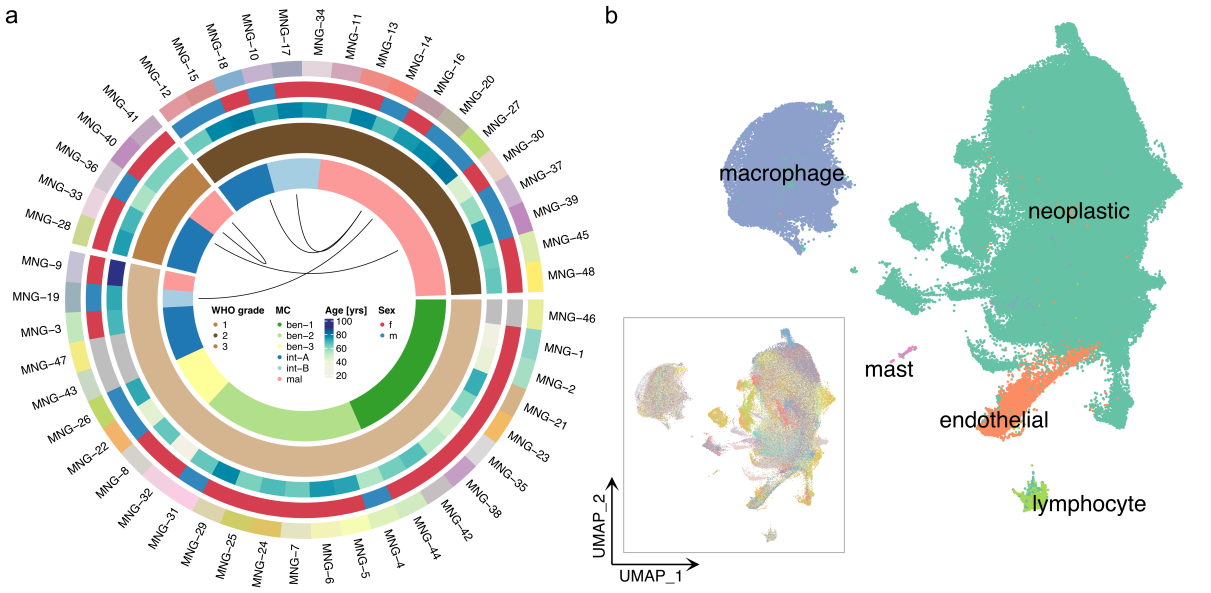

*Figure 8. **a** Meningioma samples included in the scRNA-Seq dataset and their respective WHO grades and MCs. Connecting lines indicate primary and recurrent sample pairs from the same patient. **b** UMAP representation of the integrated dataset with colors indicating cell type, and sample of origin for each cell in the inset, respectively.*

DIFFERENTIAL EXPRESSION ANALYSIS OF TUMOR CELL POPULATIONS

For identification of expressional patters specific for the tumor cell subset, I performed a DE analysis that compared the gene expression in neoplastic cells from samples of a respective MC with that in neoplastic cells from all other samples. To avoid the problem of pseudoreplication that arises from cells originating from the same tumor, I applied a pseudobulk approach. To this end, the expression of the tumor cells from the same sample is averaged and treated as a single sample, which can then be compared using conventional bulk DE methods (Squair et al. 2021). The greatest number of differentially expressed genes was identified in MC ben-2 meningiomas, followed by MC ben-3 tumors (**Supplementary Figure 3**), in line with the typical differences in their genetic background compared to other MCs (Sahm et al. 2017). Only a small number of genes was detected as differentially expressed in MC int-A and int-B meningiomas, possibly due to the lower number of samples for these classes or caused by similarities to MC mal that shares genetic features. Interestingly, many HOX genes showed an elevated expression in MC mal tumor cells (**Supplementary Figure 3**f), confirming previously discovered associations of an increase in HOX gene expression with malignancy (Paramasivam et al. 2019).

To gain a better understanding of the expressional signatures beyond individual genes, I performed a gene set enrichment analysis based on the Molecular Signatures Database hallmark gene set collection (Liberzon et al. 2015) on the differentially expressed genes for each MC. MC mal tumor cells showed an enrichment in genes related to the G2-M checkpoint and epithelial mesenchymal transition (**Figure 9**a), which is in line with histological observations of increased proliferation (**Figure 9**b) and a loss of growth patterns typical for meningiomas, the so-called sheeting architecture (**Figure 9**c) in these tumors, respectively. H&E tissue sections and immunohistochemistry shown here were obtained by colleagues in the lab. MC ben-3 tumor cells on the other hand displayed a signature of hypoxia (**Figure 9**a), which could possibly be correlated to the frequently observed angiomatous subtype in this class. On the other hand, MC ben-1 tumor cells reflected the strong involvement of the immune system as observed on bulk level in the enrichment for immune-related pathways such as inflammatory response, which was also enriched in MC mal tumor cells, and additionally interferon gamma response and TNF-alpha signaling via NF-kB. TNF-alpha is often produced by macrophages; however, it was not detectable in the scRNA-Seq data.

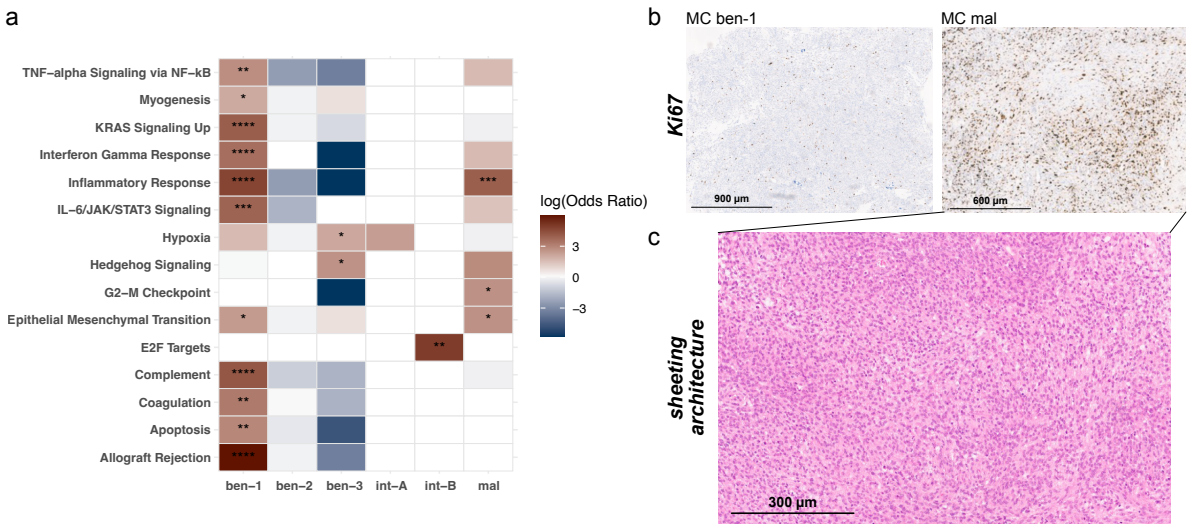

Figure 9. a *Differentially regulated hallmark gene sets for each MC. Red color indicates upregulation of the pathway in the respective MC (odds ratio > 1), blue indicates downregulation (odds ratio < 1). Asterisks indicate significant p-values. **** … p < 0.0001, *** … p < 0.001, ** … p < 0.01, * … p < 0.05.* ***b*** *Immunohistochemistry for the proliferation marker Ki67 for an MC ben-1 meningioma (left) and an MC mal meningioma (right).* ***c*** *H&E staining of the MC mal meningioma from (b) displaying its sheeting architecture. H&E and immunohistochemistry sections (b,c) were obtained by colleagues in the lab.*

TUMOR CELL SPECIFIC BEHAVIOR OF MENINGIOMA RISK FACTORS

CDKN2A expression and deletion in high grade meningiomas

Besides the more general pathway patterns that I have here identified to be linked to meningioma subtypes, the expression of some genes has already been associated with malignancy in meningiomas. It has for example been observed that *CDKN2A/B* homozygous deletion is associated with aggressive meningioma and has been included as diagnostic marker in the recent WHO classification (Sievers et al. 2020; Louis et al. 2021). Interestingly however, non-homozygous deleted high-grade tumors display an increased expression of the *CDKN2A* gene and its gene product p16 compared to low-grade tumors on both transcriptomic and proteomic level in the bulk datasets here (**Figure 10**a). However, whether the high *CDKN2A* expression is caused by neoplastic cells or infiltrating non-tumor cells could not be determined from bulk data. Investigating this in the scRNA-Seq dataset revealed that neoplastic cells from non-homozygous deleted MC mal cases displayed increased expression levels compared to neoplastic cells from low grade cases (**Figure 10**b). This indicates that *CDKN2A* is indeed expressed specifically in tumor cells.

It could be hypothesized that the frequent *CDKN2A/B* homozygous deletion in high-grade meningioma is preceded by an especial “openness” in chromatin structure at that locus which causes the elevated *CDKN2A* expression and enhances the risk for deletion of the gene locus. To compare the chromatin structure between *CDKN2A/B* homozygous deleted and non-deleted cases, I exploited so-called single cell Multiome data, which does not only capture transcriptomic profiles of single cells, but also their respective chromatin structure in form of an assay for

transposase-accessible chromatin using sequencing (ATAC-Seq). This sequencing method captures open structures of chromatin as peaks. The Multiome dataset employed here comprised four WHO grade 3, MC mal meningiomas in total, two of them with *CDKN2A* homozygous deletion and two non-deleted cases. As expected, *CDKN2A* homozygous deleted cases displayed no expression of *CDKN2A* and no peaks at the *CDKN2A/B* locus in the neoplastic cell populations, whereas both, *CDKN2A* expression and peaks at the *CDKN2A/B* locus, were clearly present in the neoplastic cells of the non-deleted cases (**Figure 10**c,d).

To investigate further differences in the overall chromatin structure of *CDKN2A/B* homozygous deleted and non-deleted tumors I subsequently estimated transcription factor motif activities from the ATAC assay of the Multiome data. The activity of known transcription factor binding sites was hereby estimated from the chromatin accessibility across genomic locations. Several transcription factor motifs were identified to display a differential activity between tumors with differing *CDKN2A/B* status, such as different complexes of the transcription factor activator protein 1 (AP-1) that is formed by dimers of members of transcription factor families Jun and Fos and motifs of which displayed elevated activity in *CDKN2A/B* deleted cases (**Figure 10**e). In *CDKN2A/B* non-deleted cases on the other hand binding motifs for the Myc family of transcription factors exhibited increased activity levels. This might indicate that the *CDKN2A/B* homozygous deletion causes an overall shift in regulatory mechanisms for the tumor cells.

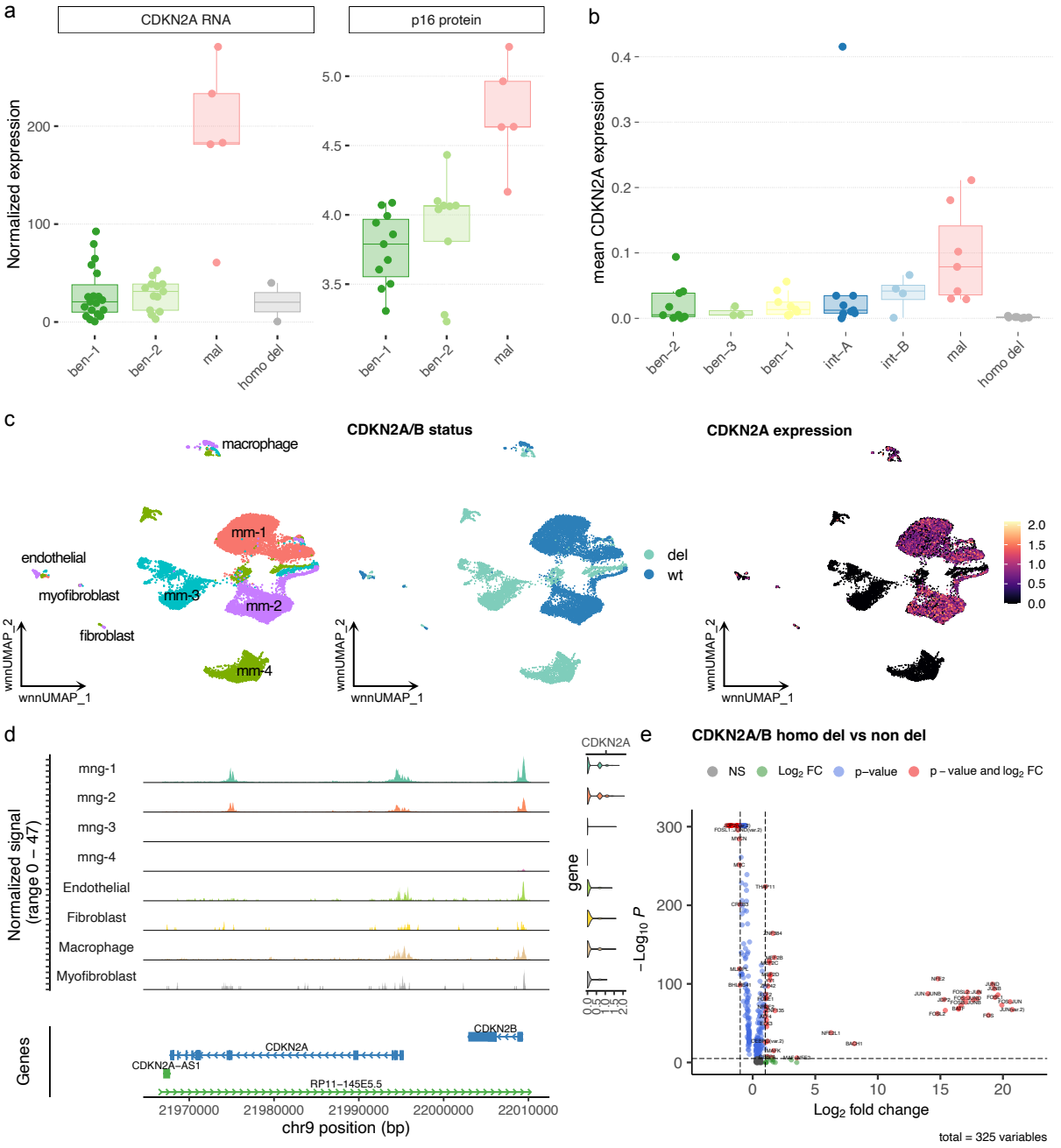

Figure 10. a *Normalized expression of* CDKN2A *in bulk RNA-Seq data (left) and of its respective protein p16 in bulk proteomic data (right). homo del …* CDKN2A *homozygous deletion.* ***b*** *Mean* CDKN2A *expression per sample in the neoplastic cell population derived from scRNA-Seq data.* ***c*** *UMAP representations of weighted nearest neighbor (WNN) graph for combined RNA-Seq and ATAC-Seq data per cell colored by sample of origin (left), status of the* CDKN2A/B *gene locus in the respective sample (middle), and normalized expression of* CDKN2A *(right). wt …* CDKN2A/B *wild type (non-deleted), del …* CDKN2A/B *homozygous deletion.* ***d*** *Cluster-wise accessibility of the* CDKN2A/B *gene locus. Peaks indicate accessible chromatin regions. Violin plots on the right reflect normalized* CDKN2A *expression in the respective cell population.* ***e*** *Transcription factor binding motifs with differential activity in cases with* CDKN2A/B *homozygous deletion compared to non-deleted cases. Positive log2FC indicates elevated activity in homozygous deleted cases.*

FOXM1 activity in high grade meningiomas

Similarly to *CDKN2A/B* homozygous deletion, increased activity of the *FOXM1* expression factor has been linked to aggressiveness in meningioma (Vasudevan et al. 2018; Paramasivam et al. 2019; H. Kim et al. 2020). Overall *FOXM1* expression levels were low in the scRNA-Seq dataset, so I inferred *FOXM1* activity from the expression of its target genes. Indeed, *FOXM1* activity was

significantly increased in MC mal meningiomas compared to MC ben-2 meningiomas (p-value = 7.8e-6 as determined by Tukey's range test). However, there was no significant difference between any of the remaining comparisons when comparing sample means. Instead, *FOXM1* activity seemed only to be elevated in a small subpopulation of cells, while the *FOXM1* activity for a majority of cells stayed consistent across MCs, with MC ben-2 as the only exception, as it had a larger population of cells with decreased *FOXM1* activity (**Figure 11**a). Moreover, the activity of *FOXM1* seemed to be connected to the cell cycle stage, with cells undergoing the G2M checkpoint displaying a higher *FOXM1* activity compared to cells in the G1 as well as the S Phase of the cell cycle (**Figure 11**b).

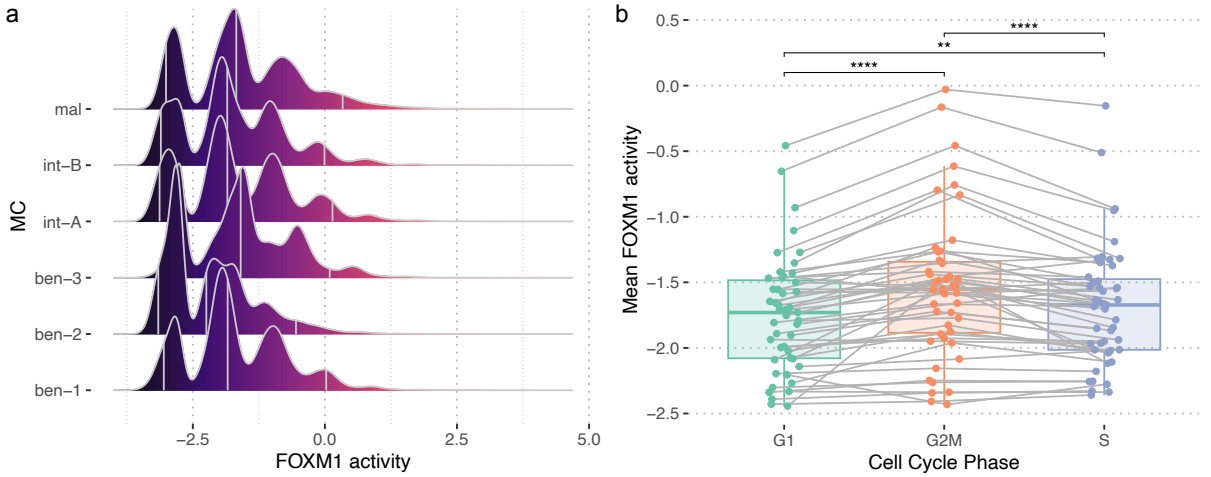

Figure 11. a *Density of* FOXM1 *activity as inferred from the expression of its target genes per MC. Vertical grey lines indicate 5%, 50%, and 95% quantiles.* ***b*** *Average* FOXM1 *activity per sample depending on the cell cycle stage. Lines connect means from the same sample. Asterisks indicate significant p-values as determined from a post-hoc paired t-tests after repeated measures ANOVA. ** … p < 0.01, **** … p < 0.0001.*

This indicates that not the overall *FOXM1* activity across neoplastic cells, but only a small subpopulation of cycling cells with elevated *FOXM1* activity is determinative of the increased aggressiveness in meningioma.

Cellular origin of endothelial structures in angiomatous meningioma

While *CDKN2A/B* homozygous deletion and increased expression as well as elevated *FOXM1* activity are associated with MC mal meningiomas, MC ben-3 tumors are frequently associated with an angiomatous histological subtype. Angiomatous meningiomas are characterized by a high amount of vascularization within the tumor tissue. Thus far it has however not been conclusively elucidated whether the numerous blood vessels are formed by infiltrating endothelial cells that are attracted by angiogenic factors secreted by tumor cells, or by the tumor cell population itself. I queried the scRNA-Seq dataset, that comprised in total four angiomatous meningiomas, to investigate this question. Comparing the expression scores for endothelial marker genes with the CNV scores for chromosomal alterations, specifically the chromosomal gains typical for this tumor class that were observed in at least one of the four samples, namely for chromosomes 3, 5, 12, 13,

18, and 20, in the tumor/endothelial cell population revealed no relationship between both (**Figure 12**a). Cells either displayed chromosomal alterations or the expression of endothelial-specific genes, but not both. This indicates that the vasculature in these tumors is not formed by neoplastic cells but infiltrating endothelial cells.

To gain insights into how the endothelial cells are attracted to the tumor site, I performed a ligand-receptor analysis between the cell populations of the angiomatous meningiomas. This analysis can infer what cell populations interact with one another through which ligands and receptors based on a common increase in the expression of matching ligand-receptor pairs in the respective two cell populations. For the angiomatous meningiomas, a strong interaction specifically between the neoplastic and the endothelial cell population was inferred, with the endothelial cells as the receiving cell population (**Figure 12**b). These interactions were frequently based on *VEGFA/B*, a growth factor involved in angiogenesis (Murphy and Fitzgerald 2001), and *SLIT2* that were expressed as ligands by the tumor cells (**Figure 12**c). *SLIT2* has previously been demonstrated to induce vascularization (Han and Geng 2011). This demonstrates possible mechanisms in which neoplastic cells attract endothelial cells for vessel formation in the tumor.

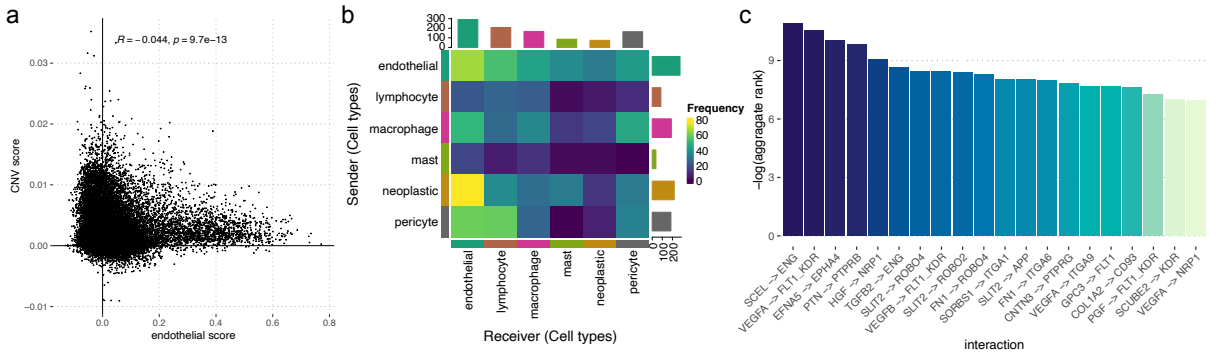

Figure 12. a *Score for endothelial marker gene expression and CNV score for chromosomal gains for each cell in the meningioma samples of angiomatous subtype. R ... Pearson correlation between both scores.* ***b*** *Frequency of interactions between cell populations with the ligand expressing cell type in rows and the receptor expressing cell type in columns.* ***c*** *Top interactions between neoplastic and endothelial cells with neoplastic cells as source (expressing the ligand) and endothelial cells as target (expressing the receptor).*

Shared transcriptomic signatures across tumor stages

While so far I have considered the neoplastic cell population of a tumor as a whole, it is likely that a tumor undergoing progression is formed by different tumor cell subpopulations at different stages of progression. Some of these may be responsible for a more aggressive behavior, such as the capability of tissue invasion, or later give rise to recurrences. Therefore, I aimed to identify such tumor cell subpopulations and their phenotypes to compare how they are shared between tumors of differing malignancy. For identification of tumor cell subpopulations, I applied non-negative matrix factorization (NMF) to the neoplastic cell population of each individual sample to dissect transcriptomic signatures and subsequently determined similarities in the transcriptomic

signatures across samples. This analysis revealed six transcriptomic signatures that were shared across samples. I scored all neoplastic cells according to their expression of the respective signature genes of each transcriptomic signature and thus assigned them to six tumor subpopulations, each with a specific phenotype. Based on the transcriptomic signature genes, a subpopulation consisting of cycling cells was identified, as well as a population of neoplastic cells expressing genes related to cell adhesion. Another subpopulation displayed an elevated expression of genes linked to epithelial-mesenchymal transition (EMT), hypoxia, and inflammation. The remaining three transcriptomic signatures covered genes connected to *KRAS* signaling, oxidative phosphorylation, and androgen response, respectively.

The proportions at which each of these tumor cell subpopulations occurred within the neoplastic cell population varied strongly between the tumor subtypes (**Figure 13**). As one would expect, the cycling cell population increased significantly with malignancy from the benign MCs to MC mal (adjusted p-value = 0.033 in MC ben-1 versus MC mal as determined by Tukey's range test). All remaining comparisons did not indicate a significant difference in proportions of the tumor cell subpopulations between MCs, most likely due to the high inter-sample variance within MCs. Nonetheless, the tumor cell population with an adhesive phenotype tended to be more prominent in the benign MCs as compared to the intermediate and malignant MCs, with highest proportions in MC ben-3 and ben-2, both MCs with lowest risk for metastasis and tumor recurrence. Interestingly, a majority of samples of the *NF2*-mutant MCs ben-1, int-A/B, and mal, but not all, presented with a high proportion of cells highly active in oxidative phosphorylation, while tumors of the non-*NF2* mutant MCs ben-2 and ben-3 tended to contain higher proportions of cells with active *KRAS* signaling.

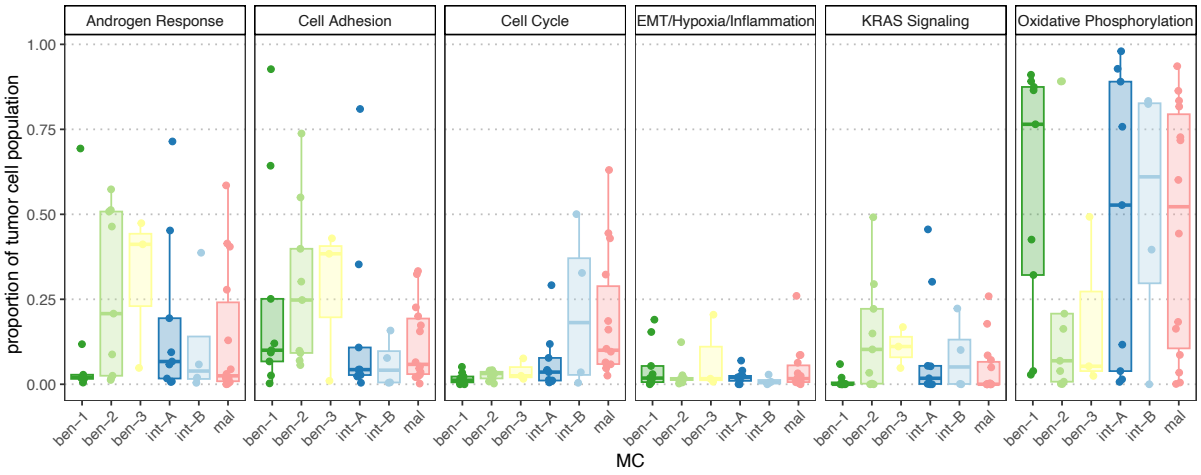

Figure 13. *Proportion of tumor cells from total tumor cells per sample for each tumor cell subpopulation.*

Altogether, these results demonstrate that tumor cell subpopulations exist with shared transcriptomic profiles across samples, albeit at varying proportions depending on the tumor subtype and genetic background. Further investigations will however be necessary to understand in detail how these subpopulations are linked to tumor progression.

SPATIAL DISTRIBUTION OF TUMOR MCS AND TUMOR CELL SUBPOPULATIONS

On single cell level, I have discovered tumor cell subpopulations with shared transcriptional programs across samples, which occur at differing proportions depending on the tumor class. A fundamental limitation of the scRNA-Seq data is that it is not possible to infer whether these subpopulations tend to co-locate or whether they appear at spatially distinct locations within the tumor tissue. Thus, I queried spatial transcriptomics data that was obtained for 17 meningiomas of WHO grades 1 to 3 and MCs ben-1, int-A, and mal, however with an overrepresentation of MC int-A and MC mal cases (**Supplementary Table 3**).

First, I investigated whether the transcriptional programs of the six MCs can occur together within the same tumor and if any of them tend to associate with certain histological structures. The scRNA-Seq data was used as a reference to deconvolute the expression profile of each spot in the spatial transcriptomics to predict individual cell populations as they were observed on single cell level. This included infiltrating cell types as well as neoplastic cells. The latter were annotated according to the MC of their sample of origin. The distribution of MCs within the tumors was surprisingly mixed, especially for benign samples (**Figure 14**a). Two MC ben-1 samples for example also displayed an enrichment for the int-B transcriptional signature in parts of the tumor tissue (**Figure 14**b). And while one MC int-A case displayed a very clear enrichment for only the int-A transcriptional signature (**Figure 14**c), the remaining MC int-A samples exhibited mixed enrichments with a tendency either towards the ben-2 or the mal transcriptional signature. MC mal tumors on the other hand were uniformly enriched for the mal transcriptional signature, however focal enrichment for ben-2 and ben-3 signatures could also be identified in small sections of the tissue (**Figure 14**d).

Taken together, these results indicate that transcriptional signatures for different MCs might coexist within the same tumor. Interestingly, this seems to be independent of the genetic background that is typically observed for the individual MCs, as also MCs with different genetic profiles were identified within the same tissue.

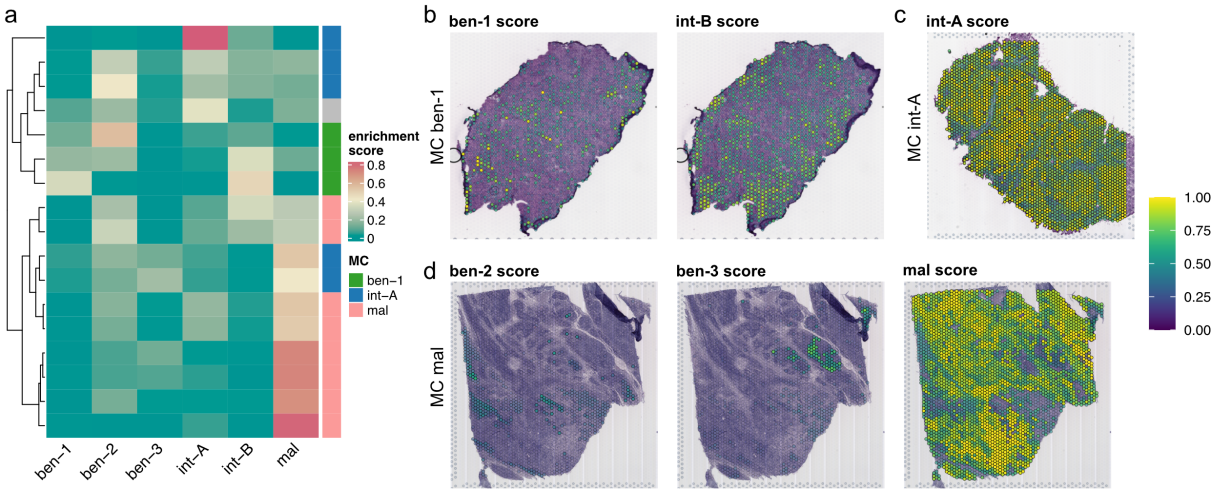

Figure 14. ***a*** *Average enrichment per sample (rows) for each of the MC-specific transcriptional signatures (columns) as derived from scRNA-Seq data.* ***b-d*** *Spot-wise enrichment scores for MC-specific transcriptional signatures for an MC ben-1 meningioma (b), an MC int-A meningioma (c), and an MC mal meningioma (d).*

Similarly as for the MCs, the localization of the six tumor cell subpopulations identified by NMF was inferred from the scRNA-Seq data to identify their spatial associations. First, I investigated whether any of the tumor cell subpopulations tended to occur in the same tissue areas by correlating their spot-wise enrichment scores for each of the six subpopulations. Thereby, the subpopulation active in oxidative phosphorylation seemed negatively associated with the presence of the cycling and hypoxic subpopulations as well as the subpopulation with active *KRAS* signaling (**Figure 15**a). Histologically, the oxidative phosphorylation subpopulation colocalized with the perinecrotic zone surrounding necrotic regions in tissue sections with necrosis (**Figure 15**b). Apart from this, there was no apparent correlation between the spatial localization of any two tumor cell subpopulations or an association with visible histological features. This means that the subpopulations on one hand do not seem to be mutually exclusive within the same tissue area. On the other hand, it might also indicate that there is no interdependence between the tumor cell subpopulations, where one would provide a favorable environment for another one.

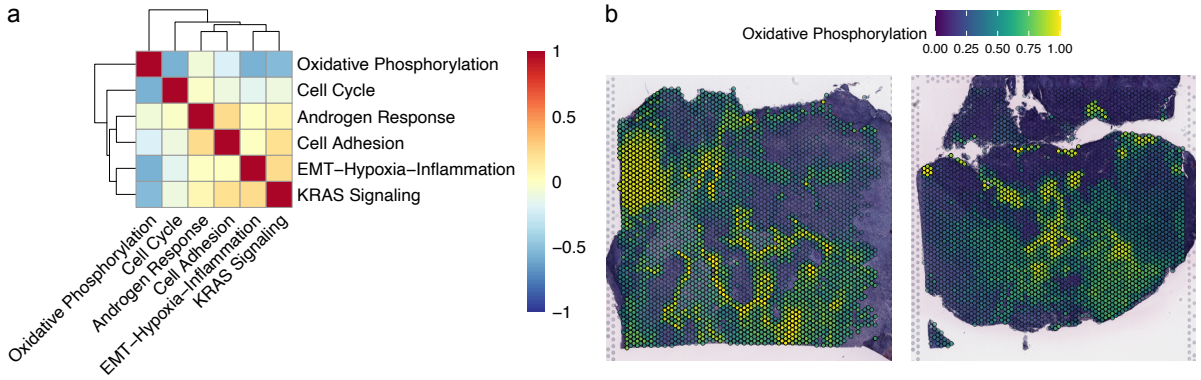

Figure 15. ***a*** *Correlation of spot-wise enrichment scores for the tumor subpopulations. Color legend represents Pearson correlation scores, with red color indicating positive correlation and blue indicating negative correlation.* ***b*** *Spot-wise enrichment scores for the tumor subpopulation with high activity in oxidative phosphorylation for two WHO grade 3 and MC mal meningiomas with necrosis.*

TRANSCRIPTIONAL CHANGES ALONG THE INFILTRATION ZONE

Another advantage of spatial transcriptomics data is the possibility to link histologically interesting properties directly to expressional changes. One of the meningiomas included in the spatial transcriptomics dataset for example captured a brain invasive region of a meningioma (**Figure 16**a). Analyzing this in detail could identify changes in expression specific to invasive tumor cells that might facilitate or even be required for tumor infiltration in meningioma. Thus, in the following I analyzed the infiltration zone in greater detail.

The tumor regions could be reliably separated from the non-tumor regions through the identification of tumor specific CNVs (**Figure 16**b), consolidating the histology. I defined an infiltration trajectory from the tumor regions crossing the infiltration zone up to the healthy brain tissue (**Figure 16**c). Spots located along this trajectory were used for differential expression and pathway enrichment analysis. As expected, the Reactome pathway 'Degradation of the extracellular matrix' displayed a peak in enrichment along the infiltration trajectory at the infiltration zone (**Figure 16**d). The same was observed with other pathways connected to tumor infiltration, such as collagen degradation. A number of genes was similarly differentially expressed along the trajectory. Among those were matrix metalloproteinases that exhibited expression peaks at different regions along the trajectory (**Figure 16**e). Matrix metalloproteinase 2 (*MMP2*) displayed the highest peak in expression. This peak also concurred directly with the infiltration zone.

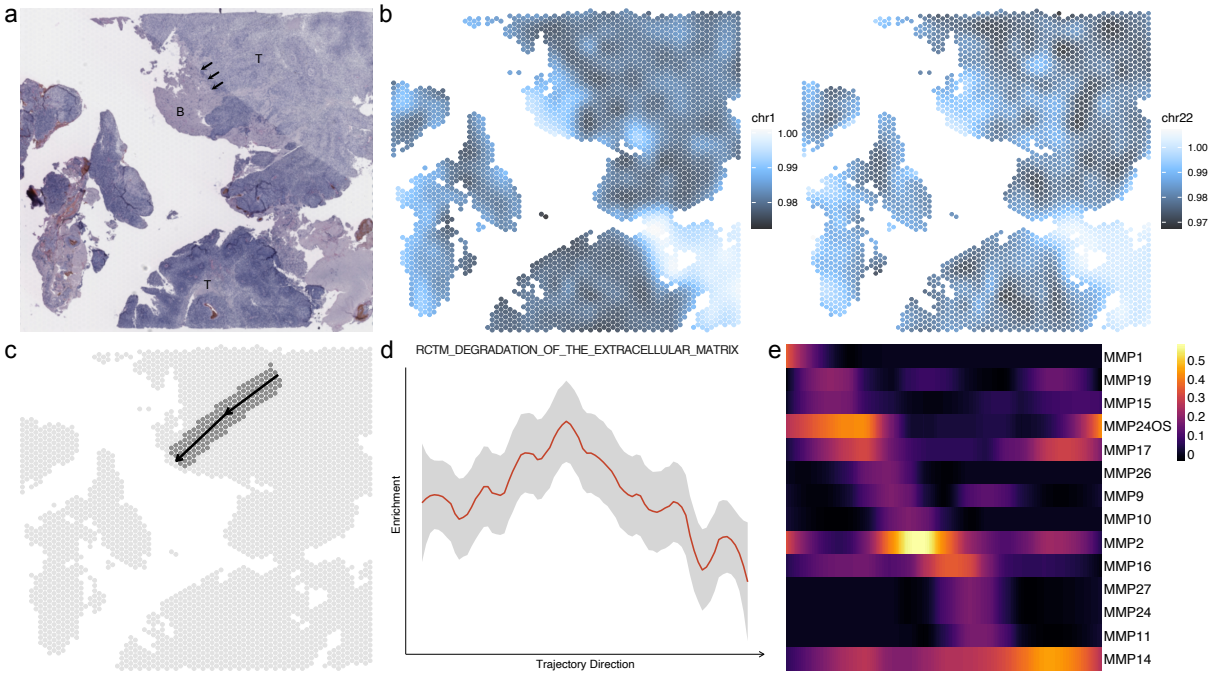

***Figure 16. a** H&E section of a WHO grade 3 and MC mal meningioma with brain invasion. Arrows mark the infiltration zone between tumor (T) and brain (B). **b** Spot-wise scores for a copy number change of chromosomes 1 (left) and 22 (right), with a score of 1 indicating a copy number neutral status and a score below 1 indicating a deletion of the respective chromosome. **c** Trajectory along the infiltration zone of the tumor. Dark spots were included for analysis of the infiltration trajectory. **d** Enrichment for the Reactome pathway 'Degradation of the extracellular matrix' along the infiltration trajectory from (c). Grey area represents the confidence interval after smoothing. **e** Average expression of metalloproteinases along the infiltration trajectory from (c).*

These results indicate that several matrix metalloproteinases play a role in brain invasion that is often observed in aggressive meningiomas, with *MMP2* seemingly being of specific importance. Further analysis and more samples will however be necessary to unravel the mechanisms driving brain invasion in meningioma.

3.3. Meningioma tumor microenvironment

Differences in infiltrating cell populations depending on tumor grade and MC

Besides neoplastic cells, a number of infiltrating cell types were identified in the scRNA-Seq dataset, including myeloid cells, lymphocytes, endothelial cells, and mast cells. It has been extensively shown that these cells, which together with the molecules they secrete make up the TME, heavily influence the tumor's ability to progress, infiltrate the surrounding tissue, and metastasize (Chen et al. 2015; Jin and Jin 2020). With this knowledge, I next investigated these non-neoplastic cell populations more closely and compared their abundance and phenotype across tumor classes, as they might affect meningioma malignancy. Comparing proportions of infiltrating cells already highlighted stark differences between meningioma grades and MCs (**Figure 17**a). While there was no significant difference in the proportion of total lymphocytes between grades or MCs, CD4 positive T cells were enriched in low grade versus high grade cases (**Supplementary Figure 4**, WHO grade 1 versus WHO grade 3: adjusted p-value = 0.032 as determined by Tukey's range test). A similar tendency was observed for NK cells, although no significant difference was detected. CD8 positive T cells on the other hand tended to be enriched in high grade cases, but also without significant difference.

Most striking was however the difference in tumor-associated macrophages (TAMs). TAMs were present at significantly greater numbers in MC ben-1 meningiomas as compared to MC mal tumors (**Figure 17**b, Tukey's range test adjusted p-value = 0.00040). Interestingly, also MC ben-2 meningiomas displayed significantly lower numbers of TAMs compared to MC ben-1 cases (Tukey's range test adjusted p-value = 0.0021). No clear difference could be observed between WHO grade 1 and grade 3 tumors, most likely due to the opposing behavior of MCs ben-1 and ben-2/-3 tumors. A similar tendency was detected between matched primary and recurrent tumors of the same patient, with lower numbers of infiltrating TAMs in the recurrence compared to the respective primary tumor (**Figure 17**c). However, only five such matched pairs were included in the dataset, so that the variance was too great for a stable result (paired Wilcoxon signed-rank test p-value = 0.062).

To subsequently exclude the possibility of a sampling bias during nuclei extraction for single cell sequencing, I deconvoluted the bulk RNA-Seq data using xCell to predict the enrichment of

cell types from the bulk transcriptional profiles. As expected, macrophages were greatly enriched in MC ben-1 cases compared to MCs ben-2 and mal (**Supplementary Figure 5**). This was also in line with the enrichment for immune-related pathways for MC ben-1 meningiomas in the bulk DE analyses. Immunohistochemistry stainings for the macrophage marker CD68 that were obtained by my colleague Helin Dogan in the lab further consolidated this finding (**Figure 17**d).

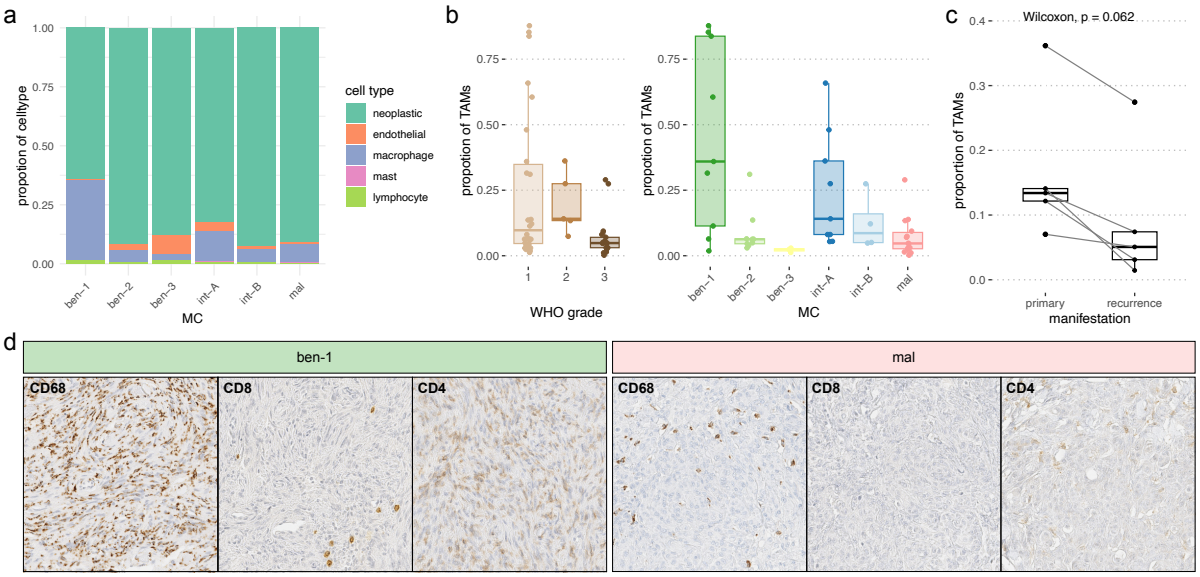

***Figure 17. a** Proportion of individual cell types across all samples of each MC. **b** Proportion of macrophages in each sample with respect to WHO grade (left) and MC (right). **c** Changes in macrophage proportions between primary and recurrent tumor of the same patient. Lines indicate matching sample pairs. **d** Immunohistochemistry stainings for the macrophage marker CD68 and T cell markers CD8 (CD8+ T cells) and CD4 (CD4+ T cells) in an MC ben-1 meningioma (left) and an MC mal meningioma (right).*

Differential activation of tumor-associated macrophages between MCs

Macrophages are known to influence tumor cell behavior and progression. At that, they can exert both protumoral as well as antitumoral effects. Given the stark differences in the macrophages that already became apparent by comparing abundances, in a subsequent step I closely analyzed the activation status of the TAMs depending on tumor grade and MC to predict their potential impact on the tumor cells. To this end, a DE analysis was performed comparing the TAM population of each MC to all other TAMs applying the same pseudobulk approach as for the neoplastic cell population. The differentially expressed genes were then probed for activation patterns of interleukin (IL) signaling pathways. Indeed, differences between the TAM populations of the individual MCs became apparent. TAMs infiltrating MC mal meningiomas for example displayed a strong activation of the IL-4 and IL-13 signaling pathway as well as the IL-6 signaling pathway (**Figure 18**), both of which are known to have protumoral effects (Hirano 2021; Suzuki et al. 2015). TAMs of MC ben-1 tumors on the other hand were enriched for IL-2 and IL-21 signaling pathways, which have been demonstrated to have antitumoral effects (Waldmann

2018). Thus, the activation status of the TAM population strongly differs between MCs, with an activation favorable for the tumor prevalent in MC mal cases.

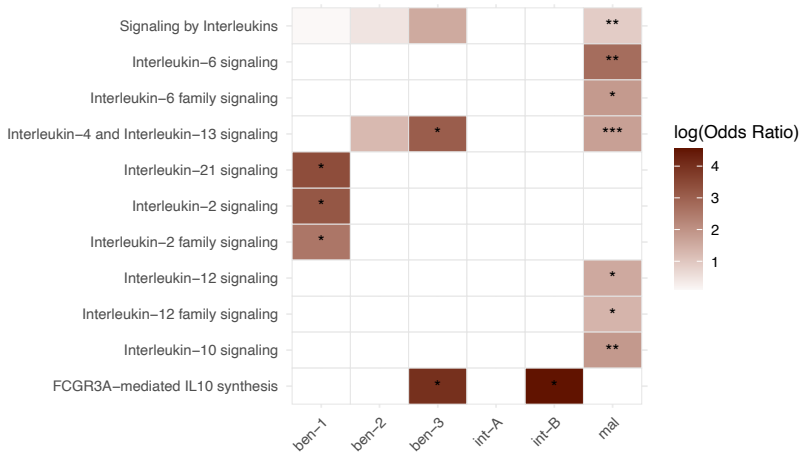

Figure 18. *Differential activation of interleukin signaling pathways between MCs. Asterisks indicate significance. *** … p < 0.001, ** … p < 0.01, * … p < 0.05*

Given these differences in abundance and activation, I investigated whether they could be caused by the neoplastic cell population that stimulate the macrophages in one way or another. Thus, a ligand-receptor analysis was performed to test for interactions between neoplastic cells and macrophages depending on the tumor class. Thereby, macrophages were predicted to be stimulated by several factors secreted by the neoplastic cells. Among these was the *CSF1/IL34* ligand complex that interacted with the CSF1 receptor (*CSF1R*) on the macrophages in MC ben-1 and MC int-A tumors (**Figure 19**a). The same interaction was not predicted for MC ben-2, int-B, and mal tumors, the tumor classes with typical lower macrophage infiltration. For MC ben-3, no sufficient expression of the ligand-receptor pair could be observed for any conclusions. In line with this were the significantly decreased *CSF1* expression levels in the neoplastic cells of these MCs as compared to MC ben-1 meningiomas (**Figure 19**b). On the other hand, no difference in the *CSF1R* expression of the macrophage population could be observed between MCs (**Figure 19**c). This might indicate that a shift in stimulation occurs in the neoplastic cell population during progression, where tumor cells cease to stimulate macrophages vis *CSF1*. Coincidentally, the *CSF1* gene is located on chromosome 1p, a gene locus that is frequently deleted in high grade meningioma.

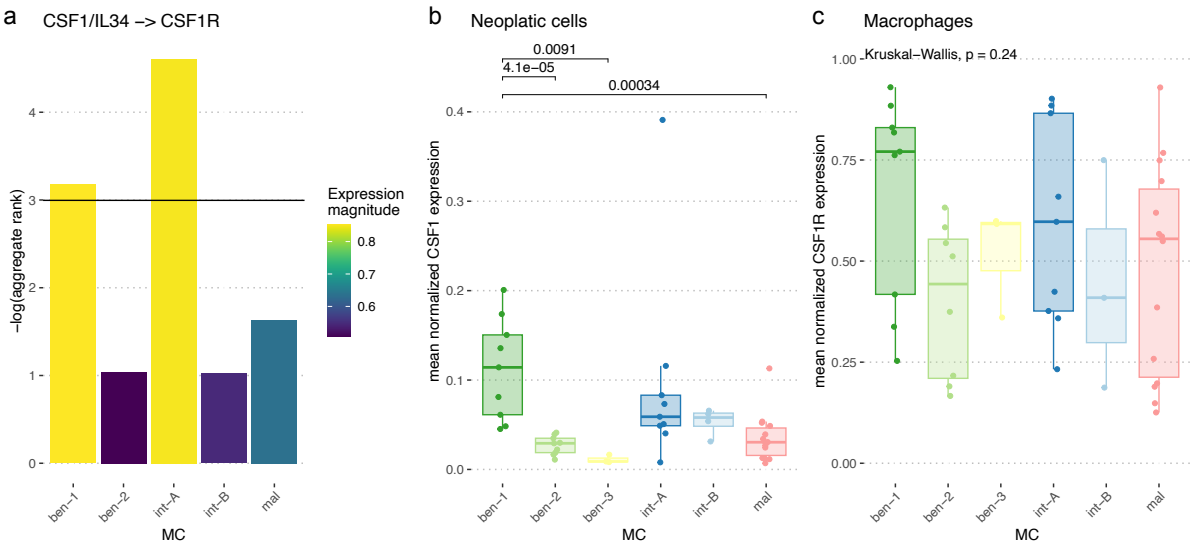

Figure 19. a *Aggregate rank across ligand-receptor analysis methods for the interaction via the* CSF1/IL34 *complex expressed by neoplastic cells and* CSF1R *expressed by macrophages. The black line resembles a significance level of 0.05. Colors represent extent of expression for ligand and receptor in the source and target cell population, respectively.* ***b*** CSF1 *expression in the neoplastic cell population depending on MC. Significant differences in mean expression according to Tukey's rank test are annotated with the respective p-values.* ***c*** CSF1R *expression in the macrophage population depending on MC.*

Interestingly, a subpopulation of TAMs also expressed typical microglial markers (*TMEM119*, *P2RY13*, *P2RY12*, *GPR34*, *SLCA5*). The proportion of TAMs with microglial marker gene expression was increased in low-grade compared to high-grade cases (MC ben-1 versus MC mal adjusted p-value = 0.0078 as determined by Tukey's rank test; WHO grade 1 versus WHO grade 3 adjusted p-value = 0.0228 as determined by Tukey's rank test; **Figure 20**). This was an unexpected finding, given that especially low-grade cases rarely present with brain invasion, and might point towards a specialized cell type.

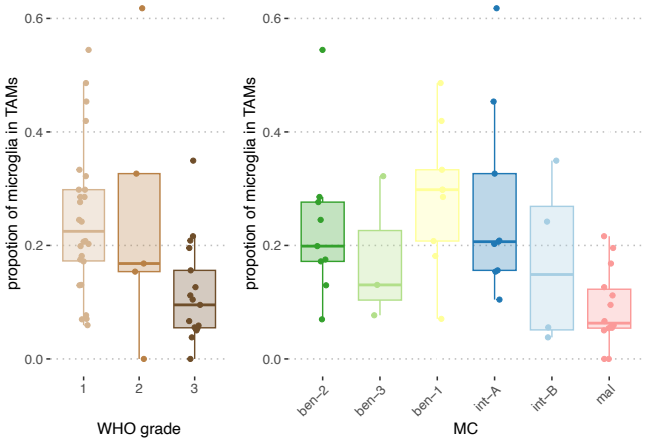

Figure 20. *Proportion of microglia in the total TAM population of each tumor by WHO grade (left) and MC (right).*

Altogether, the significant differences in TAM phenotypes depending on meningioma subtype indicate that they might heavily influence tumor aggressiveness and progression by shaping the tumor microenvironment.

Spatial distribution of tumor-associated macrophages within the meningioma tissue

As the TAMs will mainly exert their pro- and antitumoral effects on tumor cells in their direct vicinity, I next investigated the spatial distribution of TAMs in the spatial transcriptomics data. Confirming the previous findings, MC ben-1 tumors displayed a higher enrichment for TAMs as compared to higher-grade meningiomas (**Figure 21**a). However, the enrichment was rather homogenously distributed in the tumor (**Figure 21**b). A focal enrichment for TAMs could be observed only in tumors with necrotic regions, all of them WHO grade 3 and MC mal, where TAMs accumulated in the perinecrotic regions surrounding the necrosis (**Figure 21**b,c, **Supplementary Figure 6**a,b).

A closer analysis of these perinecrotic regions revealed an enrichment of metallothionein expression (**Figure 21**d, **Supplementary Figure 6**c). Moreover, an expression of ferroptotic markers (*FTL*, *FTH1*, *TF*, *TFRC*) could be observed (**Figure 21**e, **Supplementary Figure 6**d), whereas no expression of apoptosis or necrosis related genes was detected around the histologically visible necrotic areas (**Supplementary Figure 6**e,f). To investigate whether signs of ferroptosis could be found in the scRNA-Seq data, the same marker genes were queried in this dataset. However, there was no apparent correlation between the expression of ferroptosis related genes and the tumor MC, although there was a tendency of elevated ferroptotic marker gene expression levels in tumors of WHO grade 3. This might not be surprising, as no visibly necrotic regions were included when generating the scRNA-Seq data. Taken together, the data suggest that ferroptotic processes might contribute to the histologically observed necrosis in MC mal/WHO grade 3 meningiomas.

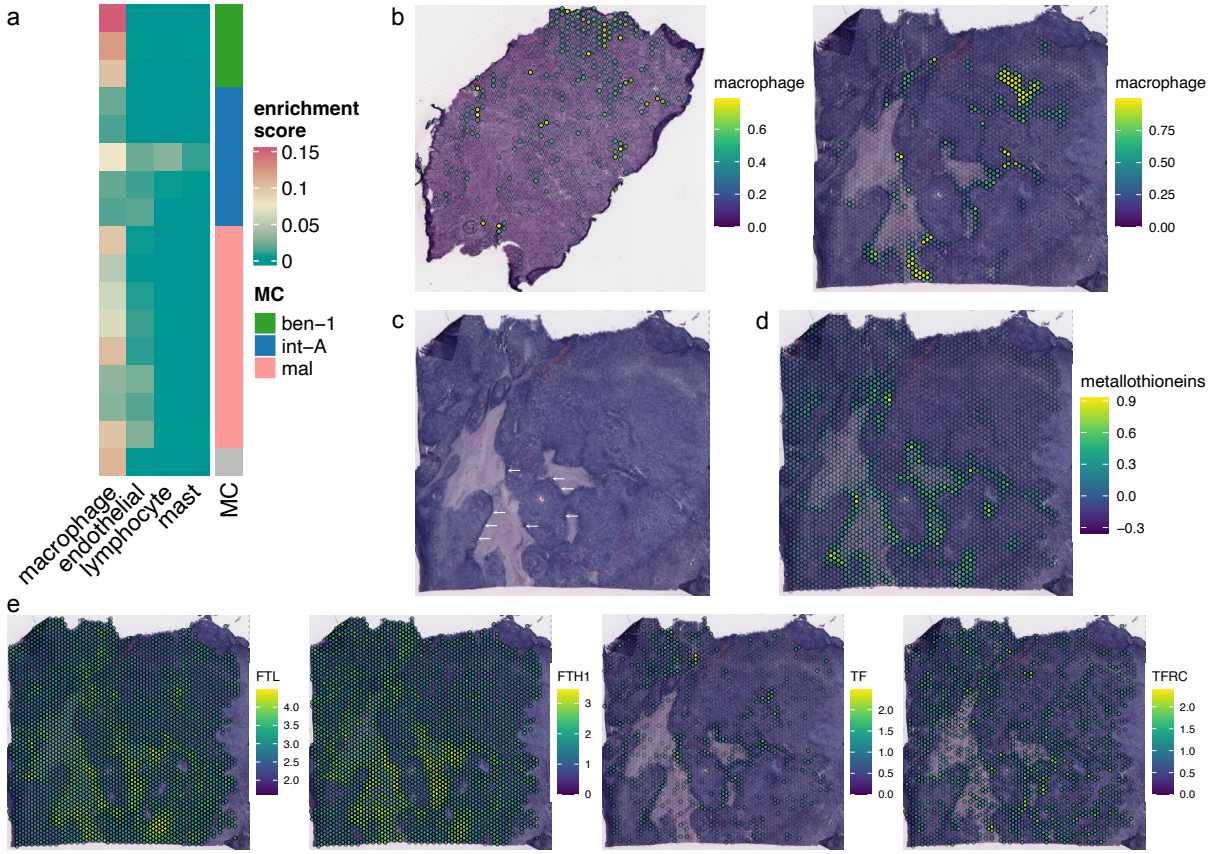

Figure 21. a *Average enrichment per sample (rows) of each non-tumor single cell population (columns).* ***b*** *Spot-wise enrichment score for macrophages as inferred from scRNA-Seq data for an MC ben-1 meningioma (left) and an MC mal meningioma with necrosis (right).* ***c*** *H&E staining of the WHO grade 3 and MC mal meningioma from (b) with necrosis and perinecrotic regions (arrows).* ***d*** *Spot-wise enrichment scores for metallothionein expression for the tissue section in (c).* ***d*** *Spot-wise expression of four ferroptotic marker genes for the tissue section in (c).*

Correlation of tumor-associated macrophages with progression free survival

The stark differences in numbers as well as activation of the TAM population depending on the tumor MC suggested that these cells influence tumor progression and with that, the outcome for the patient. Therefore, I investigated a cohort of 806 meningioma samples, for which methylation array as well as progression-free survival data was available. First, I deconvoluted the methylation array data to predict the proportion of infiltrating immune cells in each of the samples using public methylation sets for each cell type as reference (Dekkers 2019; Hassler et al. 2016; Lucero et al. 2020; Vizoso et al. 2015). As expected from the scRNA-Seq dataset, the proportion of infiltrating immune cells was elevated in MC ben-1 samples (**Figure 22**a). I then compared these numbers for the infiltrating immune cell population with the progression-free survival of the patients. To this end, I grouped the samples into tumors with low (below the first quartile), medium (between the first and third quartile), and high (above the third quartile) immune infiltration (**Figure 22**b). Between all samples, tumors with high immune infiltration presented with significantly prolonged progression-free survival as compared to tumors with low immune infiltration (**Figure 22**c).

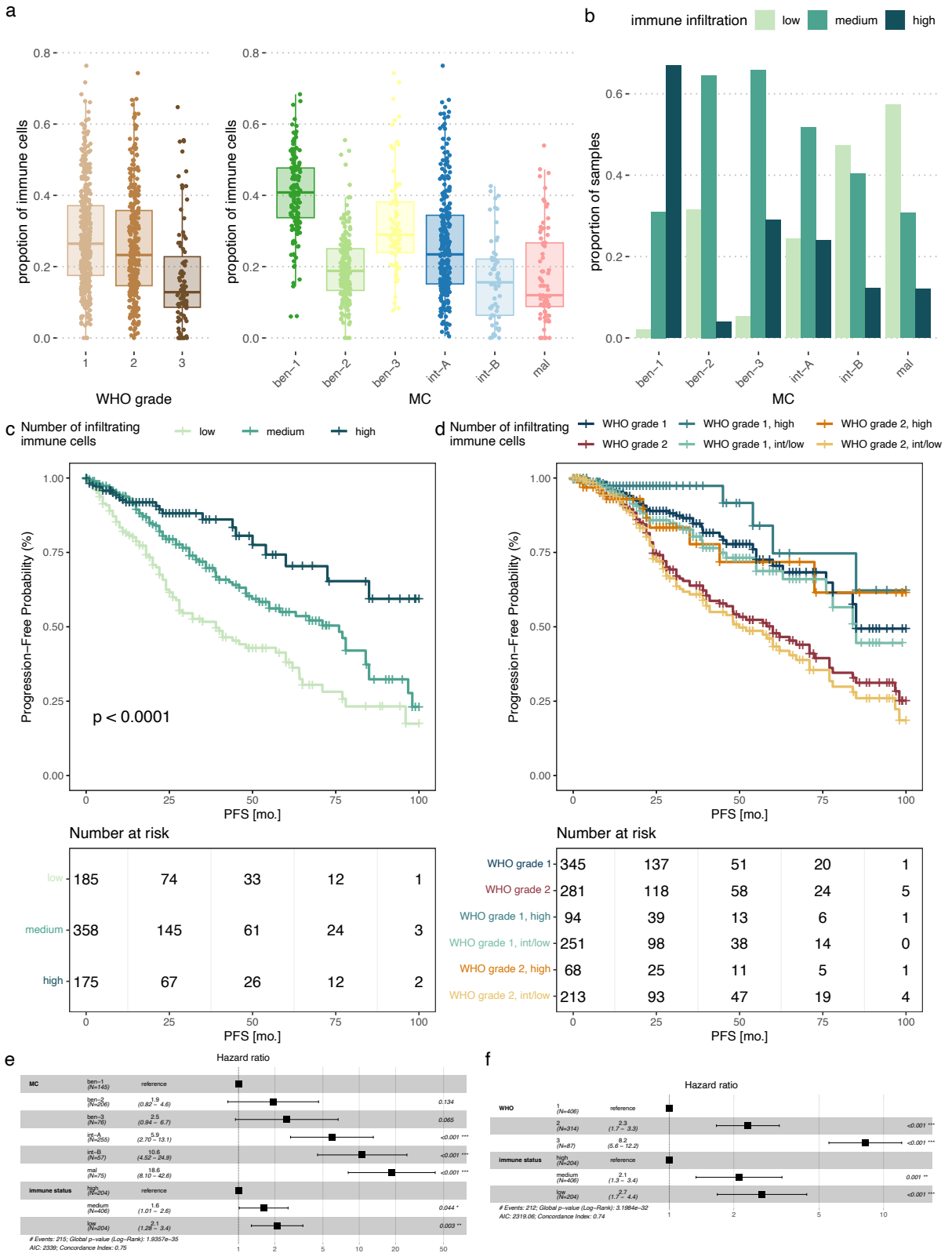

*Figure 22. **a** Proportion of immune cells as predicted by deconvolution of methylation array data. **b** Proportion of samples assigned to groups of meningiomas with high, intermediate, and low immune infiltration, respectively. **c** Progression free survival of patients depending on their immune status. **d** Progression free survival of patients depending on WHO grade and combined WHO grade and immune status. **e,f** Hazard ratio for a Cox proportional hazard model of progression free survival including immune status as well as WHO grade (e) or MC (f).*

This was still true when accounting for MC as well as WHO grade of the tumor (**Figure 22**d-f). Especially for WHO grade 1 and 2 cases, for which risk stratification is generally more difficult, the proportion of infiltrating immune cells had a significant correlation with progression-free survival, while the effect was mitigated for WHO grade 3 cases (**Supplementary Figure 7**). The Brier score for the proportion of immune cells alone was not able to compete with MCs in prediction of the progression-free survival, but it slightly improved the prediction in combination with the MCs (**Table 1**).

	IBS (10 years)
Reference	0.198
Immune status	0.184
WHO	0.166
WHO + immune status	0.159
MC	0.152
MC + immune status	0.150

Table 1. *Integrated Brier Score (IBS) after ten years for a Cox proportional hazard model of progression free survival.*

A comparison of the hazard ratio of the immune subgroup for each WHO grade separately revealed that the effect of the immune infiltration made a significance difference in patient outcome for WHO grade 1 and 2 tumors, but not in WHO grade 3 tumors (**Supplementary Figure 8**). This indicates that the effect size of the immune infiltration might depend on the tumor grade. To test for this possible subgroup effect, I compared an additive Cox proportional hazard model with WHO grade and immune subgroup as covariates with a multiplicative model of the same covariates, representing a model without and with interaction between the covariates, respectively. The difference between both models was not significant (analysis of variance p-value = 0.155), indicating that the effect of the immune infiltrate is independent of the WHO grade.

In any case, the information on the immune infiltration of the tumor will be most useful for the lower grade meningiomas, for which risk stratification is more difficult. Here, the immune infiltration can add valuable information to the WHO grading and methylation classification in terms of risk stratification for patients.

3.4. Comparison of Heidelberg MCs with UCSF classifier

Altogether, the data shown here seem to emphasize the value of methylation classification and furthermore suggest a correlation with the immune infiltration. However, the Heidelberg methylation classification that was basis for the analysis thus far is only one of the methylation classification systems that have been suggested for meningioma. Therefore, I next investigated

how these classification systems compare, especially given that the UCSF and Toronto classification systems both include one subgroup of tumors with high immune infiltration. I therefore applied the published UCSF classifier (Choudhury, Magill, et al. 2022) to our 806 meningioma samples with data on the progression-free survival. As expected, most MC ben-2 tumors were assigned to the Merlin-intact subgroup, fitting their mutational background (**Figure 23**b). MC int-B and MC mal tumors fell mostly into the hypermitotic UCSF subgroup, all subgroups with most unfavorable outcome. The immune-enriched UCSF subgroup matched well with MC ben-1, which I observed to typically present with high immune infiltration. Only MC int-A tumors composed a mixture of all three UCSF subgroups, albeit most adhered to the hypermitotic UCSF subgroup. Interestingly, the UCSF subgroup assignment to the immune-enriched group mostly reflected the tumors with high immune infiltration according to the deconvolution (**Figure 23**a).

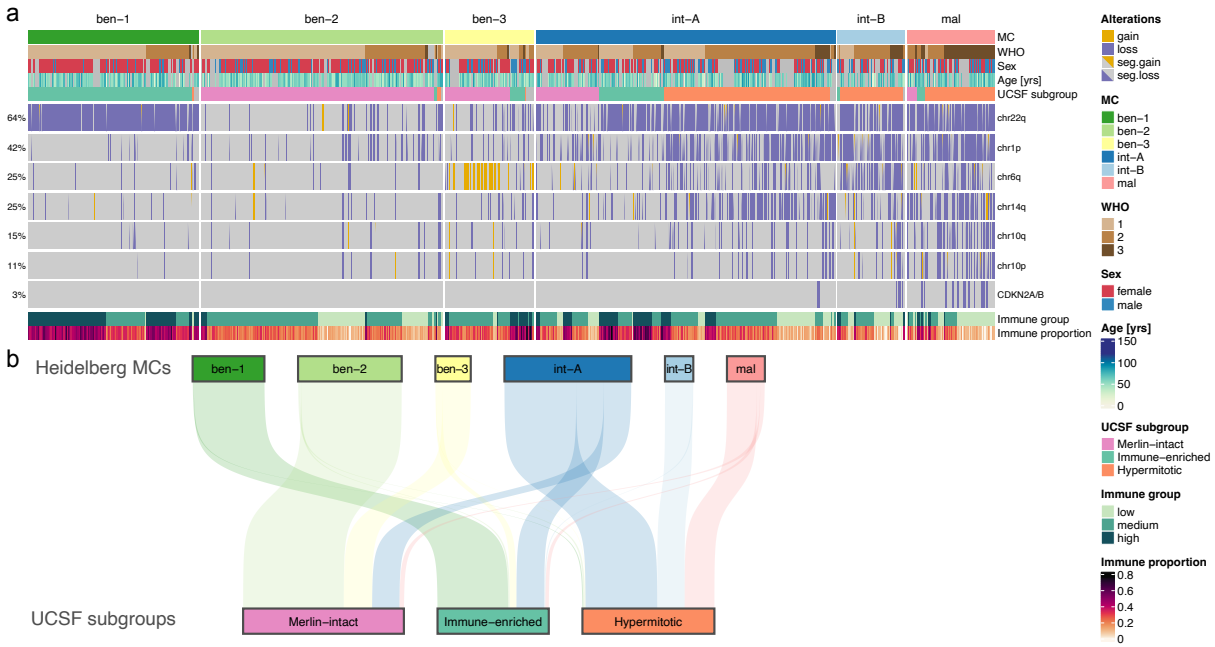

Figure 23. *Comparison of Heidelberg MCs and UCSF classifier for meningioma.* ***a*** *Most relevant CNVs for all samples from methylation array with respect to MC, WHO grade, and UCSF subgroup. Proportions of infiltrating immune cells as estimated from deconvolution and the respective immune group for each sample are annotated at the bottom.* ***b*** *Concordance between Heidelberg MCs and UCSF meningioma subgroups.*

Exploring the progression-free survival in correlation to Heidelberg MCs and UCSF subgroups revealed a slight benefit of the Heidelberg MCs in comparison to the UCSF subgroups, even when adding the information on the immune infiltration (**Table 1** and **Table 2**). Interestingly, the immune status was able to improve risk stratification in combination with the UCSF subgroups, even though the UCSF classification subgroup comprises the immune-enriched subgroup. Taken together, these findings indicate that the Heidelberg MCs seem to have a slight advantage at risk stratification.

	IBS (10 years)
Reference	0.197
UCSF	0.158
UCSF + immune status	0.156

Table 2. *Integrated Briers Score (IBS) after ten years for a Cox proportional hazard model of progression free survival.*

IV. Discussion

4.1. Consistency of epigenetic subgroups across regulatory levels

Besides the conventional grading of meningiomas based on their histopathology, molecular evaluation of the tumors has gained increasing importance for risk stratification. Several classification systems based on epigenomic profiles have been established for meningioma, which all have been demonstrated to be of additional prognostic value compared to the WHO grading (Sahm et al. 2017; Nassiri, Liu, et al. 2021; Choudhury, Magill, et al. 2022). In only one of these classification systems, the epigenomic classification has been put into perspective to additional molecular layers, however (Nassiri, Liu, et al. 2021). One of the aims of this thesis was to investigate how the Heidelberg MCs are recapitulated on RNA and protein level. Despite major discrepancies in differentially expressed genes and proteins as well as in the pathway regulation on both levels, transcriptomic and proteomic data combined consistently replicated the subgroups on epigenomic level in an SNF analysis. This underlines the relevance of the MCs past the epigenome, which is relatively upstream in regulation of expression, and implicates a more direct correspondence with the phenotype.

A consistent differential regulation of signaling pathways could not be observed across RNA and protein level. However, active signaling pathways are not always immediately associated with a change in expression, but rather with a change in conformation or phosphorylation status. For this reason, transcriptomic and proteomic datasets are not the best suited modalities to capture such differences. Thus, I analyzed the phosphoproteome for differences in signaling pathway regulation. Thereby I indeed identified kinases with differential activity depending on the tumor subgroup. Not surprisingly, cyclin-dependent kinases displayed increased activity in MC mal meningiomas. They regulate the cell cycle and are therefore indicative of the increased rate of proliferation that is generally characteristic of high grade meningiomas (Shapiro 2006). In MCs ben-1 and ben-2 on the other hand, kinases of the MAPK family were observed at increased activity levels compared to MC mal cases. Previously, a reduced activation of MAPK has been correlated to an increased rate of recurrence in meningioma (Mawrin et al. 2005). This indicates that the MAPK signaling pathway might play a protective role in tumor progression. However, this will require more in-depth investigations. In the same study, WHO grade 2 and 3 tumors were demonstrated to display elevated activity in the PI3K/AKT signaling pathway (Mawrin et al. 2005). This is somewhat contradictory to the increased *AKT1* activity that I observed on phosphoproteomic level in MC ben-2 meningiomas, which are typically WHO grade 1. However, other benign MCs contribute to WHO grade 1, and could therefore skew the observation.

Especially since the increase in *AKT1* activity is on the other hand in line with the frequent *AKT1* and *PI3KCA* mutation in MC ben-2, which are both typically activating mutations and thus lead to a constituent activation of the Pi3K/AKT signaling pathway (Carpten et al. 2007; Zadeh, Karimi, and Aldape 2016). Overall, the size of the phosphoproteomic dataset is however too small for any major conclusion. Data will have to be generated for a larger cohort to obtain conclusive results.

4.2. Intra- and intertumoral heterogeneity of neoplastic cells

As such investigations on bulk level are likely to miss more intricate differences in tumor cell subpopulations, I next investigated differential transcriptomic signatures on single cell level. Thereby I could also eliminate any confounding effects of infiltrating non-tumor cell populations. First, I generally compared the neoplastic cell population between MCs. Some of the pathways I identified to be differentially regulated had a direct counterpart in the histopathology of the tumors. For example, MC mal neoplastic cells displayed an elevated cell cycle activity, which again is in line with the increased proliferation in these tumors and can be directly observed as an increase in Ki67-positive cells in immunohistochemistry. Similarly, the activity in epithelial-mesenchymal transition for MC mal neoplastic cells can be inferred to be the regulatory equivalent to the sheeting architecture often observed in the histology of high-grade meningiomas, where typical histological meningioma growth patterns are lost. On the level of differentially expressed genes, several genes of the HOX family displayed an increased expression in MC mal neoplastic cells. This further corroborates the hypothesis that HOX genes contribute to meningioma aggressiveness, as has been previously suggested based on the presence of a super enhancer near the *HOXD* gene locus and an upregulation of HOX genes in MC mal in bulk analyses (Paramasivam et al. 2019).

Having compared the tumor cell population as a whole between samples in a pseudobulk fashion, I subsequently leveraged the full potential of single cell sequencing to identify intratumoral subpopulations of neoplastic cells and how they overlap between tumor subgroups. This allows for the identification of cellular subpopulations associated with aggressiveness, with the ultimate goal to discern what cellular phenotypes are correlated to a higher risk of tumor progression and recurrence. Here, I have identified six tumor cell subpopulations with distinct phenotypes that could be identified across samples. Proportions at which each of the subpopulations was present varied between MCs, but partially also between samples within each MC, preventing conclusions on the role of each subpopulation in tumor progression. Yet, enrichments of subpopulations in groups of specific clinical presentation could be found: Once again, the proportion of the cycling neoplastic cell population increased with malignancy, corresponding to the definition of higher grade meningiomas according to the number of mitoses

(Louis et al. 2021). A neoplastic cell subpopulation with elevated activity in the KRAS signaling pathway tended to be more prominent in MC ben-2 and ben-3 tumors as compared to the remaining MCs that are characterized by a loss of *NF2*. This is in line with results from the analysis of phosphoproteomic data on bulk level, where I have found an increased activity of *MAPK1*/ERK2 and *MAPK3*/ERK1, both downstream targets of Ras in the MAPK signaling pathway, to be significantly enriched in MC ben-2 meningiomas. Merlin, the gene product of *NF2*, has previously been demonstrated to be necessary for accurate regulation of Ras (Cui et al. 2019). Surprisingly, Merlin appears to suppress Ras activity in an indirect manner (Morrison et al. 2007). This is contradictory to the observation I made here. However, I have not investigated the activity in the KRAS signaling pathway in direct correlation to *NF2* expression, which might not be present in the same cell population. On the other hand, a cellular subpopulation with increased activity in oxidative phosphorylation displayed an inverse pattern in abundancy, with high proportions in the ben-1, intermediate, and malignant MCs and decreased proportions in MCs ben-2 and ben-3. Previously, complexes involved in oxidative phosphorylation have been demonstrated to be downregulated in WHO grade 1 meningiomas compared to higher grade tumors (Feichtinger et al. 2016). A hypermetabolic meningioma subgroup was also observed in the Toronto methylation classification system, with enrichment in metabolic pathways such as the electron transport chain, fatty acid oxidation, and mitochondrial translation (Nassiri, Liu, et al. 2021). This could be reflective of a dominating presence of the cellular subpopulation that I identified on single cell level. A neoplastic cell population expressing genes related to cell adhesion was observed at increased proportions at the benign MCs compared to the intermediate and malignant MCs, which could be indicative of the tumor's ability to invade surrounding structures or metastasize. However, this subpopulation rarely composed the majority of neoplastic cells, even for low-risk cases. Altogether, the results did not provide sufficient evidence to determine a subpopulation of neoplastic cells with a clear tendency to progress or metastasize. A larger cohort, possibly including more primary and recurrent tumor pairs of the same patient, could help identify such a population. In addition, the cellular subpopulations established here remain to be validated in an independent dataset.

4.3. Vascular origin in angiomatous meningioma

Dissecting tumor cells from non-tumor cells was not only important to gather differential expression profiles specific to the neoplastic cell population, but also of specific relevance in the context of angiomatous meningiomas. This usually benign histological subtype is characterized by exceptionally high vascularization. Thus far, it has not been investigated what causes the high vascularization in these tumors and where the endothelial structures originate from. Here, I

demonstrated that the vessels are formed not by the neoplastic cells themselves, but by infiltrating endothelial cells. Most likely, the endothelial cells are recruited into the tumor tissue by the neoplastic cells expressing the vascular endothelial growth factors *VEGFA/B* as well as *SLIT2*. While the role of *SLIT2* in meningioma has not been studied thus far, a positive correlation has been previously shown for *VEGFA* expression on neoplastic cells with the expression of its receptors on vessels in meningioma (Bernatz et al. 2021). Interestingly, this study demonstrated a correlation of high *VEGFA* expression with a decreased overall survival of patients. However, only WHO grade 2 and 3 meningiomas were investigated, thus likely missing the angiomatous meningioma subtype that typically presents at WHO grade 1. Besides that, several studies have investigated VEGF in the context of meningiomas with contradicting results, some demonstrating a correlation of its expression with malignancy, others an absence thereof (Lamszus et al. 2000; Barresi and Tuccari 2010). A possible explanation would be that angiomatous meningiomas are a special case, in which high vascularization is not associated with increased malignancy, while this might still be the case for other meningioma subtypes, hence introducing a bias when investigating the relationship of VEGF and tumor grade in meningiomas.

4.4. Molecular risk factors at single cell level

Besides leveraging the single cell transcriptomic data to characterize phenotypic changes in neoplastic cell populations, I have applied the dataset to investigate the behavior of known molecular risk factors in meningioma on cellular level. The homozygous loss of the *CDKN2A/B* gene locus has for example been integrated in the recent WHO grading, promptly assigning tumors to WHO grade 3 if present (Louis et al. 2021). Interestingly, I demonstrated here that on bulk level, both *CDKN2A* and its gene product p16 displayed an increased expression in malignant MC tumors compared to low-grade tumors in those cases without deletion of the gene locus. I subsequently deployed the scRNA-Seq dataset to investigate whether this expression increase was a general mechanism in the neoplastic cell population. Indeed, *CDKN2A* expression was universally increased in the neoplastic cells of MC mal tumors without *CDKN2A/B* deletion. A comparison with ATAC-Seq data in addition revealed a high accessibility of the gene locus in these cases. One hypothesis to explain the correlation of malignancy in meningioma with increased *CDKN2A* expression as well as homozygous deletion of its gene locus would be that expression of the cell cycle inhibitor *CDKN2A* is upregulated as a means to counteract the elevated proliferation rate with increasing malignancy. Due to the higher accessibility of the gene locus that this entails, this locus may be more prone to deletion, thus eliminating an important check point to prevent cells from proliferation. However, the regulatory mechanisms to support this hypothesis remain to be investigated.

Another molecular risk factor in meningioma is an increased activity of *FOXM1* (Paramasivam et al. 2019). By investigating *FOXM1* activity on single cell level, I demonstrated here that the observed increase in activity is in fact not generally observed across the neoplastic cell population but limited to a subset of cells. This subset of cells with elevated *FOXM1* activity corresponded to neoplastic cells undergoing cell cycle. As *FOXM1* plays an important role during cell cycle progression (Wierstra and Alves 2007), its elevated activity in malignant cases could be simply reflective of the high proliferation rate. Nonetheless, *FOXM1* might have an impact on driving this increase in proliferation in aggressive meningioma. Further investigations will be required to elucidate the mechanisms of action for *FOXM1* in meningioma.

4.5. The role of the immune compartment in meningioma progression

Having investigated the transcriptomic signatures of the neoplastic cells in detail, a logical next step was to further dissect the infiltrating immune cells which were also captured in the scRNA-Seq dataset. A huge disparity in numbers depending on MC already indicated pronounced differences in the immune microenvironment between tumor subgroups. MC ben-1 tumors displayed a significantly higher number of infiltrating TAMs compared to MC mal meningiomas. Since TAMs can have both tumor promoting as well as tumor suppressing effects, I next examined the phenotypes of the TAMs across subtypes. TAMs in MC mal meningiomas displayed activity in the IL-4 and IL-13 signaling pathway as well as the IL-6 signaling pathway. Both have been demonstrated to execute roles promoting tumor growth and progression (Suzuki et al. 2015; Hirano 2021). TAMs infiltrating ben-1 tumors on the other hand exhibited activity in anti-tumorigenic pathways such as the IL-2 and the IL-21 signaling pathway (Waldmann 2018). Considering both the variation in numbers of infiltrating TAMs as well as their differing activation status, these results strongly suggest an important role of the TAM population in tumor progression. Possibly, the number and anti-tumorigenic phenotype of the TAMs in MC ben-1 meningiomas could be preventative of tumor progression and only if lost, the tumor will adapt a more aggressive phenotype. It could also be that the neoplastic cells actively influence the infiltration and phenotype of the TAMs and thus create a TME that is favorable to them. This would be supported by the interaction between *CSF1* expressed by neoplastic cells and *CSF1R* on the cellular membrane of TAMs that I predicted in my analyses here for the MC ben-1 and int-A cases with high immune infiltration. Considering that the *CSF1* gene is located on chromosome 1p, a gene locus that is frequently deleted in high-grade meningioma, this mechanism of TAM recruitment could be lost during tumor progression. In the end, it remains to be investigated whether the TAM population is shaped by the neoplastic cells depending on their aggressivity or

whether the TAMs themselves determine the ability of the neoplastic cells to progress. Both might be the case, but the exact mechanisms of either remain to be elucidated.

To better correlate the presence of infiltrating TAMs with patient outcome, I deconvoluted epigenomic data with available information on progression-free survival for the immune compartment. Thereby I discovered a positive correlation of the proportion of infiltrating immune cells with the progression-free survival. For WHO grade 1 and 2 tumors, this was true even within the respective WHO grade. This could have important implications for prognosis, as for WHO grade 1 and 2 meningiomas risk stratification if often difficult. TAM infiltration could however be easily and cost-effectively determined by immunohistochemistry to aid risk stratification for these cases in the future.

4.6. Ferroptosis as cell death-inducing process in meningioma

Through the analysis of spatial sequencing data, I in addition investigated the spatial distribution of infiltrating TAMs within the tumor tissue. While no specific enrichment could be observed in benign cases, an accumulation of TAMs could be observed in the perinecrotic regions in those MC mal/WHO grade 3 tumors with necrosis. The same region further displayed an increased expression of metallothioneins. Metallothioneins are cytoplasmatic proteins with the ability to bind metals (Dai et al. 2021). They have been demonstrated to be expressed in meningiomas, with increasing frequency in WHO grade 2 and 3 meningiomas (Tews et al. 2001). As WHO grade 1 meningiomas rarely present with necrosis, this could at least be partially explained with their association to perinecrotic regions as I have detected here. In addition, metallothioneins have been illustrated to enhance an inflammatory response to an LPS stimulus in macrophages (Dai et al. 2021). This could further contribute to the phenotypical shift in the TAMs of malignant as compared to benign tumors. As iron-chelators, metallothioneins also exert an anti-ferroptotic role by sequestering excessive iron (Sun et al. 2016). Ferroptosis is an alternative pathway leading to cell death and relies mainly on the oxidative damage caused by iron (Chen et al. 2015). Since I have observed the expression of ferroptosis-related genes within the perinecrotic regions as well, the increased metallothionein expression could be the result of an attempt to counteract the underlying processes causative for ferroptosis. Previously, *NF2* loss has been shown to promote ferroptosis in meningioma cells (Bao et al. 2021). The same study demonstrated that the induction of ferroptosis was thereby dependent on cell density. Considering that apoptotic and necrotic markers were absent in perinecrotic regions, one could hypothesize that ferroptosis plays an important role in causing cell death in the tumor center with high cell density. This susceptibility to ferroptosis could be leveraged in novel therapy approaches

by triggering ferroptotic processes in meningioma. However, ferroptosis as well as the possibility to target it therapeutically has not been sufficiently studied in meningioma thus far.

4.7. Prognostic value of methylation classification systems

Despite recent advances with the establishment of molecular markers, risk prediction remains difficult in many cases for meningioma patients. Especially for *NF2*-mutated cases that occur at the entire bandwidth of WHO grades for meningioma, tumors that later progress or recur are sometimes initially classified as WHO grade 1. A more accurate risk prediction would be highly valuable for patients and selection of the treatment strategy. Several studies have attempted to tackle this problem by introducing molecular classification systems based on the epigenome of the tumors (Sahm et al. 2017; Nassiri, Liu, et al. 2021; Choudhury, Magill, et al. 2022). Two of these, the classification system of UCSF and Toronto, share a subgroup of meningiomas without the frequent *NF2* mutation. This is also reflected in the MC ben-2 of the Heidelberg classification system, which usually does not harbor a mutation in *NF2* or a loss of chromosome 22q, comprising the *NF2* gene locus. Both the UCSF and the Toronto classification systems further harbor an immune-enriched meningioma subgroup. Similarly, I have found the Heidelberg MC ben-1 and a subset of MC int-A here to display a high amount of immune infiltration, making up the counterpart for the immune-enriched subgroup. I confirmed this by applying the UCSF classifier to the dataset here, where MC ben-1 samples and a subset of MC int-A samples, consistently those with high immune infiltration, typically were assigned to the immune-enriched subgroup. However, the deconvolution for the immune cells that I performed on the epigenomic data revealed not two distinct groups in the distribution of proportion of immune cells, but a continuum in immune infiltration. This indicates that an immune-enriched subgroup is possibly not that clearly to be separated. Nevertheless, it reflects the beneficial outcome for patients with an increased immune infiltration. A possible way to implement this in the clinic with direct impact for patients would be to analyze the immune infiltration through immunohistochemistry and define a high immune infiltration as indicator for a low risk of progression. The by far more cost and time intensive molecular profiling would then only have to be performed for the remaining cases. However, a suitable cutoff would have to be defined and extensively validated in further studies.

Among the existing methylation classification systems, risk stratification with the UCSF and the Toronto classifier leads to comparable results, with largely overlapping subgroups between both (Choudhury, Chen, et al. 2022). Parallels can also be observed to the Heidelberg classifier. However, the Heidelberg classifier comprises additional groups, especially two intermediate MCs with no immediate counterpart in the other two classification systems. Here, I demonstrated that

the Heidelberg classifier allows for an improved risk stratification as compared to the UCSF classification system, both if including the immune infiltration status and if not. In both cases however the epigenomic classification was superior to the WHO grading, and for both classification systems including the immune infiltration status improved risk stratification. This was especially remarkable for the UCSF classifier, as this classification system already considers an immune-enriched subgroup.

Altogether, these results suggest a further use of the Heidelberg methylation classification for risk stratification in combination with the evaluation of the immune infiltration. How the immune status is best integrated will have to be validated in further studies, ideally with a prospective patient cohort.

V. Conclusion & Future Perspectives

5.1. Conclusion

In this thesis, I have conclusively investigated the inter- and intratumoral heterogeneity of tumor cell populations as well as of infiltrating immune cells with specific focus on tumor-infiltrating TAMs in meningiomas. Thereby, I have identified broad changes in the expression profiles of neoplastic cells between tumor subgroups, which are partially reflected in the tumor's histopathology. Furthermore, I have discovered six tumor cell subpopulations with distinct phenotypes that could be detected across samples, with varying abundancies depending on the tumor grade. Besides these differences in the tumor expression profiles, I have unveiled significant differences between tumor subgroups with respect to the infiltrating immune cells, especially infiltrating TAMs, in terms of numbers as well as activation status. TAMs were thereby highly abundant in the low-grade MC ben-1 meningiomas, but only present at small numbers in high-grade MC mal meningiomas. Their activation transitioned from an anti-tumorigenic status in MC ben-1 tumors to a pro-tumorigenic activation in MC mal tumors. Given this profound variability, TAMs seem to play a crucial role in guiding tumor progression. The TAM population could thereby influence the tumor cells' ability to progress, while the tumor cells in high-grade cases at the same time might shape TAM infiltration as well as their activation status to their favor. Altogether, the immune microenvironment is thereby possibly an interesting target that could be leveraged in novel therapy approaches in meningioma.

Furthermore, I have highlighted the coherence of epigenetic subgroups in meningiomas across molecular levels as well as their importance in risk stratification. Despite the MCs having been defined purely based on the tumor epigenome, these subgroups were recapitulated when jointly grouping according to the transcriptome and proteome. This underlines the fact that the differences on the regulatory upstream level of DNA methylation propagate further downstream to transcriptional and translational processes, resulting in phenotypical differences. Epigenomic classification for meningiomas has gained prognostic value and has been included in the recent 2021 WHO classification. I have demonstrated here that among existing methylation classification systems, the Heidelberg methylation classifier appears to be superior. However, it could be further refined by including information on the immune status for risk stratification, as patients with high immune infiltration have a significantly improved progression-free survival. Examination of the immune status could therefore easily be integrated during tumor grading to improve risk stratification for patients.

5.2. Limitations & future perspectives

Despite the relevant conclusions with impact on risk stratification and potential therapeutic targets in meningioma, some key aspects remain topic for further research to substantiate the findings of this thesis.

Importantly, although distinct tumor cell subpopulations with differing phenotypes have been defined which can be present simultaneously within the same tumor, their impact on the tumor's ability to progress and metastasize still has to be elucidated. First, their presence will have to be validated in another, independent meningioma dataset. Then, a potentially bigger cohort with information on progression-free survival of patients could aid the stratification of the risk that each of the subpopulation carries for tumor recurrence. Ideally, the cohort would further contain more primary and recurrent tumor sample pairs from the same patient, so that the abundance of the subpopulations could be extensively compared before and after tumor recurrence.

Furthermore, the mechanisms of interaction between tumor cells and TAMs remain to be elucidated. While I have demonstrated the differences in TAM infiltration and activation between tumor subgroups and have identified the *CSF1*/*CSF1R* ligand-receptor pair as possible way of interaction between tumor cells and TAMs, the exact effects that TAMs exert on tumor cells and vice versa still need to be investigated. Further insights on the ongoing regulatory mechanisms would then also allow inferences on possibilities to leverage the involvement on TAMs in tumor progression for novel therapy approaches.

While I have shown in detail how the immune infiltration positively correlates to the progression-free survival, I have not drawn final conclusions how this could be applied in a clinical setting. In an immediate next step, the correspondence of the results from my deconvolution approach from DNA methylation to estimate the proportion of infiltrating immune cells with the quantification of infiltrating TAMs via immunohistochemistry would have to be established. Should both be in line as expected, immunohistochemistry could be applied to estimate immune infiltration and render the more time and cost consuming molecular profiling unnecessary in a subset of cases that were thereby assigned a low risk of progression. Ideally, criteria for assigning tumors to a subgroup of samples with high immune infiltration based on immunohistochemistry would be defined in a retrospective cohort and its significant difference in patient outcome validated in a prospective cohort. If it is thereby possible to define criteria to assign meningiomas a low risk based on this, this could possibly make molecular profiling unnecessary for these cases. At least however, it would greatly aid risk stratification for patients.

Bibliography

Abedalthagafi, Malak, Wenya Linda Bi, Ayal A. Aizer, Parker H. Merrill, Ryan Brewster, Pankaj K. Agarwalla, Marc L. Listewnik, et al. 2016. 'Oncogenic PI3K Mutations Are as Common as AKT1 and SMO Mutations in Meningioma'. *Neuro-Oncology* 18 (5): 649–55. https://doi.org/10.1093/neuonc/nov316.

Ahronowitz, Iris, Winnie Xin, Rosemary Kiely, Katherine Sims, Mia MacCollin, and Fabio P. Nunes. 2007. 'Mutational Spectrum of the NF2 Gene: A Meta-Analysis of 12 Years of Research and Diagnostic Laboratory Findings'. *Human Mutation* 28 (1): 1–12. https://doi.org/10.1002/humu.20393.

Alvarez, Mariano J., Yao Shen, Federico M. Giorgi, Alexander Lachmann, B. Belinda Ding, B. Hilda Ye, and Andrea Califano. 2016. 'Functional Characterization of Somatic Mutations in Cancer Using Network-Based Inference of Protein Activity'. *Nature Genetics* 48 (8): 838–47. https://doi.org/10.1038/ng.3593.

Aran, Dvir. 2020. 'Cell-Type Enrichment Analysis of Bulk Transcriptomes Using XCell'. *Methods in Molecular Biology (Clifton, N.J.)* 2120: 263–76. https://doi.org/10.1007/978-1-0716-0327-7_19.

Aran, Dvir, Agnieszka P. Looney, Leqian Liu, Esther Wu, Valerie Fong, Austin Hsu, Suzanna Chak, et al. 2019. 'Reference-Based Analysis of Lung Single-Cell Sequencing Reveals a Transitional Profibrotic Macrophage'. *Nature Immunology* 20 (2): 163–72. https://doi.org/10.1038/s41590-018-0276-y.

Bao, Zhongyuan, Lingyang Hua, Yangfan Ye, Daijun Wang, Chong Li, Qing Xie, Hiroaki Wakimoto, Ye Gong, and Jing Ji. 2021. 'MEF2C Silencing Downregulates NF2 and E-Cadherin and Enhances Erastin-Induced Ferroptosis in Meningioma'. *Neuro-Oncology* 23 (12): 2014–27. https://doi.org/10.1093/neuonc/noab114.

Barresi, Valeria, and Giovanni Tuccari. 2010. 'Increased Ratio of Vascular Endothelial Growth Factor to Semaphorin3A Is a Negative Prognostic Factor in Human Meningiomas'. *Neuropathology* 30 (5): 537–46. https://doi.org/10.1111/j.1440-1789.2010.01105.x.

Behling, Felix, Christina Fodi, Irina Gepfner-Tuma, Kristina Kaltenbach, Mirjam Renovanz, Frank Paulsen, Marco Skardelly, et al. 2021. 'H3K27me3 Loss Indicates an Increased Risk of Recurrence in the Tübingen Meningioma Cohort'. *Neuro-Oncology* 23 (8): 1273–81. https://doi.org/10.1093/neuonc/noaa303.

Bernatz, Simon, Daniel Monden, Florian Gessler, Tijana Radic, Elke Hattingen, Christian Senft, Volker Seifert, et al. 2021. 'Influence of VEGF-A, VEGFR-1-3, and Neuropilin 1-2 on Progression-Free: And Overall Survival in WHO Grade II and III Meningioma Patients'. *Journal of Molecular Histology* 52 (2): 233–43. https://doi.org/10.1007/s10735-020-09940-2.

Brastianos, Priscilla K., Peleg M. Horowitz, Sandro Santagata, Robert T. Jones, Aaron McKenna, Gad Getz, Keith L. Ligon, et al. 2013. 'Genomic Sequencing of Meningiomas Identifies Oncogenic SMO and AKT1 Mutations'. *Nature Genetics* 45 (3): 285–89. https://doi.org/10.1038/ng.2526.

Buerki, Robin A, Craig M Horbinski, Timothy Kruser, Peleg M Horowitz, Charles David James, and Rimas V Lukas. 2018. 'An Overview of Meningiomas'. *Future Oncology* 14 (21): 2161–77. https://doi.org/10.2217/fon-2018-0006.

Capper, David, Damian Stichel, Felix Sahm, David T. W. Jones, Daniel Schrimpf, Martin Sill, Simone Schmid, et al. 2018. 'Practical Implementation of DNA Methylation and Copy-Number-Based CNS Tumor Diagnostics: The Heidelberg Experience'. *Acta Neuropathologica* 136 (2): 181–210. https://doi.org/10.1007/s00401-018-1879-y.

Carpten, John D., Andrew L. Faber, Candice Horn, Gregory P. Donoho, Stephen L. Briggs, Christiane M. Robbins, Galen Hostetter, et al. 2007. 'A Transforming Mutation in the Pleckstrin Homology Domain of AKT1 in Cancer'. *Nature* 448 (7152): 439–44. https://doi.org/10.1038/nature05933.

Chen, Fei, Xueqian Zhuang, Liangyu Lin, Pengfei Yu, Ying Wang, Yufang Shi, Guohong Hu, and Yu Sun. 2015. 'New Horizons in Tumor Microenvironment Biology: Challenges and Opportunities'. *BMC Medicine* 13 (March): 45. https://doi.org/10.1186/s12916-015-0278-7.

Choudhury, Abrar, William C. Chen, Calixto-Hope G. Lucas, James C. Bayley, Akdes S. Harmanci, Sybren L. N. Maas, Sandro Santagata, et al. 2022. 'Hypermitotic Meningiomas Harbor DNA Methylation Subgroups with Distinct Biological and Clinical Features'. *Neuro-Oncology*, October, noac224. https://doi.org/10.1093/neuonc/noac224.

Choudhury, Abrar, Stephen T. Magill, Charlotte D. Eaton, Briana C. Prager, William C. Chen, Martha A. Cady, Kyounghee Seo, et al. 2022. 'Meningioma DNA Methylation Groups Identify Biological Drivers and Therapeutic Vulnerabilities'. *Nature Genetics* 54 (5): 649–59. https://doi.org/10.1038/s41588-022-01061-8.

Clark, Victoria E., E. Zeynep Erson-Omay, Akdes Serin, Jun Yin, Justin Cotney, Koray Özduman, Timuçin Avşar, et al. 2013. 'Genomic Analysis of Non-NF2 Meningiomas Reveals Mutations in TRAF7, KLF4, AKT1, and SMO'. *Science* 339 (6123): 1077–80. https://doi.org/10.1126/science.1233009.

Coscia, Fabian, Sophia Doll, Jacob Mathias Bech, Lisa Schweizer, Andreas Mund, Ernst Lengyel, Jan Lindebjerg, Gunvor Iben Madsen, José Ma Moreira, and Matthias Mann. 2020. 'A Streamlined Mass Spectrometry-Based Proteomics Workflow for Large-Scale FFPE Tissue Analysis'. *The Journal of Pathology* 251 (1): 100–112. https://doi.org/10.1002/path.5420.

Cui, Yan, Susann Groth, Scott Troutman, Annemarie Carlstedt, Tobias Sperka, Lars Björn Riecken, Joseph L. Kissil, Hongchuan Jin, and Helen Morrison. 2019. 'The NF2 Tumor Suppressor Merlin Interacts with Ras and RasGAP, Which May Modulate Ras Signaling'. *Oncogene* 38 (36): 6370–81. https://doi.org/10.1038/s41388-019-0883-6.

Dai, Hanying, Lu Wang, Lingyun Li, Zhong Huang, and Liang Ye. 2021. 'Metallothionein 1: A New Spotlight on Inflammatory Diseases'. *Frontiers in Immunology* 12. https://www.frontiersin.org/articles/10.3389/fimmu.2021.739918.

Davson, H., and M. Segal. 1996. 'Physiology of the CSF and Blood-Brain Barriers'. In . https://www.semanticscholar.org/paper/Physiology-of-the-CSF-and-Blood-Brain-Barriers-Davson-Segal/4c1131b1232d8f7a0cd8ee27c502ab8eea1dba96.

Dekkers, KF. 2019. 'Monocyte-to-Macrophage Differentiation Is Defined by Gain and Loss of DNA Methylation at Transcription Factor Binding Sites'. GEO. https://geo.metadataplus.biothings.io/geo/query/acc.cgi?acc=GSE118696.

Derk, Julia, Hannah E. Jones, Christina Como, Bradley Pawlikowski, and Julie A. Siegenthaler. 2021. 'Living on the Edge of the CNS: Meninges Cell Diversity in Health and Disease'. *Frontiers in Cellular Neuroscience* 15. https://www.frontiersin.org/articles/10.3389/fncel.2021.703944.

Dimitrov, Daniel, Dénes Türei, Martin Garrido-Rodriguez, Paul L. Burmedi, James S. Nagai, Charlotte Boys, Ricardo O. Ramirez Flores, et al. 2022. 'Comparison of Methods and Resources for Cell-Cell Communication Inference from Single-Cell RNA-Seq Data'. *Nature Communications* 13 (1): 3224. https://doi.org/10.1038/s41467-022-30755-0.

Dobin, Alexander, Carrie A. Davis, Felix Schlesinger, Jorg Drenkow, Chris Zaleski, Sonali Jha, Philippe Batut, Mark Chaisson, and Thomas R. Gingeras. 2013. 'STAR: Ultrafast Universal RNA-Seq Aligner'. *Bioinformatics (Oxford, England)* 29 (1): 15–21. https://doi.org/10.1093/bioinformatics/bts635.

Du, Ziming, Malak Abedalthagafi, Ayal A. Aizer, Allison R. McHenry, Heather H. Sun, Mark-Anthony Bray, Omar Viramontes, et al. 2015. 'Increased Expression of the Immune Modulatory

Molecule PD-L1 (CD274) in Anaplastic Meningioma'. *Oncotarget* 6 (7): 4704–16. https://doi.org/10.18632/oncotarget.3082.

Fang, Liangjuan, Daniel E. Lowther, Matthew L. Meizlish, Richard C. E. Anderson, Jeffrey N. Bruce, Lesley Devine, Anita J. Huttner, et al. 2013. 'The Immune Cell Infiltrate Populating Meningiomas Is Composed of Mature, Antigen-Experienced T and B Cells'. *Neuro-Oncology* 15 (11): 1479–90. https://doi.org/10.1093/neuonc/not110.

Feichtinger, René G., Serge Weis, Johannes A. Mayr, Franz A. Zimmermann, Barbara Bogner, Wolfgang Sperl, and Barbara Kofler. 2016. 'Alterations of Oxidative Phosphorylation in Meningiomas and Peripheral Nerve Sheath Tumors'. *Neuro-Oncology* 18 (2): 184–94. https://doi.org/10.1093/neuonc/nov105.

Franzén, Oscar, Li-Ming Gan, and Johan L M Björkegren. 2019. 'PanglaoDB: A Web Server for Exploration of Mouse and Human Single-Cell RNA Sequencing Data'. *Database* 2019 (January): baz046. https://doi.org/10.1093/database/baz046.

Garcia-Alonso, Luz, Christian H. Holland, Mahmoud M. Ibrahim, Denes Turei, and Julio Saez-Rodriguez. 2019. 'Benchmark and Integration of Resources for the Estimation of Human Transcription Factor Activities'. *Genome Research* 29 (8): 1363–75. https://doi.org/10.1101/gr.240663.118.

Gaujoux, Renaud, and Cathal Seoighe. 2010. 'A Flexible R Package for Nonnegative Matrix Factorization'. *BMC Bioinformatics* 11 (1): 367. https://doi.org/10.1186/1471-2105-11-367.

Gillespie, Marc, Bijay Jassal, Ralf Stephan, Marija Milacic, Karen Rothfels, Andrea Senff-Ribeiro, Johannes Griss, et al. 2022. 'The Reactome Pathway Knowledgebase 2022'. *Nucleic Acids Research* 50 (D1): D687–92. https://doi.org/10.1093/nar/gkab1028.

Ginhoux, Florent, Melanie Greter, Marylene Leboeuf, Sayan Nandi, Peter See, Solen Gokhan, Mark F. Mehler, et al. 2010. 'Fate Mapping Analysis Reveals That Adult Microglia Derive from Primitive Macrophages'. *Science* 330 (6005): 841–45. https://doi.org/10.1126/science.1194637.

Gomez Perdiguero, Elisa, Kay Klapproth, Christian Schulz, Katrin Busch, Emanuele Azzoni, Lucile Crozet, Hannah Garner, et al. 2015. 'Tissue-Resident Macrophages Originate from Yolk-Sac-Derived Erythro-Myeloid Progenitors'. *Nature* 518 (7540): 547–51. https://doi.org/10.1038/nature13989.

Goutagny, Stéphane, Jean C. Nault, Maxime Mallet, Dominique Henin, Jessica Z. Rossi, and Michel Kalamarides. 2014. 'High Incidence of Activating TERT Promoter Mutations in Meningiomas Undergoing Malignant Progression'. *Brain Pathology (Zurich, Switzerland)* 24 (2): 184–89. https://doi.org/10.1111/bpa.12110.

Haage, Verena, Marcus Semtner, Ramon Oliveira Vidal, Daniel Perez Hernandez, Winnie W. Pong, Zhihong Chen, Dolores Hambardzumyan, et al. 2019. 'Comprehensive Gene Expression Meta-Analysis Identifies Signature Genes That Distinguish Microglia from Peripheral Monocytes/Macrophages in Health and Glioma'. *Acta Neuropathologica Communications* 7 (1): 20. https://doi.org/10.1186/s40478-019-0665-y.

Han, Hai-xiong, and Jian-guo Geng. 2011. 'Over-Expression of Slit2 Induces Vessel Formation and Changes Blood Vessel Permeability in Mouse Brain'. *Acta Pharmacologica Sinica* 32 (11): 1327–36. https://doi.org/10.1038/aps.2011.106.

Hao, Yuhan, Stephanie Hao, Erica Andersen-Nissen, William M. Mauck, Shiwei Zheng, Andrew Butler, Maddie J. Lee, et al. 2021. 'Integrated Analysis of Multimodal Single-Cell Data'. *Cell* 184 (13): 3573-3587.e29. https://doi.org/10.1016/j.cell.2021.04.048.

Hassler, Melanie R., Walter Pulverer, Ranjani Lakshminarasimhan, Elisa Redl, Julia Hacker, Gavin D. Garland, Olaf Merkel, et al. 2016. 'Insights into the Pathogenesis of Anaplastic Large-Cell Lymphoma through Genome-Wide DNA Methylation Profiling'. *Cell Reports* 17 (2): 596–608. https://doi.org/10.1016/j.celrep.2016.09.018.

Hirano, Toshio. 2021. 'IL-6 in Inflammation, Autoimmunity and Cancer'. *International Immunology* 33 (3): 127–48. https://doi.org/10.1093/intimm/dxaa078.

Jin, Ming-Zhu, and Wei-Lin Jin. 2020. 'The Updated Landscape of Tumor Microenvironment and Drug Repurposing'. *Signal Transduction and Targeted Therapy* 5 (1): 1–16. https://doi.org/10.1038/s41392-020-00280-x.

Kalamarides, M., A. O. Stemmer-Rachamimov, M. Niwa-Kawakita, F. Chareyre, E. Taranchon, Z.-Y. Han, C. Martinelli, et al. 2011. 'Identification of a Progenitor Cell of Origin Capable of Generating Diverse Meningioma Histological Subtypes'. *Oncogene* 30 (20): 2333–44. https://doi.org/10.1038/onc.2010.609.

Katz, Leah M., Thomas Hielscher, Benjamin Liechty, Joshua Silverman, David Zagzag, Rajeev Sen, Peter Wu, et al. 2018. 'Loss of Histone H3K27me3 Identifies a Subset of Meningiomas with Increased Risk of Recurrence'. *Acta Neuropathologica* 135 (6): 955–63. https://doi.org/10.1007/s00401-018-1844-9.

Ketter, Ralf, Steffi Urbschat, Wolfram Henn, Wolfgang Feiden, Niko Beerenwinkel, Thomas Lengauer, Wolf-Ingo Steudel, Klaus D. Zang, and Jörg Rahnenführer. 2007. 'Application of Oncogenetic Trees Mixtures as a Biostatistical Model of the Clonal Cytogenetic Evolution of Meningiomas'. *International Journal of Cancer* 121 (7): 1473–80. https://doi.org/10.1002/ijc.22855.

Kim, H., K.-J. Park, B.-K. Ryu, D.-H. Park, D.-S. Kong, K. Chong, Y.-S. Chae, Y.-G. Chung, S. I. Park, and S.-H. Kang. 2020. 'Forkhead Box M1 (FOXM1) Transcription Factor Is a Key Oncogenic Driver of Aggressive Human Meningioma Progression'. *Neuropathology and Applied Neurobiology* 46 (2): 125–41. https://doi.org/10.1111/nan.12571.

Kim, Hyunsoo, and Haesun Park. 2007. 'Sparse Non-Negative Matrix Factorizations via Alternating Non-Negativity-Constrained Least Squares for Microarray Data Analysis'. *Bioinformatics (Oxford, England)* 23 (12): 1495–1502. https://doi.org/10.1093/bioinformatics/btm134.

Korsunsky, Ilya, Nghia Millard, Jean Fan, Kamil Slowikowski, Fan Zhang, Kevin Wei, Yuriy Baglaenko, Michael Brenner, Po-ru Loh, and Soumya Raychaudhuri. 2019. 'Fast, Sensitive and Accurate Integration of Single-Cell Data with Harmony'. *Nature Methods* 16 (12): 1289–96. https://doi.org/10.1038/s41592-019-0619-0.

Kresak, Jesse Lee, and Meggen Walsh. 2016. 'Neurofibromatosis: A Review of NF1, NF2, and Schwannomatosis'. *Journal of Pediatric Genetics* 5 (2): 98–104. https://doi.org/10.1055/s-0036-1579766.

Kuleshov, Maxim V., Matthew R. Jones, Andrew D. Rouillard, Nicolas F. Fernandez, Qiaonan Duan, Zichen Wang, Simon Koplev, et al. 2016. 'Enrichr: A Comprehensive Gene Set Enrichment Analysis Web Server 2016 Update'. *Nucleic Acids Research* 44 (W1): W90–97. https://doi.org/10.1093/nar/gkw377.

Lamszus, Katrin, Ulrike Lengler, Nils Ole Schmidt, Dimitrios Stavrou, Süleyman Ergün, and Manfred Westphal. 2000. 'Vascular Endothelial Growth Factor, Hepatocyte Growth Factor/Scatter Factor, Basic Fibroblast Growth Factor, and Placenta Growth Factor in Human Meningiomas and Their Relation to Angiogenesis and Malignancy'. *Neurosurgery* 46 (4): 938.

Lee, Young Suk, and Youn Soo Lee. 2020. 'Molecular Characteristics of Meningiomas'. *Journal of Pathology and Translational Medicine* 54 (1): 45–63. https://doi.org/10.4132/jptm.2019.11.05.

Li, Bo, and Colin N. Dewey. 2011. 'RSEM: Accurate Transcript Quantification from RNA-Seq Data with or without a Reference Genome'. *BMC Bioinformatics* 12 (1): 323. https://doi.org/10.1186/1471-2105-12-323.

Liberzon, Arthur, Chet Birger, Helga Thorvaldsdóttir, Mahmoud Ghandi, Jill P. Mesirov, and Pablo Tamayo. 2015. 'The Molecular Signatures Database (MSigDB) Hallmark Gene Set Collection'. *Cell Systems* 1 (6): 417–25. https://doi.org/10.1016/j.cels.2015.12.004.

Louis, David N., Arie Perry, Pieter Wesseling, Daniel J. Brat, Ian A. Cree, Dominique Figarella-Branger, Cynthia Hawkins, et al. 2021. 'The 2021 WHO Classification of Tumors of the Central

Nervous System: A Summary'. *Neuro-Oncology* 23 (8): 1231–51. https://doi.org/10.1093/neuonc/noab106.

Love, Michael I, Wolfgang Huber, and Simon Anders. 2014. 'Moderated Estimation of Fold Change and Dispersion for RNA-Seq Data with DESeq2'. *Genome Biology* 15 (12). https://doi.org/10.1186/s13059-014-0550-8.

Lucero, Rocco, Valentina Zappulli, Alessandro Sammarco, Oscar D. Murillo, Pike See Cheah, Srimeenakshi Srinivasan, Eric Tai, et al. 2020. 'Glioma-Derived MiRNA-Containing Extracellular Vesicles Induce Angiogenesis by Reprogramming Brain Endothelial Cells'. *Cell Reports* 30 (7): 2065-2074.e4. https://doi.org/10.1016/j.celrep.2020.01.073.

Maas, Sybren L. N., Damian Stichel, Thomas Hielscher, Philipp Sievers, Anna S. Berghoff, Daniel Schrimpf, Martin Sill, et al. 2021. 'Integrated Molecular-Morphologic Meningioma Classification: A Multicenter Retrospective Analysis, Retrospectively and Prospectively Validated'. *Journal of Clinical Oncology* 39 (34): 3839–52. https://doi.org/10.1200/JCO.21.00784.

Mabbott, Neil A., J. Kenneth Baillie, Helen Brown, Tom C. Freeman, and David A. Hume. 2013. 'An Expression Atlas of Human Primary Cells: Inference of Gene Function from Coexpression Networks'. *BMC Genomics* 14 (1): 632. https://doi.org/10.1186/1471-2164-14-632.

Maillo, Angel, Alberto Orfao, José María Sayagues, Pedro Diaz, Juan Antonio Gómez-Moreta, Marcelino Caballero, David Santamarta, Angel Santos-Briz, Francisco Morales, and María Dolores Tabernero. 2003. 'New Classification Scheme for the Prognostic Stratification of Meningioma on the Basis of Chromosome 14 Abnormalities, Patient Age, and Tumor Histopathology'. *Journal of Clinical Oncology: Official Journal of the American Society of Clinical Oncology* 21 (17): 3285–95. https://doi.org/10.1200/JCO.2003.07.156.

Mawrin, Christian, Tina Sasse, Elmar Kirches, Siegfried Kropf, Thomas Schneider, Christoph Grimm, Claudia Pambor, et al. 2005. 'Different Activation of Mitogen-Activated Protein Kinase and Akt Signaling Is Associated with Aggressive Phenotype of Human Meningiomas'. *Clinical Cancer Research* 11 (11): 4074–82. https://doi.org/10.1158/1078-0432.CCR-04-2550.

McGinnis, Christopher S., Lyndsay M. Murrow, and Zev J. Gartner. 2019. 'DoubletFinder: Doublet Detection in Single-Cell RNA Sequencing Data Using Artificial Nearest Neighbors'. *Cell Systems* 8 (4): 329-337.e4. https://doi.org/10.1016/j.cels.2019.03.003.

Mogensen, Ulla B., Hemant Ishwaran, and Thomas A. Gerds. 2012. 'Evaluating Random Forests for Survival Analysis Using Prediction Error Curves'. *Journal of Statistical Software* 050 (i11). https://ideas.repec.org//a/jss/jstsof/v050i11.html.

Morrison, Helen, Tobias Sperka, Jan Manent, Marco Giovannini, Helmut Ponta, and Peter Herrlich. 2007. 'Merlin/Neurofibromatosis Type 2 Suppresses Growth by Inhibiting the Activation of Ras and Rac'. *Cancer Research* 67 (2): 520–27. https://doi.org/10.1158/0008-5472.CAN-06-1608.

Murphy, J. F., and D. J. Fitzgerald. 2001. 'Vascular Endothelial Growth Factor Induces Cyclooxygenase-Dependent Proliferation of Endothelial Cells via the VEGF-2 Receptor'. *FASEB Journal: Official Publication of the Federation of American Societies for Experimental Biology* 15 (9): 1667–69. https://doi.org/10.1096/fj.00-0757fje.

Nassiri, Farshad, Jeff Liu, Vikas Patil, Yasin Mamatjan, Justin Z. Wang, Rupert Hugh-White, Andrew M. Macklin, et al. 2021. 'A Clinically Applicable Integrative Molecular Classification of Meningiomas'. *Nature* 597 (7874): 119–25. https://doi.org/10.1038/s41586-021-03850-3.

Nassiri, Farshad, Justin Z Wang, Olivia Singh, Shirin Karimi, Tatyana Dalcourt, Nazanin Ijad, Neda Pirouzmand, et al. 2021. 'Loss of H3K27me3 in Meningiomas'. *Neuro-Oncology* 23 (8): 1282–91. https://doi.org/10.1093/neuonc/noab036.

Ogasawara, Christian, Brandon D. Philbrick, and D. Cory Adamson. 2021. 'Meningioma: A Review of Epidemiology, Pathology, Diagnosis, Treatment, and Future Directions'. *Biomedicines* 9 (3): 319. https://doi.org/10.3390/biomedicines9030319.

Onuchic, Vitor. 2022. 'EDec: Cell Type Specific Analysis of Complex Tissues through Epigenomic Deconvolution'. R. BRL-BCM. https://github.com/BRL-BCM/EDec.

O'Rahilly, R., and F. Müller. 1986. 'The Meninges in Human Development'. *Journal of Neuropathology and Experimental Neurology* 45 (5): 588–608.

Ostrom, Quinn T, Gino Cioffi, Kristin Waite, Carol Kruchko, and Jill S Barnholtz-Sloan. 2021. 'CBTRUS Statistical Report: Primary Brain and Other Central Nervous System Tumors Diagnosed in the United States in 2014–2018'. *Neuro-Oncology* 23 (Suppl 3): iii1–105. https://doi.org/10.1093/neuonc/noab200.

Paramasivam, Nagarajan, Daniel Hübschmann, Umut H. Toprak, Naveed Ishaque, Marian Neidert, Daniel Schrimpf, Damian Stichel, et al. 2019. 'Mutational Patterns and Regulatory Networks in Epigenetic Subgroups of Meningioma'. *Acta Neuropathologica* 138 (2): 295–308. https://doi.org/10.1007/s00401-019-02008-w.

Picelli, Simone, Omid R. Faridani, Åsa K. Björklund, Gösta Winberg, Sven Sagasser, and Rickard Sandberg. 2014. 'Full-Length RNA-Seq from Single Cells Using Smart-Seq2'. *Nature Protocols* 9 (1): 171–81. https://doi.org/10.1038/nprot.2014.006.

Pinton, Laura, Samantha Solito, Elena Masetto, Marina Vettore, Stefania Canè, Alessandro Della Puppa, and Susanna Mandruzzato. 2018. 'Immunosuppressive Activity of Tumor-Infiltrating Myeloid Cells in Patients with Meningioma'. *Oncoimmunology* 7 (7): e1440931. https://doi.org/10.1080/2162402X.2018.1440931.

Rao, Anjali, Dalia Barkley, Gustavo S. França, and Itai Yanai. 2021. 'Exploring Tissue Architecture Using Spatial Transcriptomics'. *Nature* 596 (7871): 211–20. https://doi.org/10.1038/s41586-021-03634-9.

Ravi, Vidhya M., Paulina Will, Jan Kueckelhaus, Na Sun, Kevin Joseph, Henrike Salié, Lea Vollmer, et al. 2022. 'Spatially Resolved Multi-Omics Deciphers Bidirectional Tumor-Host Interdependence in Glioblastoma'. *Cancer Cell* 40 (6): 639-655.e13. https://doi.org/10.1016/j.ccell.2022.05.009.

Reuss, David E., Rosario M. Piro, David T. W. Jones, Matthias Simon, Ralf Ketter, Marcel Kool, Albert Becker, et al. 2013. 'Secretory Meningiomas Are Defined by Combined KLF4 K409Q and TRAF7 Mutations'. *Acta Neuropathologica* 125 (3): 351–58. https://doi.org/10.1007/s00401-013-1093-x.

Riemenschneider, Markus J, Arie Perry, and Guido Reifenberger. 2006. 'Histological Classification and Molecular Genetics of Meningiomas'. *The Lancet Neurology* 5 (12): 1045–54. https://doi.org/10.1016/S1474-4422(06)70625-1.

Robinson, Mark D., Davis J. McCarthy, and Gordon K. Smyth. 2010. 'EdgeR: A Bioconductor Package for Differential Expression Analysis of Digital Gene Expression Data'. *Bioinformatics* 26 (1): 139–40. https://doi.org/10.1093/bioinformatics/btp616.

Sahab-Negah, Sajad, and Ali Gorji. 2020. 'Meningioma Tumor Microenvironment'. In *Tumor Microenvironments in Organs: From the Brain to the Skin – Part B*, edited by Alexander Birbrair, 33–48. Advances in Experimental Medicine and Biology. Cham: Springer International Publishing. https://doi.org/10.1007/978-3-030-59038-3_3.

Sahm, Felix, Daniel Schrimpf, Adriana Olar, Christian Koelsche, David Reuss, Juliane Bissel, Annekathrin Kratz, et al. 2015. 'TERT Promoter Mutations and Risk of Recurrence in Meningioma'. *JNCI Journal of the National Cancer Institute* 108 (5). https://doi.org/10.1093/jnci/djv377.

Sahm, Felix, Daniel Schrimpf, Damian Stichel, David T. W. Jones, Thomas Hielscher, Sebastian Schefzyk, Konstantin Okonechnikov, et al. 2017. 'DNA Methylation-Based Classification and Grading System for Meningioma: A Multicentre, Retrospective Analysis'. *The Lancet. Oncology* 18 (5): 682–94. https://doi.org/10.1016/S1470-2045(17)30155-9.

Samanic, Claudine M., Anneclaire J. De Roos, Patricia A. Stewart, Preetha Rajaraman, Martha A. Waters, and Peter D. Inskip. 2008. 'Occupational Exposure to Pesticides and Risk of Adult Brain

Tumors'. *American Journal of Epidemiology* 167 (8): 976–85. https://doi.org/10.1093/aje/kwm401.

Schep, Alicia N., Beijing Wu, Jason D. Buenrostro, and William J. Greenleaf. 2017. 'ChromVAR: Inferring Transcription-Factor-Associated Accessibility from Single-Cell Epigenomic Data'. *Nature Methods* 14 (10): 975–78. https://doi.org/10.1038/nmeth.4401.

Shapiro, Geoffrey I. 2006. 'Cyclin-Dependent Kinase Pathways As Targets for Cancer Treatment'. *Journal of Clinical Oncology* 24 (11): 1770–83. https://doi.org/10.1200/JCO.2005.03.7689.

Sievers, Philipp, Thomas Hielscher, Daniel Schrimpf, Damian Stichel, David E. Reuss, Anna S. Berghoff, Marian C. Neidert, et al. 2020. 'CDKN2A/B Homozygous Deletion Is Associated with Early Recurrence in Meningiomas'. *Acta Neuropathologica* 140 (3): 409–13. https://doi.org/10.1007/s00401-020-02188-w.

Squair, Jordan W., Matthieu Gautier, Claudia Kathe, Mark A. Anderson, Nicholas D. James, Thomas H. Hutson, Rémi Hudelle, et al. 2021. 'Confronting False Discoveries in Single-Cell Differential Expression'. bioRxiv. https://doi.org/10.1101/2021.03.12.435024.

Stamenkovic, Ivan, and Qin Yu. 2010. 'Merlin, a "Magic" Linker Between the Extracellular Cues and Intracellular Signaling Pathways That Regulate Cell Motility, Proliferation, and Survival'. *Current Protein & Peptide Science* 11 (6): 471–84.

Stichel, Damian, Daniel Schrimpf, Belén Casalini, Jochen Meyer, Annika K. Wefers, Philipp Sievers, Andrey Korshunov, et al. 2019. 'Routine RNA Sequencing of Formalin-Fixed Paraffin-Embedded Specimens in Neuropathology Diagnostics Identifies Diagnostically and Therapeutically Relevant Gene Fusions'. *Acta Neuropathologica* 138 (5): 827–35. https://doi.org/10.1007/s00401-019-02039-3.

Stuart, Tim, Andrew Butler, Paul Hoffman, Christoph Hafemeister, Efthymia Papalexi, William M. Mauck, Yuhan Hao, Marlon Stoeckius, Peter Smibert, and Rahul Satija. 2019. 'Comprehensive Integration of Single-Cell Data'. *Cell* 177 (7): 1888-1902.e21. https://doi.org/10.1016/j.cell.2019.05.031.

Stuart, Tim, Avi Srivastava, Shaista Madad, Caleb A. Lareau, and Rahul Satija. 2021. 'Single-Cell Chromatin State Analysis with Signac'. *Nature Methods* 18 (11): 1333–41. https://doi.org/10.1038/s41592-021-01282-5.

Sun, Xiaofang, Xiaohua Niu, Ruochan Chen, Wenyin He, De Chen, Rui Kang, and Daolin Tang. 2016. 'Metallothionein-1G Facilitates Sorafenib Resistance through Inhibition of Ferroptosis'. *Hepatology* 64 (2): 488–500. https://doi.org/10.1002/hep.28574.

Suzuki, Akiko, Pamela Leland, Bharat H. Joshi, and Raj K. Puri. 2015. 'Targeting of IL-4 and IL-13 Receptors for Cancer Therapy'. *Cytokine*, IL 4/IL 13 family, 75 (1): 79–88. https://doi.org/10.1016/j.cyto.2015.05.026.

Takahashi, Hannah, Alex J. Cornish, Amit Sud, Philip J. Law, Linden Disney-Hogg, Lisa Calvocoressi, Lingeng Lu, et al. 2019. 'Mendelian Randomization Provides Support for Obesity as a Risk Factor for Meningioma'. *Scientific Reports* 9 (1): 309. https://doi.org/10.1038/s41598-018-36186-6.

Tews, Dominique S., Claudia Fleissner, Barbara Tiziani, and Andreas K. A. Gaumann. 2001. 'Intrinsic Expression of Drug Resistance-Associated Factors in Meningiomas'. *Applied Immunohistochemistry & Molecular Morphology* 9 (3): 242.

Therneau, Terry M., Thomas Lumley (original S.->R port and R. maintainer until 2009), Atkinson Elizabeth, and Crowson Cynthia. 2022. 'A Package for Survival Analysis in R'. https://CRAN.R-project.org/package=survival.

Tickle, Timothy, Itay Tirosh, Christophe Georgescu, Maxwell Brown, and Brian Haas. 2019. 'InferCNV of the Trinity CTAT Project.' Klarman Cell Observatory, Broad Institute of MIT and Harvard. https://doi.org/10.18129/B9.bioc.infercnv.

Torp, Sverre Helge, Ole Solheim, and Anne Jarstein Skjulsvik. 2022. 'The WHO 2021 Classification of Central Nervous System Tumours: A Practical Update on What Neurosurgeons Need to Know—a Minireview'. *Acta Neurochirurgica* 164 (9): 2453–64. https://doi.org/10.1007/s00701-022-05301-y.

Utz, Sebastian G., and Melanie Greter. 2019. 'Checking Macrophages at the Border'. *Nature Neuroscience* 22 (6): 848–50. https://doi.org/10.1038/s41593-019-0411-6.

Vasudevan, Harish N., Steve E. Braunstein, Joanna J. Phillips, Melike Pekmezci, Bryan A. Tomlin, Ashley Wu, Gerald F. Reis, et al. 2018. 'Comprehensive Molecular Profiling Identifies FOXM1 as a Key Transcription Factor for Meningioma Proliferation'. *Cell Reports* 22 (13): 3672–83. https://doi.org/10.1016/j.celrep.2018.03.013.

Veglia, Filippo, Emilio Sanseviero, and Dmitry I. Gabrilovich. 2021. 'Myeloid-Derived Suppressor Cells in the Era of Increasing Myeloid Cell Diversity'. *Nature Reviews Immunology* 21 (8): 485–98. https://doi.org/10.1038/s41577-020-00490-y.

Vizoso, Miguel, Marta Puig, F. Javier Carmona, María Maqueda, Adriana Velásquez, Antonio Gómez, Anna Labernadie, et al. 2015. 'Aberrant DNA Methylation in Non-Small Cell Lung Cancer-Associated Fibroblasts'. *Carcinogenesis* 36 (12): 1453–63. https://doi.org/10.1093/carcin/bgv146.

Waldmann, Thomas A. 2018. 'Cytokines in Cancer Immunotherapy'. *Cold Spring Harbor Perspectives in Biology* 10 (12): a028472. https://doi.org/10.1101/cshperspect.a028472.

Wang, Bo, Aziz Mezlini, Feyyaz Demir, Marc Fiume, Zhuowen Tu, Michael Brudno, Benjamin Haibe-Kains, and Anna Goldenberg. 2018. 'SNFtool: Similarity Network Fusion'. https://CRAN.R-project.org/package=SNFtool.

Wang, Xiliang, Yao He, Qiming Zhang, Xianwen Ren, and Zemin Zhang. 2021. 'Direct Comparative Analyses of 10X Genomics Chromium and Smart-Seq2'. *Genomics, Proteomics & Bioinformatics*, Single-cell Omics Analysis, 19 (2): 253–66. https://doi.org/10.1016/j.gpb.2020.02.005.

Weller, Roy O., Matthew M. Sharp, Myron Christodoulides, Roxana O. Carare, and Kjeld Møllgård. 2018. 'The Meninges as Barriers and Facilitators for the Movement of Fluid, Cells and Pathogens Related to the Rodent and Human CNS'. *Acta Neuropathologica* 135 (3): 363–85. https://doi.org/10.1007/s00401-018-1809-z.

Wiemels, Joseph, Margaret Wrensch, and Elizabeth B. Claus. 2010. 'Epidemiology and Etiology of Meningioma'. *Journal of Neuro-Oncology* 99 (3): 307–14. https://doi.org/10.1007/s11060-010-0386-3.

Wierstra, Inken, and Jürgen Alves. 2007. 'FOXM1, a Typical Proliferation-Associated Transcription Factor' 388 (12): 1257–74. https://doi.org/10.1515/BC.2007.159.

Wiredja, Danica D. 2017. 'KSEAapp: Kinase-Substrate Enrichment Analysis'. https://CRAN.R-project.org/package=KSEAapp.

Yuzawa, Sayaka, Hiroshi Nishihara, and Shinya Tanaka. 2016. 'Genetic Landscape of Meningioma'. *Brain Tumor Pathology* 33 (4): 237–47. https://doi.org/10.1007/s10014-016-0271-7.

Zadeh, Gelareh, Shirin Karimi, and Kenneth D. Aldape. 2016. 'PIK3CA Mutations in Meningioma'. *Neuro-Oncology* 18 (5): 603–4. https://doi.org/10.1093/neuonc/now029.

Zhang, X., H. Jia, Y. Lu, C. Dong, J. Hou, Z. Wang, F. Wang, H. Zhong, L. Wang, and K. Wang. 2014. 'Exome Sequencing on Malignant Meningiomas Identified Mutations in Neurofibromatosis Type 2 (NF2) and Meningioma 1 (MN1) Genes'. *Discovery Medicine* 18 (101): 301–11.

Zotti, Tiziana, Ivan Scudiero, Pasquale Vito, and Romania Stilo. 2017. 'The Emerging Role of TRAF7 in Tumor Development'. *Journal of Cellular Physiology* 232 (6): 1233–38. https://doi.org/10.1002/jcp.25676.

Supplement

Supplementary Figures

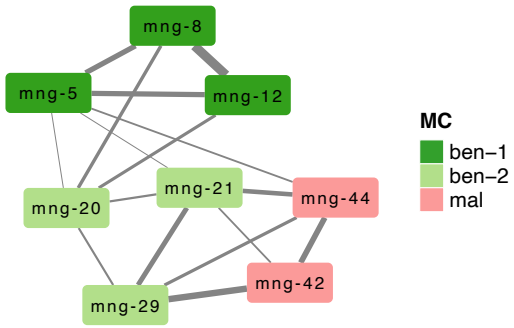

Supplementary Figure 1. *Similarity network fusion graph combining transcriptomic, proteomic, and phosphoproteomic data. Nodes represent samples, edges indicate similarity between samples. Edge widths are proportional to the extent of similarity.*

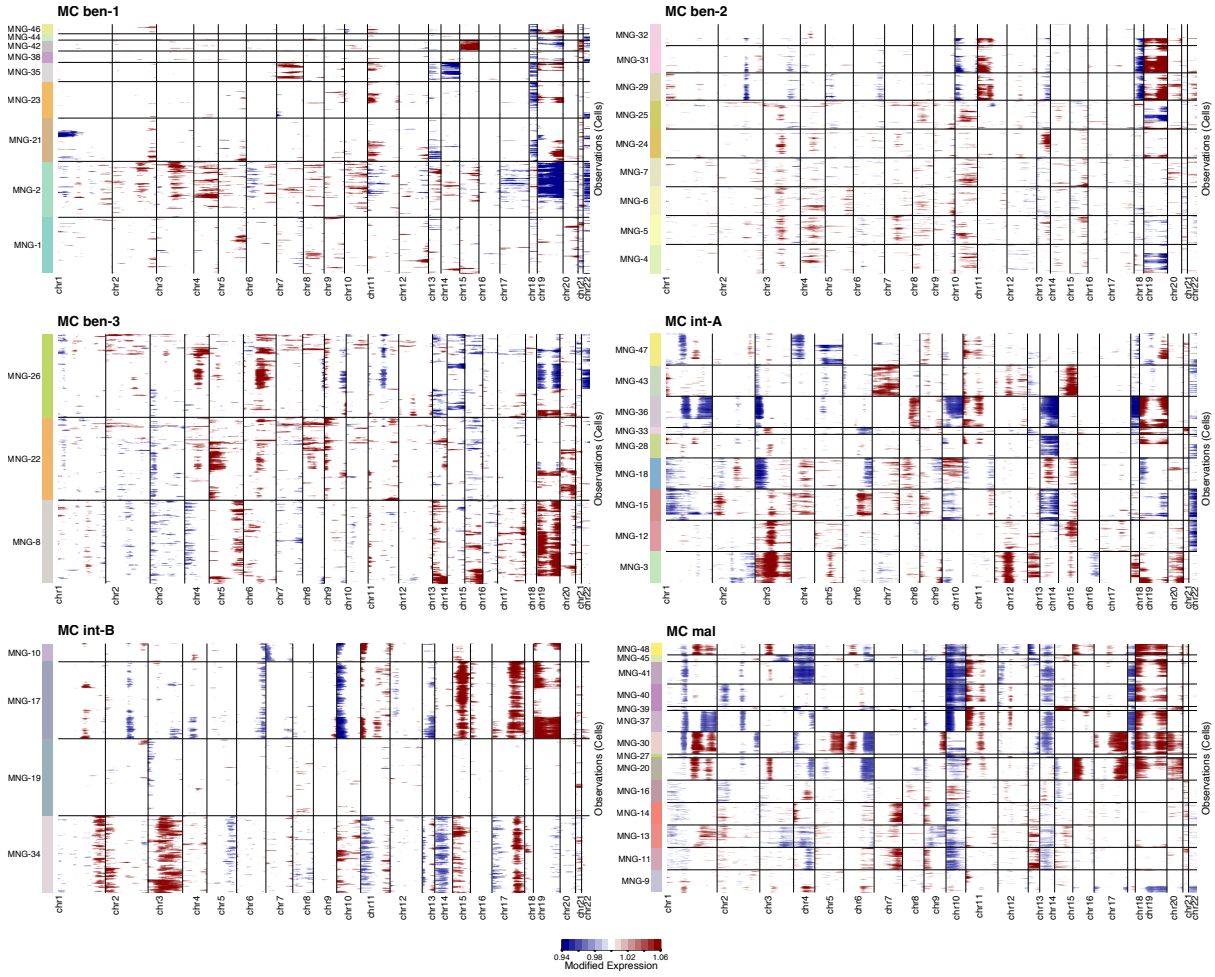

Supplementary Figure 2. *CNV profiles as estimated from single cellular expression profiles individually for each MC. Red color indicates chromosomal gains, blue color indicates chromosomal loss.*

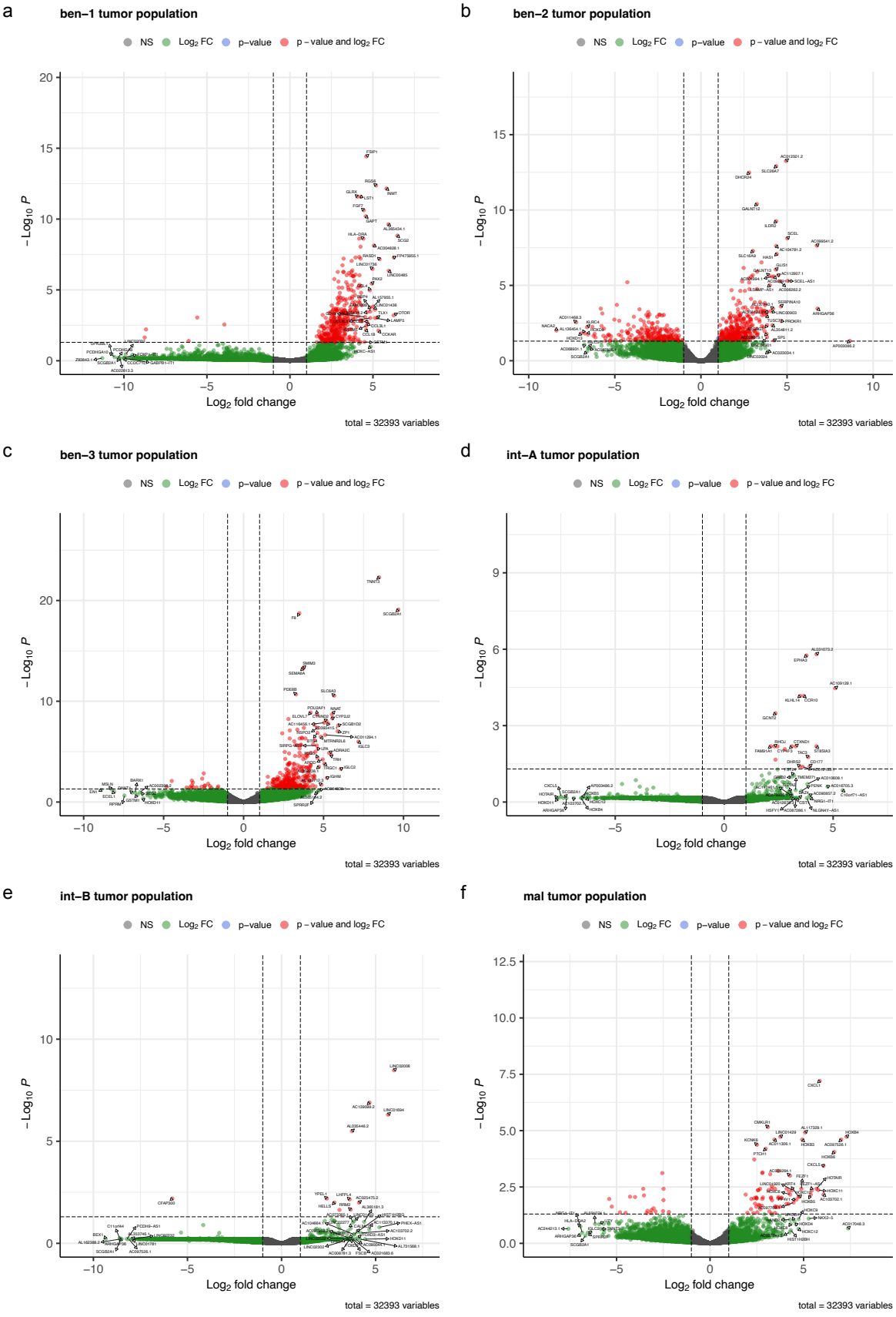

Supplementary Figure 3. *Differentially expressed genes between the neoplastic cells of one MC versus all other neoplastic cells. Genes with a higher expression in the respective MC have a positive log2FC.*

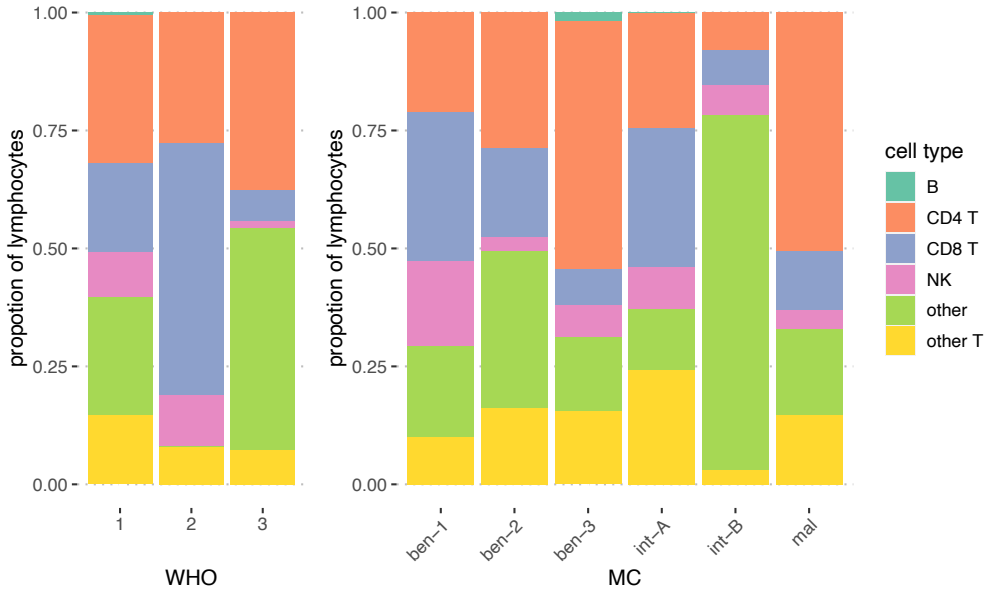

Supplementary Figure 4. *Proportion of lymphocyte subtypes in the total lymphocyte population of each WHO grade (left) and MC (right).*

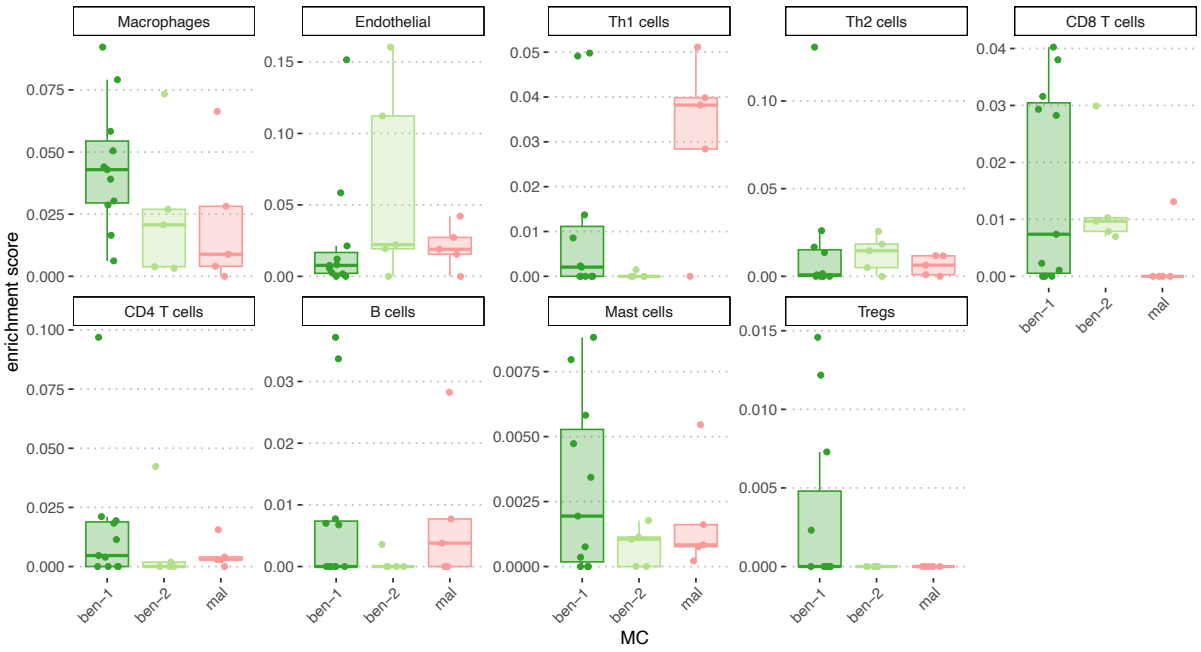

Supplementary Figure 5. *Cell type enrichment scores as estimated from bulk RNA-Seq data for selected infiltrating non-malignant cell types.*

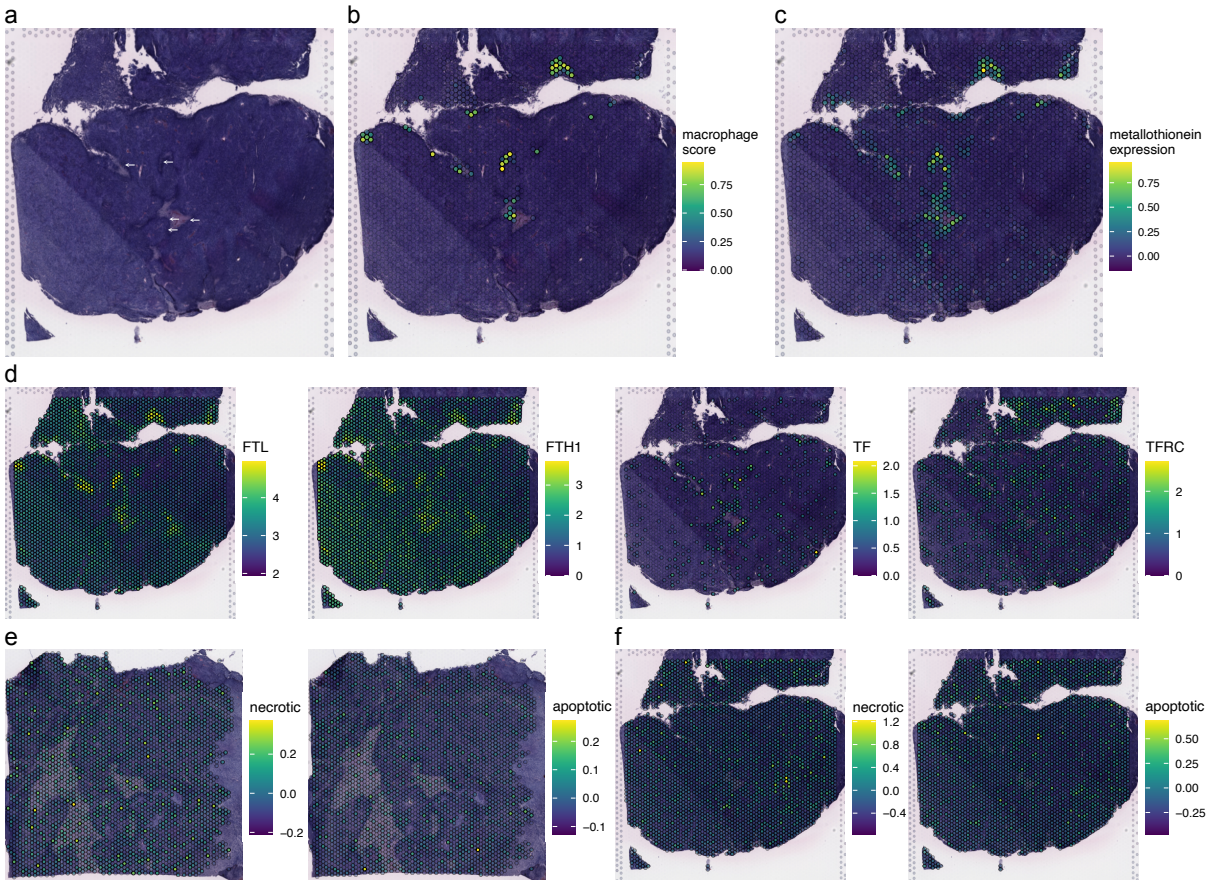

Supplementary Figure 6. ***a*** *H&E staining of a WHO grade 3 and MC mal meningioma with necrosis and perinecrotic zones (arrows).* ***b*** *Spot-wise enrichment score for macrophages as inferred from scRNA-Seq data for the MC mal meningioma from (a).* ***c*** *Spot-wise enrichment scores for metallothionein expression.* ***d*** *Spot-wise expression of four ferroptotic marker genes.* ***e,f*** *Spot-wise enrichment scores for necrotic (left) and apoptotic (right) marker genes in two MC mal meningiomas with histologically visible necrosis.*

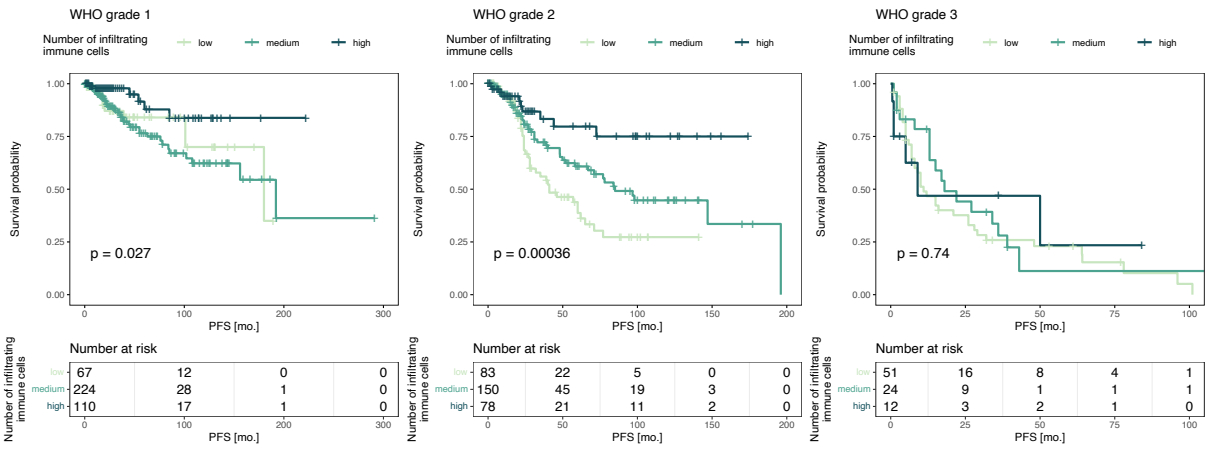

Supplementary Figure 7. *Progression free survival of patients depending on the number of infiltrating immune cells split by WHO grades.*

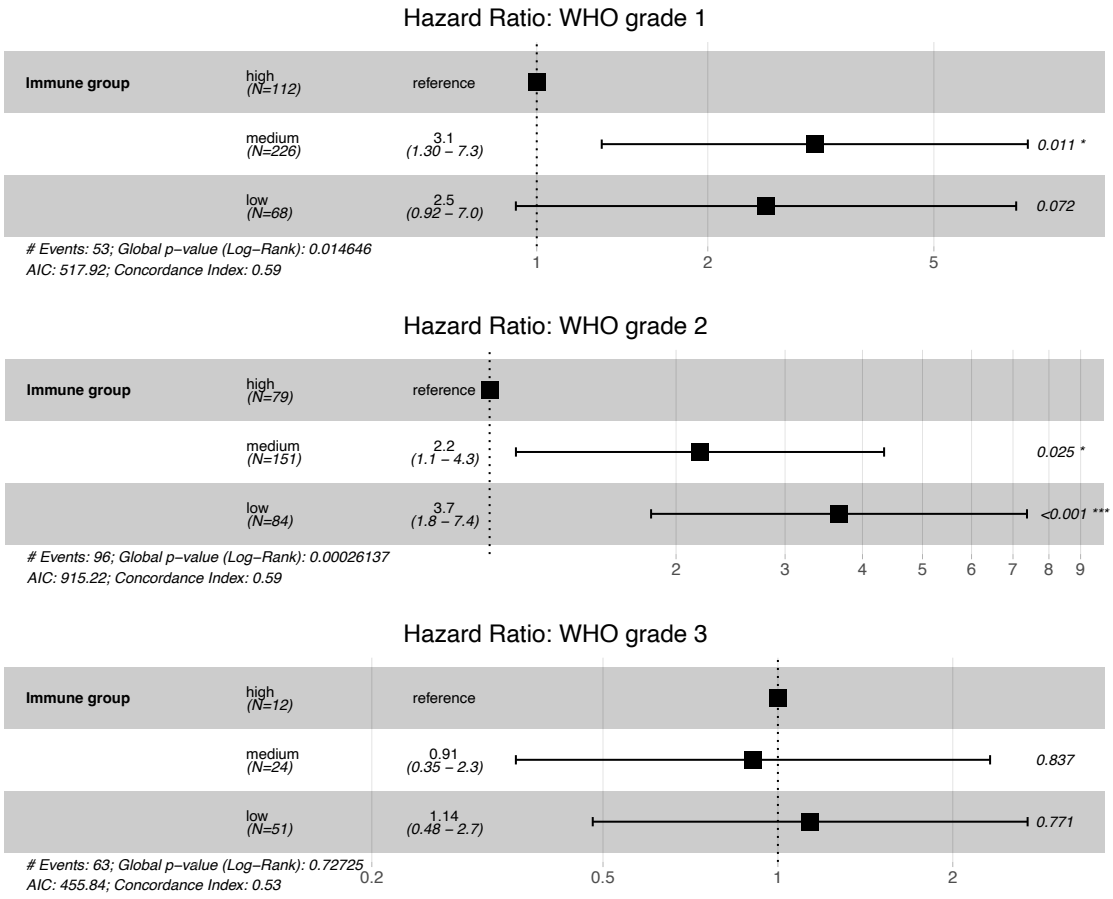

Supplementary Figure 8. *Hazard ratio of immune infiltration separated by WHO grades.*

Supplementary Tables

Supplementary Table 1. *Antibodies and dilutions used for immunohistochemical staining.*

Antibody	*Manufacturer*	*Clone*	*Catalogue No.*	*Pretreatment*	*Dilution*	*Incubation*
CD4	Cell Marque	SP35	104R-16	CC2 (pH=6,0), 56min	1:50	32min
CD8	Dako	C8/144B	M7103	CC1 (pH=8,4), 52min	1:50	32min
CD68	Dako	PG-M1	M0876	CC1 (pH=8,4), 36min	1:20	32min

Supplementary Table 2. *Meningiomas that were included in the scRNA-Seq dataset. n.a. … data not available.*

	WHO grade	*MC*	*Sex*	*Age*	*Batch*	*No. of cells*
MNG-1	1	ben-1	f	36	batch 2	11,164
MNG-2	1	ben-1	f	41	batch 2	5,120

MNG-3	1	int-A	f	69	batch 2	16,980
MNG-4	1	ben-2	m	54	batch 2	1,207
MNG-5	1	ben-2	f	73	batch 2	9,756
MNG-6	1	ben-2	f	75	batch 2	8,424
MNG-7	1	ben-2	f	64	batch 2	9,878
MNG-8	1	ben-3	f	65	batch 2	11,855
MNG-9	1	mal	f	90	batch 2	14,251
MNG-10	3	int-B	m	72	batch 2	5,358
MNG-11	3	mal	f	67	batch 2	4,396
MNG-12	3	int-A	m	64	batch 2	12,857
MNG-13	3	mal	f	79	batch 2	6,123
MNG-14	3	mal	m	68	batch 2	3,555
MNG-15	3	int-A	m	78	batch 2	4,081
MNG-16	3	mal	f	75	batch 2	17,094
MNG-17	3	int-B	f	79	batch 2	13,428
MNG-18	3	int-A	f	80	batch 2	18,928
MNG-19	1	int-B	m	72	batch 1	4,292
MNG-20	3	mal	m	78	batch 1	1,096
MNG-21	1	ben-1	f	71	batch 1	2,314
MNG-22	1	ben-3	m	43	batch 2	3,511
MNG-23	1	ben-1	f	60	batch 1	1,034
MNG-24	1	ben-2	f	68	batch 2	25,764
MNG-25	1	ben-2	f	62	batch 2	5,043
MNG-26	1	ben-3	m	72	batch 2	4,243
MNG-27	3	mal	m	81	batch 1	181
MNG-28	2	int-A	f	74	batch 1	1,135
MNG-29	1	ben-2	f	78	batch 1	1,065
MNG-30	3	mal	f	46	batch 1	3,017
MNG-31	1	ben-2	m	65	batch 1	1,462
MNG-32	1	ben-2	f	35	batch 1	896
MNG-33	2	int-A	f	69	batch 1	318
MNG-34	3	int-B	f	75	batch 1	317
MNG-35	1	ben-1	f	47	batch 1	3,135
MNG-36	2	int-A	m	55	batch 1	2,363
MNG-37	3	mal	m	58	batch 1	972

MNG-38	1	ben-1	f	52	batch 1	2,924
MNG-39	3	mal	m	75	batch 1	196
MNG-40	2	mal	f	62	batch 1	4,881
MNG-41	2	mal	f	62	batch 1	3,402
MNG-42	1	ben-1	f	67	batch 1	229
MNG-43	1	int-A	n.a.	n.a.	batch 1	3,762
MNG-44	1	ben-1	f	63	batch 1	178
MNG-45	3	mal	f	63	batch 1	442
MNG-46	1	ben-1	n.a.	n.a.	batch 1	1,522
MNG-47	1	int-A	n.a.	n.a.	batch 1	2,650
MNG-48	3	mal	f	65	batch 1	484

Supplementary Table 3. *Meningiomas included in the spatial transcriptomics dataset. n.a. ... data not available.*

	WHO grade	*MC*	*matching SC sample*
spMG-1	1	ben-1	MNG-1
spMG-2	1	ben-1	MNG-2
spMG-3	1	int-A	MNG-3
spMG-4	3	mal	MNG-37
spMG-5	1	ben-2	MNG-38
spMG-6	2	mal	MNG-41
spMG-7	3	mal	MNG-45
spMG-8	3	mal	–
spMG-9	3	int-A	–
spMG-10	3	mal	–
spMG-11	3	int-A	–
spMG-12	3	int-A	–
spMG-13	3	int-A	–
spMG-14	3	n.a.	–
spMG-15	3	mal	–
spMG-16	3	mal	–
spMG-17	3	mal	–